PROCESSING AND THERMAL BEHAVIOR OF ALUMINA HYBRID NANOCOMPOSITES

BY

UMER HAYAT

A Thesis Presented to the
DEANSHIP OF GRADUATE STUDIES

KING FAHD UNIVERSITY OF PETROLEUM & MINERALS

DHAHRAN, SAUDI ARABIA

In Partial Fulfillment of the
Requirements for the Degree of

MASTER OF SCIENCE

In

MECHANICAL ENGINEERING

DECEMBER, 2016

KING FAHD UNIVERSITY OF PETROLEUM & MINERALS

DHAHRAN- 31261, SAUDI ARABIA

DEANSHIP OF GRADUATE STUDIES

This thesis, written by **UMER HAYAT** under the direction his thesis advisor and approved by his thesis committee, has been presented and accepted by the Dean of Graduate Studies, in partial fulfillment of the requirements for the degree of **MASTER OF SCIENCE IN MECHANICAL ENGINEERING.**

Dr. Saheb Nouari
(Advisor)

Dr. Abul Fazal M. Arif
(Member)

Dr. Zuhair M. Gasem
Department Chairman

Dr. Ahsan-Ul-Haq Qurashi
(Member)

Dr. Salam A. Zummo
Dean of Graduate Studies

19/1/17
Date

To my family for their support and love

ACKNOWLEDGMENTS

I would like to express my gratitude to my advisor, Dr. Saheb Nouari, for his support and guidance throughout my Master's research. His continuous motivation, encouragement and cooperation have helped me to complete this thesis work. I am also grateful to my committee members, Dr. Abul Fazal M. Arif and Dr. Ahsan-Ul-Haq Qurashi, for their support and cooperation.

I would also like to express my gratitude to King Fahd University of Petroleum and Minerals (KFUPM), Dhahran, Saudi Arabia for providing me scholarship during my Master's study. I would also like to acknowledge King Abdulaziz City for Science and Technology (KACST) for providing research grant for this project.

I am very much thankful to my group members, Mr. Khwaja Muhammad and Ibrahim Momohjimoh, for their continuous help and support during various stages of this research. I am also thankful to all my friends especially Umer Ayub, Hafiz Khurram and Muhammad Faizan for helping me in various aspects during my stay at KFUPM.

I am also highly obliged to Mr. Latif, technical staff member at Materials Science Lab., for providing assistance during various experimental stages. I also want to acknowledge the help provided by Mr. Idris during SPS sintering and Dr. Abbas S. Hakem during SEM analysis.

At last, I would like to express my deepest gratitude to my parents for their love, prayers and support. I would also like to thank my brother and sisters for their moral support and encouragement.

TABLE OF CONTENTS

LIST OF TABLES

LIST OF FIGURES

LIST OF ABBREVIATIONS

SiC	:	Silicon Carbide
CNT	:	Carbon Nanotube
SWCNT	:	Single-walled Carbon Nanotubes
MWCNT	:	Multi-walled Carbon Nanotubes
CS	:	Conventional Sintering
SPS	:	Spark Plasma Sintering
HIP	:	Hot Isostatic Pressing
HP	:	Hot Pressing
CIP	:	Cold Isostatic Pressing
XRD	:	X-ray Diffraction
SEM	:	Scanning Electron Microscopy
EDX	:	Energy Dispersive X-ray Spectroscopy
FE-SEM	:	Field Emission Scanning Electron Microscopy
TEM	:	Transmission Electron Microscopy
RD	:	Relative Density
TD	:	Theoretical Density

ABSTRACT

Full Name : UMER HAYAT

Thesis Title : Processing and thermal behavior of alumina hybrid nanocomposites

Major Field : Mechanical Engineering

Date of Degree : December, 2016

The quest to improve the mechanical and functional properties of monolithic ceramics, to meet the growing demand for advanced ceramic materials, had led to the development of ceramic matrix composites and nanocomposites. Further improvement in mechanical properties was possible through hybrid microstructure design, the so-called hybrid nanocomposites, achieved by reinforcing a ceramic matrix with two nanoreinforcements that have different morphologies. Alumina is among advanced ceramic materials used to manufacture cutting tools, biomedical implants, and insulators. Improvement in physical and mechanical properties of alumina was possible through the incorporation of a nanoscale phase. Furthermore, production of commercial nanoreinforcements such as SiC nanoparticles and carbon nanotubes facilitated the development of hybrid alumina nanocomposites that have tailored nanostructures and outstanding properties. However, the majority of published research work, on alumina hybrid nanocomposites, has been devoted to the characterization of the microstructure and evaluation of mechanical properties and very limited work was dedicated to the study of the thermal properties and electrical conductivity. In this research work, temperature-dependent thermal properties of alumina were reported and the influence of SiC and CNTs on thermal properties and electrical conductivity of Al_2O_3-SiC-CNT hybrid nanocomposites was investigated. The

properties were correlated with the microstructure and possible transport mechanisms were discussed. The Al_2O_3-SiC-CNT hybrid nanocomposites were produced using ball milling and spark plasma sintering. The room temperature thermal conductivity, thermal diffusivity and heat capacity of monolithic alumina decreased from 34.44W/mK, 7.62mm^2/s and 1.24J/gK to 21.2W/mK, 6.64mm^2/s and 0.87J/gK for Al_2O_3-5SiC-1CNT hybrid nanocomposite and these thermal properties kept on decreasing with further addition of reinforcement content. The increase in temperature decreased the thermal conductivity and thermal diffusivity, but increased the specific heat of the monolithic alumina and the hybrid nanocomposites. The SiC and CNT reinforced alumina hybrid nanocomposites showed significant increase in room temperature electrical conductivity. This makes the hybrid composites suitable for EDM and allows for the manufacturing of low cost products that have intricate shapes, irrespective of their hardness or strength. Al_2O_3-5SiC-2CNTs had a high electrical conductivity value of 8.85S/m compared to a low value of $6.87x10^{-10}$S/m for the monolithic alumina.

ملخص الرسالة

الاسم الكامل: **عمر حياة**

عنوان الرسالة: التصنيع و السلوك الحراري للمادة المركبة الهجينة من أكسيد الألمنيوم

التخصص: الهندسة الميكانيكية

تاريخ الدرجة العلمية: ديسمبر 2016

أدت الحاجة إلى تطوير الخصائص الميكانيكية والوظيفية للمواد الخزفية أحادية الطور- لتلبية الطلب المتزايد على المواد الخزفية المتقدمة- إلى تطوير المواد الخزفية المركبة و المواد المركبة النانوية، بالإضافة إلى تطوير البنية المجهرية الهجينة عن طريق المواد المركبة الهجينة، والتي أمكن الحصول عليها عن طريق تدعيم الطور الأساسي بطورين نانونويين مقويين يملكان تركيبا أشكالا مختلفة.

يعتبر أكسيد الألمنيوم من المواد الخزفية المتقدمة، والذي يستخدم في صناعة أدوات القطع و الأعضاء الصناعية و العوازل. يمكن تحسين الخواص الفيزيائية والميكانيكة لأكسيد الألمنيوم عن طريق دمج طور نانوي. بالإضافة إلى ذلك، فإن إضافة جسيمات كاربيد السيليكون النانوية و أنابيب الكربون النانوية تساهم في تشكيل مادة أكسيد الألمنيوم النانوي المركبة ببنية مجهرية مغايرة وخواص متميزة. بالنظر إلى ما نشر في هذا المجال، يمكن ملاحظة أن أغلبه متعلق بتحليل البنية المجهرية والخصائص الميكانيكية ، بينما صرف القليل من البحث في دراسة الخواص الحرارية و التوصيل الكهربائي لهذه المواد المركبة

درس هذا العمل البحثي الخواص الحرارية لأكسيد الألمنيوم بدلالة درجة الحرارة، بالإضافة إلى تأثير كاربيد السيليكون وأنابيب الكربون النانوية على الخواص الحرارية والتوصيل الكهربائي لهذه المادة المركبة النانوية الهجينة، حيث ربطت هذه الخصائص مع البنية المجهرية للمادة . ناقش البحث كذلك آليات التوصيل المحتملة. صنعت المادة المركبة الهجينة النانوية- والمكونة من أكسيد الألمنيوم و كاربيد السيليكون وأنابيب الكاربون- باستخدام الطحن الميكانيكي وتقنية التلبيد بشرارة البلازما. وجد أن قيمة معامل التوصيل الحراري في درجة حرارة الغرفة انخفضت من 21.2 W/mK إلى 34.44 W/mK بينما انخفض معامل انتشار الحرارة من 7.62 mm^2/s إلى 6.64

mm^2/s وانخفضت السعة الحرارية من 1.24 J/gK إلى 0.87 J/gK ، وذلك عند مقارنة أكسيد الألمنيوم أحادي الطور مع المادة المركبة النانوية، والتي احتوت على 5% كاربيد السيليكون و 1% أنابيب الكاربون النانوية. استمر الانخفاض في الخواص الحرارية مع زيادة إضافة المواد المقوية. أدى ارتفاع درجة الحرارة إلى تخفيض كل من معامل التوصيل الحراري و معامل الانتشار الحراري، بينما زاد من قيمة الحرارة النوعية لكل من أكسيد الألمنيوم أحادي الطور و المادة المركبة الهجينة النانوية. أثبت البحث كذلك أن هذه المادة - والتي احتوت على أكسيد الألمنيوم و كاربيد السيليكون وأنابيب الكربون النانوية- تزيد من التوصيل الكهربائي في درجة حرارة الغرفة، والذي يجعلها مادة مناسب تصنيعها بالتفريغ الكهربائي ، و تسهل كذلك تصنيع المنتجات ذات الأشكال المعقدة بغض النظر عن قوتها و صلابتها. أظهر استخدام 5% كاربيد السيليكون و 2% أنابيب الكاربون النانوية زيادة في معامل التوصيل الكهربائي (8.85 S/m) مقارنة بأكسيد الألمنيوم أحادي الطور ($6.87x10^{-10}$ S/m).

CHAPTER 1

INTRODUCTION

1.1 Overview

Structural ceramics exhibit excellent properties such as high mechanical strength, high thermal resistance and good chemical stability. Because of these properties, they are used in extreme environments. However, the use of ceramics is limited because of their inherent brittleness. Low fracture toughness of ceramics is the only obstacle for their use in wide range of applications. A lot of research has been done in finding the ways to increase the fracture toughness of ceramics. It was found that the most effective technique is to reinforce ceramics with some reinforcements, resulting in formation of composites. These reinforcements can be in form of particles, whiskers, rods, tubes [1].

A composite is a multiphase material, which exhibit the properties of both of its constituents. Composites are produced by the combination of two or more materials having distinct properties, to get a combination of properties of all its constituents. Components of composite are selected in such a way to get unusual combination of properties i-e strength, stiffness, hardness, fracture toughness, thermal properties and corrosion resistance. The properties of composites are a function of properties of its constituent phases, relative amounts, geometry of the reinforced phase and distribution of reinforced phase [2]. When any one or both of the phases (i.e matrix and dispersed phase) have a nano size (1nm-100nm), then the composite which is formed by the mixture of

these two phases is called nanocomposite. This research area of nanocomposites was first introduced by Niihara who reported significant enhancements in properties of ceramic, when it was reinforced with nanoparticles [3]. The most common reinforcements used for the synthesis of nanocomposites include the metals such as Ni, W, Cu, Mo, Co, Fe and non-metals such as boron, carbon fibre, alumina, SiC and CNT so on [4].

Alumina (Al_2O_3) is the most widely studied ceramic because of its relative abundance, low cost, availability in highly purified grades [5]. Alumina is also an attractive ceramic because of its good mechanical properties, high thermal stability and resistance to corrosion. It is used in high speed cutting tools, gas laser turbines, dental implants, electrical and thermal insulators, wear resistant parts and coatings [6]. A lot of research has been done on monolithic alumina ceramic by sintering it through conventional sintering, hot-isostatic pressing (HIP) and spark plasma sintering (SPS) [7-12]. Some of the properties of sintered alumina are given in Table 1. Very high brittleness, lower fracture toughness, insulating electrical nature and lower thermal conductivity limits the use of alumina ceramic in various commercial applications [13]. In order to overcome these limitations, researchers have reinforced alumina with different types of reinforcements like Mo, Ni, Fe, Cr, Al, TiAl, Ni_3Al, Fe_3Al, SiC, CNT etc. Significant enhancements in properties were reported for alumina based nanocomposites [6, 13].

One of the most important applications of alumina is in cutting tools industry [14]. Some of the typical properties required for cutting tools are: high hardness, toughness, hot strength, high wear resistance and appreciable thermal conductivity. Pure alumina cutting tools, having all these properties, were developed and used during start of twentieth century for cutting low hardness steel and grey cast iron [15]. However, because of low

fracture toughness, they were prone to brittle failure. With development of high speed machining, properties requirements for cutting tools also became higher, resulting in shifting of single phase ceramic tools to multiphase composite tools. Some of the additives used in alumina are; ZrO_2, TiC, TiN, WC, Ti(C,N), Zr(C,N), SiC and CNTs [16-19]. H. Xiao et al [20] reported that alumina-based cutting tools were most suitable as compared to other ceramic tools for hardened steel machining because of superior flank wear resistance. A. Chakraborty et al [21] studied the comparative wear behavior of pure alumina, zirconia-toughened alumina and WC tools during high speed machining of low alloy steel. He reported that both alumina and zirconia-toughened alumina showed low wear rates and better surface finish as compared to WC tools, especially at high machining speeds.

Silicon Carbide (SiC) is a ceramic material having high strength, hardness, ability to retain its properties at higher temperature, good oxidation resistance, good corrosion behavior, good heat transfer coefficient. Due to these excellent properties, it is used in number of applications involving extreme conditions such as components of gas turbine, heat exchangers and refractories for high temperature furnace, seals, bearings, wear resistant components [22, 23]. Properties of sintered silicon carbide are presented in Table 1. Silicon carbide, like other ceramics, also has lower fracture toughness. Different reinforcing materials such as carbon nanotubes, graphene etc. are added to enhance the fracture toughness of silicon carbide. At the same time, silicon carbide is also used as reinforcement in wide range of materials such as Al_2O_3, SiAlON, Si_3N_4, MgO to enhance their properties [24].

Table 1. Properties of Al_2O_3 ceramic, SiC and CNTs

Property	Alumina (Al_2O_3) [5, 25-27]	Silicon Carbide (SiC) [22, 27, 28]	Carbon Nanotubes (CNT) [13, 29]
Density (g/cm^3)	3.984	3.16	1.3-2
Elastic Modulus (GPa)	416	415	1000
Fracture Toughness ($MPa.m^{1/2}$)	3.5	3.1	---
Hardness (GPa)	15	32	---
Thermal Conductivity (W/mK)	33	114	3000-6000
Electrical Conductivity (S/m)	10^{-10} - 10^{-12}	10^{-3}-10^{2}	1.85×10^{5}
Thermal expansion coefficient(K^{-1})	8.6×10^{-6}	4.5×10^{-6}	negligible

Addition of this SiC to alumina ceramic resulted in enhancement in fracture toughness, fracture strength, wear resistance and creep resistance [24]. X.L. Shi et al [30] showed that fracture toughness of alumina ceramic can be enhanced upto $7.6MPa.m^{1/2}$ by the addition of 5 wt.% SiC. He also reported enhanced flexural strength of Al_2O_3-SiC nanocomposites. M. Parchoviansky [31] reported the flexural strength of Al_2O_3-SiC nanocomposites, twice higher than pure alumina ceramic, when reinforced with 20 wt.% SiC. S. Hayun [23] found significant enhancements in hardness, flexural strength and

fracture toughness of Al_2O_3-SiC nanocomposites as compared to alumina ceramic. M. Parchoviansky et al [32] reported appreciable improvements in thermal and electrical conductivity of Al_2O_3-SiC nanocomposites when reinforced with 20 wt.% SiC.

The cutting performance of commercial tools and alumina-SiC composites have been studied by Ko et al [18]. Alumina containing 10wt%SiC showed the best cutting performance for machining heat treated AISI4140, while alumina containing 5wt% SiC composite exhibit the best cutting performance for machining grey cast iron. Thus, tool life of alumina containing 10wt%SiC and 5wt% SiC was 7 times and 1.5 times longer than that of commercial tools (Al_2O_3-TiC and Al_2O_3-TiB) on machining heat treated steel and grey cast iron, respectively. High wear resistance of SiC-reinforced alumina cutting tools was also reported by Yust et al [20], as compared to pure alumina tools.

Carbon nanotubes (CNTs), because of their exceptional mechanical, electrical and thermal properties, have gained huge importance in field of advance materials since after their discovery in 1991 [33]. Due to their very high modulus of elasticity, strength and thermal conductivity, they became an excellent reinforcement material for metals, alloys, ceramics and polymers. Some properties of CNTs are shown in Table 1. Carbon nanotubes exist in the form of single walled tubes or multi walled tubes. Single-walled CNTs have very high Young's modulus and tensile strength i-e 5 TPa and 150 GPa respectively, the values which are one to two orders of magnitude higher than the best known steels [34]. Multi-walled carbon nanotubes (MWCNTs) show somehow lower properties than single-walled carbon nanotubes but still exceptional (Young modulus 1.8TPa). However, the chemical stability of multi-walled carbon nanotubes is found to be higher than single-walled carbon nanotubes [35].

Al_2O_3-MWCNT nanocomposites showed superior properties when reinforced with different amounts of CNT. Song Bi et al [36] reported the enhancements in fracture toughness and flexural strength of Al_2O_3-CNT nanocomposites upto 61.1% and 17.2% respectively, when reinforced with 5 wt.% CNT. I. Ahmed et al [37] found the enhancements in fracture toughness, hardness and flexural strength upto 94%, 13% and 6.4% respectively, when alumina matrix was reinforced with 4 vol.% of CNT. Enhancements in thermal properties of Al_2O_3-CNT nanocomposites were also observed, with thermal conductivity reaching upto the value of 90.44 W/mK, as investigated by L. Kumari [38]. K. Ahmad et al [25] showed that reinforcement of upto 5 vol.% of CNT's can increase the electrical conductivity of alumina up to twelve orders of magnitude.

Hybrid nanocomposite is a new class of materials, in which two reinforcements are added to a matrix in order to achieve a unique combination of properties of all constituents. Although uniform dispersion of two reinforcements within a single matrix is quite challenging, yet this hybrid design has shown significant enhancements in fracture toughness and bending strength without affecting the hardness [39]. K. Mohammad et al [40] reported 33% increase in fracture toughness of Al_2O_3-5SiC-1CNT hybrid nanocomposite as compared to pure alumina. N. Saheb et al [41] showed 93.95% enhancement in facture toughness of Al_2O_3-5SiC-2CNT in comparison with alumina. Enhancement of 117% in fracture toughness and 44% in bending strength was observed by K. Ahmad et al [39] in Al_2O_3-SiC-CNT hybrid nanocomposites with different fractions of SiC and CNT. Large amount of work has been done to enhance the properties of alumina by developing Al_2O_3-SiC and Al_2O_3-CNT's nanocomposites [30, 31, 37, 42-

48]. However, the work on alumina hybrid nanocomposites is quite rare, especially on thermal and electrical behavior.

In this thesis work, spark plasma sintering parameters were optimized using alumina ceramic aiming for full densification and the effect of these sintering parameters on thermal properties was studied. Then, two reinforcements (SiC nanoparticles and multi-walled CNTs) were added to the alumina matrix in order to enhance the performance and properties of alumina matrix. To ensure the homogeneous dispersion, combination of processes i-e magnetic stirring, sonication and ball milling were used. SPS was used for sintering. Effects of SiC and CNT reinforcements on thermal and electrical properties of Al_2O_3-SiC-CNT hybrid nanocomposites were investigated and possible factors affecting the properties were discussed in detail.

1.2 Motivation

The quest to improve the mechanical and functional properties of monolithic ceramics, to meet the growing demand for advanced ceramic materials, had led to the development of ceramic matrix composites and nanocomposites. Significant improvement in mechanical properties of ceramic materials was obtained by reinforcing a ceramic matrix with a micron or nano scale phase. Further improvement in mechanical properties was possible through hybrid microstructure design, the so-called hybrid nanocomposites, achieved by reinforcing a ceramic matrix with two nanoreinforcements that have different morphologies and/or attributes. Alumina is among advanced ceramic materials used to manufacture cutting tools, biomedical implants, and insulators. Improvement in physical and mechanical properties of alumina was possible through the incorporation of a nanoscale phase. Furthermore, production of commercial nanoreinforcements such as SiC

nanoparticles and carbon nanotubes facilitated the development of hybrid alumina nanocomposites that have tailored nanostructures and outstanding properties. However, the majority of published research work, on alumina hybrid nanocomposites, has been devoted to the characterization of the microstructure and evaluation of mechanical properties and very limited work was dedicated to the study of the thermal properties and electrical conductivity.

1.3 Objectives

The overall objective of this research work is to investigate the influence of SiC and CNTs on thermal properties and electrical conductivity of ball milled and spark plasma sintered Al_2O_3-SiC-CNTs hybrid nanocomposites.

The following are the specific objectives to reach the overall objective of this research:

- Synthesis of homogenous Al_2O_3-SiC-CNTs hybrid nanocomposite powders using ball milling technique.
- Consolidation of the prepared powders to high density using spark plasma sintering method.
- Evaluation of the thermal properties of the developed materials.
- Measurement of the electrical conductivity of the developed materials.
- Correlation of the properties with the microstructure and discussion of possible transport mechanisms.

1.4 Organization of thesis

Chapter 2 contains the detailed literature review about the different powder processing and consolidation techniques, microstructural properties, mechanical properties, thermal properties and electrical properties of Al_2O_3 ceramic, Al_2O_3-SiC nanocomposites, Al_2O_3-CNT nanocomposites and Al_2O_3-based hybrid nanocomposites.

Chapter 3 provides the details about materials and experimental procedures. Detailed specifications of materials used in research, processing and consolidation techniques used and their parameters are discussed here. Characterization techniques used to study the desired properties are also discussed in this chapter.

Chapter 4 contains the results and discussion on characterization of pure alumina and Al_2O_3-SiC-CNT hybrid nanocomposites. Powders characterization, densification, crystallite size, microstructural analysis, thermal properties and electrical properties are discussed in detail.

Chapter 5 provides the conclusions and recommendations

CHAPTER 2

LITERATURE REVIEW

2.1 Introduction

Hybrid nanocomposites is relatively a new field, in which a matrix is reinforced with two or more nano-phase reinforcements having superior properties, in order to get the combination of properties of all constituents [39]. One of the difficulties faced in fabrication of hybrid nanocomposites is the homogenous dispersion of nano-phases into the matrix [49]. Nano-sized reinforcements have a very large surface area and in turn high surface energy, resulting in very high tendency for agglomeration [50]. Agglomeration of reinforcement within matrix deteriorates the expected enhanced properties of material. These agglomerates can act as a stress concentration sites within the nanocomposite materials, leading to the premature failure. Therefore, uniform dispersion of nano-phases within matrix is extremely important in case of hybrid nanocomposites.

Addition of reinforcements also hinders the densification process, resulting in less dense material with reduced properties [50]. This makes selection of consolidation process and its parameters quite challenging. Densification can be increased by subjecting material to higher sintering temperature or prolonging the sintering time, but it can result in grain growth, which also has adverse effect on properties. However, with the advancement in technology, many new techniques have been developed such as SPS, HIP to overcome

this problem of densification [51]. These new techniques offer enhanced densification rates, along with better control on microstructure.

Lot of research has been done to explore the enhanced properties of ceramic-based nanocomposites and hybrid nanocomposites. This chapter summarizes the research which has been done by different researchers along with their findings.

2.2 Powder Processing Techniques

Homogenous dispersion of reinforcement in matrix is the key to obtain enhanced properties in nanocomposites. Therefore, large number of powder processing techniques have been developed and used in order to get homogenous dispersion in nanocomposites. Some of them are; powder processing, colloidal processing, sol-gel processing, molecular level mixing, ball milling, ultrasonication, magnetic stirring [4, 13].

In the current thesis work, magnetic stirring, ultrasonication and ball milling are used in combination with each other for obtaining the better dispersion. Few of the powder processing techniques are discussed below.

2.2.1 Ball Milling

Mechanical alloying or ball milling [52] is a technique used for the production of high performance materials. It has been proven as one of the powerful powder processing technique for the uniform dispersion of reinforcement into matrix. Mechanical alloying or ball milling process involves mixing of raw powders with high energy milling balls, mostly with additives, in an inert atmosphere. During milling stage, the powders experience repeated cold welding and fracturing until fine mixed powder, which is finer than the starting constituents, is obtained as shown in Figure 1.

Characteristics of the final milled products are affected by several factors such as milling time, miller type, type of ball material, ball to powder weight ratio, milling atmosphere, process control agent or additive in the stage of milling. With the use of prolong milling time and mixing of powders with high energy milling balls, solid state chemical reaction can occur, driven by repeated plastic deformation during milling. At an optimum milling time, welding and fracture mechanism of mixed powders reach equilibrium and equiaxed particles can be obtained. If the milling time is too long, the resultant particles exhibit irregular shape and affect the mechanical properties of consolidated products. Mechanical alloying, because of its potential for uniform dispersion of reinforcement within matrix, is extensively used for the preparation of nanocomposites.

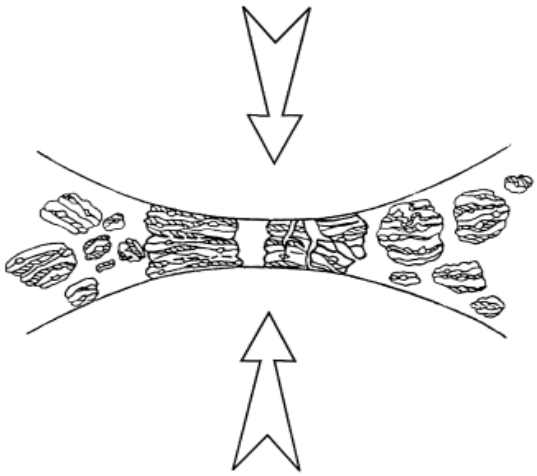

Figure 1. Cold welding and fracturing of powders during ball-powder-ball collision in ball milling [52]

2.2.2 Ultrasonication

In ultrasonication process, sound waves are used for stirring of powder mixtures within certain liquid. These ultrasonic waves are generated using equipment called sonicator, as

shown in Figure 2. These ultrasound waves travel within liquid medium, in series of compressions, where they interact with powder particles and peel off the agglomerated powder particles [53]. Ultrasonication is widely used technique for the homogeneous dispersion of nanoparticles especially for the dispersion of CNT's. Q. Cheng et al [54] showed that ultrasonication is the most effective process for dispersion of carbon nanotubes, using ultrasonic waves for breaking the Van Der Waal forces between the CNT agglomerates.

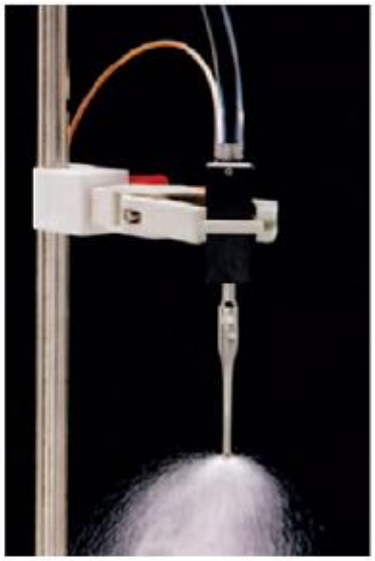

Figure 2. Probe Sonicator [53]

Different researchers have used different powder processing routes for the preparation of nanocomposite powders. F. Inam [55, 56], S.C Zhang [47] and G. D. Zhan [57] used sonication and ball milling for the preparation of alumina-CNT nanocomposites. L. Kumari [26] used chemical vapor depostion process (CVD) for the preparation of alumina-CNT nanocomposite powders. Song Bi [36] studied the properties of alumina-CNT nanocomposites by using two different routes for nanocomposite powder

preparation, hydrothermal crystallization and ball milling, and studied the effect of processing route on final properties of nanocomposite. N. Bakhsh [45] used combination of ball milling and gas purging sonication (GPS) for dispersion of carbon nanotubes in alumina powder.

J. Sun [58], J. Ning [59], G. Yamamoto [60, 61] used the colloidal processing route for the preparation of alumina-CNT nanocomposite powders. S. Ghadami [42], S. Gustafsson [43], X. L. Shi [30], J. H. Chae [44], M. Parchoviansky [31] used ball milling for the mixing of alumina-SiC nanocomposite powders. L. Gao [62] used heterogeneous precipitaion method for the preparation of alumina-SiC nanocomposites.

K. Mohammad [40] used molecular level mixing for the synthesis of Al_2O_3-SiC-CNT hybrid nanocomposite powders. K. Ahmad [39], N. Saheb [41] used combination of sonication and ball milling for the preparation of Al_2O_3-SiC-CNT hybrid nanocomposite powders.

2.3 Powder Consolidation Techniques

Powders are consolidated using different consolidation techniques such as conventional sintering (CS), hot pressing (HP), hot isostatic pressing (HIP), microwave sintering, spark plasma sintering (SPS) etc. [51]. In case of nanomaterials, the ultimate aim of consolidation is to achieve maximum densification with minimum grain growth. However, during consolidation, certain amount of grain growth occurs surely along with the densification. Therefore, selection of consolidation process and its parameters, to get the desired properties, can be a challenging task. Few of the consolidation techniques are discussed here.

2.3.1 Conventional Sintering

Conventional sintering is one of the oldest methods used for consolidation of powders. It is generally done in two steps; green compaction and sintering. In green compaction, sample is pressed in the form of pellets, with or without binder. Then, this green compact is heated into the furnace for a certain period of time. During sintering process, particles bond together and annihilate the pores and voids and form a solid compact [51]. Main advantages of conventional sintering are; complex shapes can be sintered easily, equipment is not so expensive. However, the only disadvantage of conventional sintering is that very large sintering times are required for achieving higher densification, which can sometimes lead to uncontrollable grain growth.

S. Gadami et al [42] reported a very high densification of 99.4% for alumina and 98.6% for alumina-2.5wt.% SiC nanocomposites using conventional sintering at temperature of 1750℃ for 4hr. S. Gustafsson et al [43] attained 99.3% relative density of alumina-5wt.% SiC nanocomposite using conventional sintering. S. Zhang et al [47] reported 99% relative densification, when conventionally sintered alumina-1vol.% CNT nanocomposite at 1500℃ for 2hr.

2.3.2 Hot Pressing

Hot pressing is another powder consolidation technique allowing higher densification to achieve along with better control on microstructure [51], as compared to conventional sintering. The schematic of hot pressing is shown in Figure 3. In hot pressing, variables are; temperature, pressure and time. This process involves the simultaneous application of temperature and pressure to the powder sample, resulting in higher densification. Due

to the simultaneous application of pressure along with heat, processing time is significantly reduced.

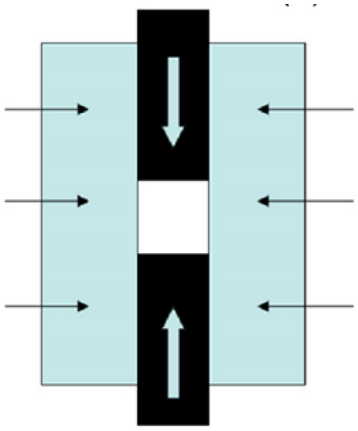

Figure 3. Schematic of Hot Pressing [51]

M. Parchoviansky et al [31] reported the densification of upto 99.5% for alumina-SiC nanocomposites using hot pressing at temperature of 1740°C, pressure of 30MPa and sintering time of 1hr. Song Bi et al [36] also reported very high densification of 99.2% for alumina-5wt.% CNT nanocomposites using hot pressing.

2.3.3 Spark Plasma Sintering

Spark plasma sintering is a pressure assisted sintering technique used to achieve higher densification within short time and at lower temperatures. However, the exact mechanism responsible for this fast densification is still not known [63]. Still it has been proven as the high speed consolidation technique having less power consumption than conventional sintering and hot pressing [64].

In spark plasma sintering, sample is loaded within a die and then pressure and heating is applied simultaneously. The difference between spark plasma sintering and hot pressing

lies only in the method used for heating. External heaters are used for heating in hot pressing while in spark plasma sintering, a pulsed DC current is made to pass through conducting dies and through the sample as shown in Figure 2. This heating mode in SPS allows very fast heating rates, which eventually contribute to the higher densification along with minimum grain growth. Three factors which are thought to be responsible for rapid densification during spark plasma sintering include: high pressure, rapid heating rates and pulsed DC current [10].

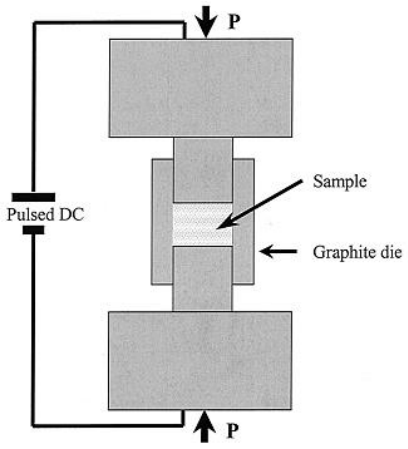

Figure 4. Schematic of Spark Plasma Sintering [10]

SPS, because of its promising results, is one of the most widely used techniques for consolidation of nanomaterials [10-12, 23, 44, 45, 65-67]. Z. Shen et al [10] showed that with proper selection of sintering parameters, even 100% relative density can be achieved using SPS for alumina ceramic. 99.5% relative density was reported by N. Bakhsh [45] for alumina-1wt.% CNT nanocomposites using SPS.

2.4 Monolithic Al_2O_3 Ceramic

2.4.1 Densification, Microstructural and Mechanical Properties

Alumina ceramic, because of its relative abundance and low cost in combination with very good mechanical and thermal properties, was extensively studied and used in applications with extreme conditions such as high speed cutting tools, dental implants, electrical and thermal insulators, wear resistant parts and coatings [6]. High thermal stability and retention of strength at elevated temperatures makes alumina one of the best materials for extreme operating conditions. Different methods such as conventional sintering, hot isostatic pressing (HIP), microwave sintering and spark plasma sintering (SPS) have been used for the consolidation of alumina submicron powder to get better properties of compacted alumina [7-12, 66]. SPS has been found to be the most effective technique for consolidation of alumina for better densification and minimum grain growth. Table 2 shows some of the reported literature on densification, microstructural and mechanical properties of spark plasma sintered specimens.

J. G. Santanach et al [9] studied the effect of various sintering parameters i-e dwell temperature, applied pressure, dwell time and pulse pattern on spark plasma sintering of alumina. Investigation of densification and grain size of spark plasma sintered alumina at various sintering parameters showed two regimes: densification without grain growth which occurred at low temperatures and grain growth without further densification which occurred at higher temperatures with threshold between 1100 to 1200 °C.

Table 2. Sintering behavior of Spark plasma sintered alumina

Powder Size (µm)	Sintering Parameters	Relative Density (% TD*)	Grain Size (µm)	Hardness (GPa)	Fracture Toughness ($MPa.m^{1/2}$)	Ref.
0.4	1200°C-150°C/min-3min-50MPa	98	0.5	21.5	3.2	[10]
	1225°C-156°C/min-3min-50MPa	98.2	1	20.6	4.5	
	1300°C-140°C/min-10min-50MPa	99.7	5.9	19.3	4.3	
0.05	1150°C-200°C/min-3min-63MPa	99.8	0.349	20.3	3.3	[66]
0.2	1350°C-100°C/min-5min-50MPa	99.8	0.529	22.9	2.9	[68]
0.21	1250°C-100°C/min-5min-5.5MPa	92	0.76	13.9	4.4	[69]
	1250°C-100°C/min-15min-5.5MPa	98	0.68	17.7	2.7	

Table 2. (Continued)

Powder Size (µm)	Sintering Parameters	Relative Density (% TD*)	Grain Size (µm)	Hardness (GPa)	Fracture Toughness ($MPa.m^{1/2}$)	Ref.
0.03	1300℃-300℃/min-5min-75MPa	97.7	0.7	19	---	[65]
0.15	1250℃-100℃/min-5min-60MPa	99.8	0.68	20.75	4.45	[11]
	1500℃-100℃/min-5min-60MPa	99.9	4	18.5	4.3	
0.14	1350℃-100℃/min-6min-150MPa	99	1.2	22	5	[70]
	1150℃-100℃/min-5min-100MPa	100	0.32	21.3	5.4	
0.3	1300℃-100℃/min-5min-30MPa	99.3	4.4	19.5	4.7	[71]

*TD is the theoretical density

Z. Shen et al [10] investigated the effects of grain growth inhibitor and different sintering parameters on the densification, grain growth, hardness and fracture toughness of spark plasma sintered alumina. 0.1% MgO was used as a grain growth inhibitor in few samples.

Grain growth was more prominent in samples without MgO. Hardness and fracture toughness remained within the range of 20-21 GPa and 3.2 ± 0.5 $MPa.m^{1/2}$. The mechanisms, grain boundary diffusion and grain boundary migration, responsible for enhanced grain growth were found to be strongly temperature dependent.

S. W. Wang et al [12] studied the effect of different particle sizes of starting powder, different sintering parameters and different thicknesses of sintered samples on densification and grain structure of spark plasma sintered alumina. Smaller initial particle size resulted in higher relative density. Driving force for densification of fine initial powder was greater than coarse powder during spark plasma sintering. Decrease in density was observed when the thickness of samples was increased.

Jinling Liu et al [72] studied the effect of different particle sizes of initial powder and sintering temperature on the grain refining of spark plasma sintered alumina. Density of the samples having smaller initial particle size was found higher than the samples with large initial particle size. Grain sizes of sintered samples with 1µm initial powder size at 1200 and 1300°C were reported as 300nm and 2.2µm respectively while for 3µm initial powder, grain sizes were 110nm and 700nm respectively. In case of 3µm initial powder, regardless of sintering temperature, the final grain size of sintered samples was found to be smaller than initial powder, revealing the grain refining effect which was not found in case of 1µm powder. This showed that grain refining effect only occurred for initial powder larger than a particular size. This grain refining effect was found probably due to rearrangement of dislocations through thermo-mechanical fatigue process. Due to lesser number of dislocations in small sized initial powder, grain refining effect was not prominent.

2.4.2 Thermal Properties

Large literature is available on densification, microstructural and mechanical characterization of sintered alumina [5, 8-11, 38]. However, not enough literature is available on thermal behavior of alumina. Thermal properties are also as much important as mechanical properties, as these materials are used in applications involving high temperatures such as refractories for glass and metal industries, gas radiant burners, high temperature structural components, wear part and cutting tools etc. [73]. Very few researchers have reported thermal properties of alumina as shown in Table 3.

L. Kumari et al (2008) [38] reported the thermal properties i-e thermal diffusivity, heat capacity, thermal conductivity of spark plasma sintered alumina. Thermal diffusivity was measured using laser flash technique and heat capacity by differential scanning calorimetry (DSC). Thermal conductivity was calculated using relation $\lambda = D\rho C_p$ (where λ is thermal conductivity, D is thermal diffusivity, ρ is bulk density, C_p is heat capacity). Thermal diffusivity was found to be decreasing with temperature increase i-e from 5.97mm^2/s at 100°C to 3.54mm^2/s 300°C. Heat capacity increased with increase in temperature from 0.77J/gK at 25°C to 1.09J/gK at 300°C. Thermal conductivity was found to be decreasing from 27.65W/mK to 19.96W/mK with the increase in temperature from 100°C to 300°C, respectively.

Guo-Dong Zhan et al (2004) [57] studied the mechanical and thermal properties of spark plasma sintered alumina. Spark plasma conditions used were 1150°C and 3 minutes. Relative density and grain size of sintered specimen were reported to be 100% and 349nm, respectively. Hardness and fracture toughness values reported were 20.3 GPa and 3.3 MPa.$m^{1/2}$, respectively. Thermal conductivity of alumina at room temperature was

Table 3. Thermal properties of sintered alumina

SPS conditions	Micro-structural parameters	Thermal characterization				Ref.
		Temp (°C)	Thermal Conductivity (W/mK)	Heat capacity (J/gK)	Thermal Diffusivity (mm^2/s)	
1150°C-100°C/min-10min-100MPa	-----	25	---	0.77	8.7	[38]
		100	27.65	0.9	5.97	
		250	22.6	1	4.6	
		300	19.96	1.09	3.54	
1150°C-3min	100% RD* 349nm grain size	25	27.3	---	---	[57]
1400°C-3min-50MPa	99.5% RD 350nm grain size	25	34	---	---	[74]

*RD is relative density

found to be 27.3 W/mK. K. Ahmed et al (2014) [74] also reported the thermal conductivity of fully dense alumina sample to be 34W/mK.

2.4.3 Electrical Conductivity

Pure alumina is electrically insulator with very low electrical conductivity in the range of 10^{-10}-10^{-12} S/m as reported by G. D. Zhan et al [57]. The values of electrical conductivity of alumina reported by different researchers are given in Table 4.

Table 4. Electrical Conductivity of monolithic alumina ceramic

Sintering Method	Electrical Conductivity (S/m)	Ref.
SPS	1.79×10^{-12}	[25]
SPS	10^{-10}	[26]
HP	7.8×10^{-6}	[32]
SPS	10^{-10}-10^{-12}	[57]
SPS	10^{-10}-10^{-12}	[75]
SPS	10^{-8}	[76]
SPS	10^{-12}	[77]
HP	1.3×10^{-10}	[78]
SPS	10^{-12}	[79]

2.5 Al_2O_3-SiC Nanocomposites

2.5.1 Densification, Microstructural and Mechanical Properties

Alumina, although having very good mechanical properties, has limited applications because of lower fracture toughness. One reason for lower fracture toughness of alumina ceramic is restricted dislocation movement due to strong ionic and covalent bonds. However, it was proposed that reinforcing alumina ceramic with nanoparticles improves both strength and fracture toughness [1, 6]. In last few years, huge research has been carried out to develop tougher and harder Al_2O_3 based nanocomposite. SiC particles are used as reinforcement in alumina because of their lower thermal expansion, higher hardness and low reactivity. Different sintering routes were used for sintering Al_2O_3-SiC nanocomposites [30, 31, 42-44].

Alumina-SiC nanocomposites show enhanced fracture toughness, fracture strength, wear resistance and creep resistance as compared to pure alumina [24]. Different mechanisms, responsible for enhancement in properties of Al_2O_3-SiC nanocomposites, were proposed by different researchers. Nihara et al [80] proposed that crack deflection by SiC carbide particles inside alumina matrix is the reason for enhancement of strength and fracture toughness of composite. G. Pezzotti et al [81] proposed residual stress model for explaining the strengthening mechanism in Al_2O_3-SiC nanocomposite. He proposed that this strengthening arises due to the micro-stresses generated within the alumina matrix because of the thermal mismatch between Al_2O_3 and SiC. Zhen-Yan et al [82] proposed that strengthening arise due to pinning effect of SiC particles within alumina matrix, which changes the fracture mode of alumina matrix from intergranular to transgranular. T. Ohji et al [83] proposed that increased creep resistance in alumina-SiC

nanocomposites, as compared to monolithic alumina, is due to very strong interfacial bond between SiC particles and alumina matrix.

Table 5 shows densification, microstructural and mechanical properties of Al_2O_3-SiC nanocomposites sintered using different sintering techniques. Enhancement in properties especially fracture toughness was reported in all cases.

Z. Dheng et al [82] reported an increase of 122% in fracture toughness, 135% in fracture strength, when alumina was reinforced with different fractions of SiC to form Al_2O_3-SiC nanocomposites. Even at temperature of 1200℃, all the Al_2O_3-SiC nanocomposites showed superior fracture toughness and fracture strength as compared to monolithic alumina. These enhancements in properties were attributed to pinning effect of SiC, which changes the fracture mode of alumina matrix from intergranular to transgranular. Alumina-SiC nanocomposites also demonstrated superior creep properties with strain rate 4-8% less than pure alumina.

O. T. Johnson et al [84] reinforced alumina with 3, 10, 30, 50 wt.% SiC and studied the effect on mechanical properties of alumina-SiC nanocomposites. X. L. Shi [30] reported a very high value of 7.6 $MPa.m^{1/2}$ for fracture toughness of Al_2O_3-5wt.%SiC nanocomposite prepared through hot pressing. L. Gao [62] reported a very high bending strength of 1000 MPa for Al_2O_3--5vol% SiC nanocomposite.

Table 5. Densification, microstructural and mechanical properties of Al_2O_3-SiC nanocomposites

Initial Powders Size (μm)	SiC (wt. %)	Sintering process and parameters	Relative Density (% TD)	Matrix Grain size (μm)	Hardness (GPa)	Fracture Toughness ($MPa.m^{1/2}$)	Ref.
Al_2O_3 (5) SiC (0.08) 0.05% MgO	0	CS Cold pressing 300MPa.Heating 1750°C, 4hr	99.4	11.04	12.1	3.05	[42]
	2.5		98.6	6.85	14.1	3.21	
	5		97.8	5.04	15.6	3.59	
	7.5		95.9	4.75	15.9	3.26	
	10		94	3.80	13.9	3.09	
Al_2O_3 (1) SiC (1)	5	HP 1635°C, 25MPa	98.2	4.8	25.2	7.6	[30]
	10		98	3.4	22.6	6	
	15		96.2	2.3	21.0	5	
	20		95.7	1.9	20	4.1	

Table 5. (Continued)

Initial Powders Size (μm)	SiC (wt. %)	Sintering process and parameters	Relative Density (% TD)	Matrix Grain size (μm)	Hardness (GPa)	Fracture Toughness ($MPa.m^{1/2}$)	Ref.
Al_2O_3 SiC	5	SPS:40MPa,5min, 1500°C,200K/min,	99	---	---	2.8	[44]
	20		99			3.6	
Al_2O_3 (0.15) SiC (0.04)	5	HP 1740°C, 30MPa, 1hr	98.7	14	19	5.5	[31]
	10		98.4	0.2	20	6	
	15		98.2	0.17	20.3	5.5	
	20		97.7	0.17	20.5	5.5	
Al_2O_3 (0.15) SiC (0.2)	5		99.4	11	18.5	5.5	
	10		99.4	2	19.5	5.5	
	15		99.5	1	19.7	5.2	
	20		99.4	0.7	20	5.2	

2.5.2 Thermal Properties

It is expected that reinforcement of SiC into alumina matrix will enhance the thermal properties of matrix alumina, especially thermal conductivity, due to its superior thermal properties as shown in Table 1. However, only moderate improvements in thermal conductivity have been reported yet, due to the influence of interfacial barriers, various impurities and defects within the material [85]. Hasselmann et al [86] proposed that the reason for this lower increase in thermal conductivity may be due to the presence of thermal barrier at matrix-reinforcement interface. Table 6 presents some of the reported literature on thermal properties of Al_2O_3-SiC nanocomposite

M. Parchovianský et al [32] reported the effect of SiC reinforcement in alumina matrix, prepared through hot pressing, on thermal properties of matrix. A small decrease in density of nanocomposites was observed, as the volume fraction of SiC increases from 3 to 20%. However, grain size of alumina kept decreasing with increase in content of SiC. The presence of SiC particles at and within grains hindered the grain growth during sintering process. Thermal conductivity and thermal diffusivity were found to be increasing with increasing SiC content and were higher than pure alumina as shown in Figure 5. However, the increase in thermal conductivity was quite lower than expected. Some of the reasons proposed for this low increase in thermal properties are; presence of porosity in composite, thermal barriers at grain-reinforcement interfaces, interfacial imperfections and residual stresses.

Table 6. Thermal properties of Al_2O_3-SiC nanocomposite

Al_2O_3-wt.%SiC nanocomposites	Sintering process and parameters	Relative Density (% TD)	Thermal properties		Ref.
			Thermal Conductivity (W/mK)	Thermal Diffusivity (cm^2/s)	
Al_2O_3- 28% SiC	HP 60min, 1900°C, 50MPa	>99	37	0.134	[85]
Al_2O_3-33.4% SiC			40.9	0.148	
Al_2O_3-38.6% SiC			43.8	0.161	
Al_2O_3-30% SiC	HP: 5MPa, 60min, 1850°C	>99	49.5	0.176	[87]
Al_2O_3-3% SiC	HP 1740°C, 1hr, 30MPa	99.2	30	0.10	[32]
Al_2O_3-5% SiC		98.7	32	0.105	
Al_2O_3-10% SiC		98.2	34	0.117	
Al_2O_3-15% SiC		97.9	37	0.122	
Al_2O_3-20% SiC		97.5	38	0.135	
Al_2O_3-20% SiC	HP: 1850°C	100	34.25	0.079	[88]

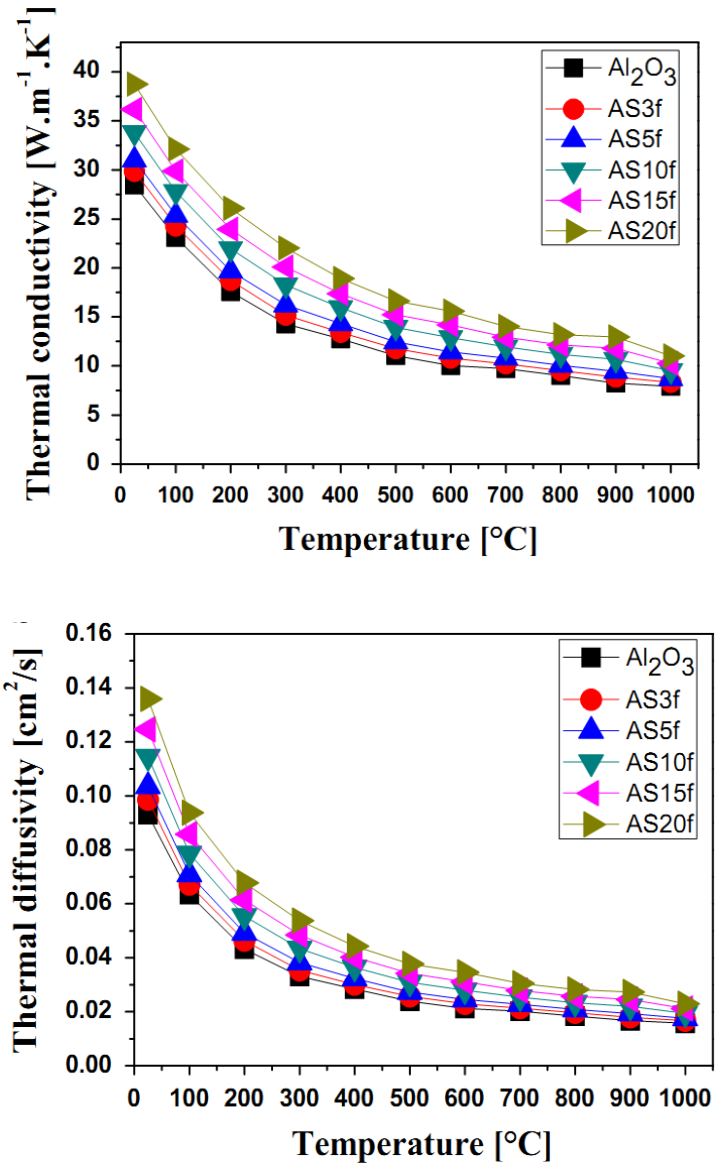

Figure 5. Thermal conductivity and thermal diffusivity curves at different temperatures for different SiC content in alumina (i-e AS3f for 3% SiC, AS5f for 5%SiC, AS10f for 10%SiC, AS15f for 15%SiC, AS20f for 20%SiC) [32]

R. Barea et al [73] studied the effect of varying the content of SiC platelets (0, 12, 20, 30%) on thermal properties of hot pressed Al_2O_3-SiC nanocomposites. Thermal conductivity was found to be increasing with increasing the content of SiC platelets, reaching the value of 43 W/mK for Al_2O_3-30% SiC nanocomposites. Likewise, thermal

diffusivity also increased with increasing SiC content, reaching from 0.092cm^2/s for monolithic alumina to 0.153cm^2/s for Al_2O_3-30% SiC nanocomposites. Both thermal conductivity and thermal diffusivity were found to be decreasing with increase in temperature. Variations in thermal conductivity and thermal diffusivity, with varying SiC content and temperature, are shown in Figure 6.

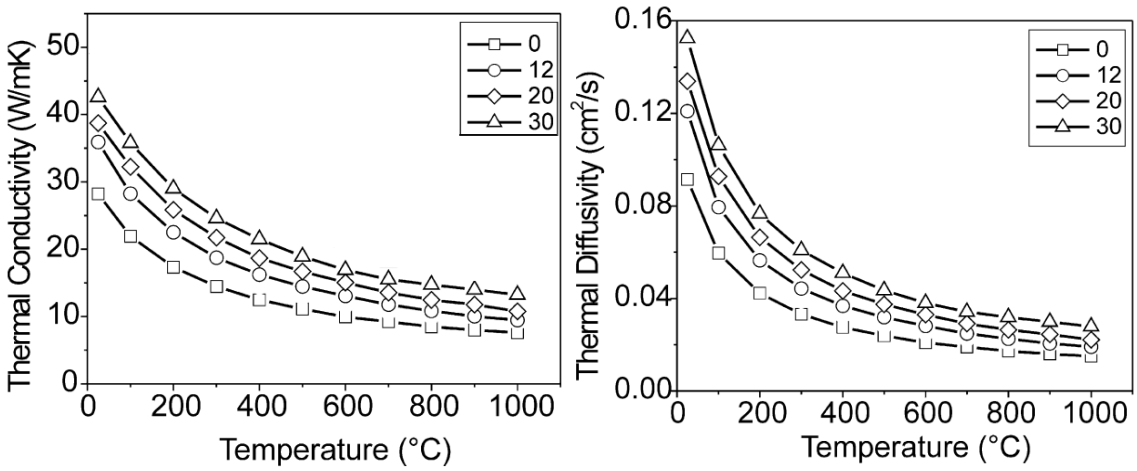

Figure 6. Thermal conductivity and thermal diffusivity for Al_2O_3-SiC nanocomposites with varying SiC content (0, 12, 20, 30) as a function of temperature [73]

2.5.3 Electrical Conductivity

SiC is a semiconductor material having electrical conductivity higher than monolithic alumina, which is electrically insulator, as shown in Table 1. The electrical conduction mechanism in Al_2O_3-SiC nanocomposites is due to the formation of interconnected continuous network of SiC reinforcement in alumina as shown in Figure 7. At particular concentration of reinforcement in matrix, continuous network of conducting or semi-conducting reinforcement is established, called percolation threshold, beyond which electrical conductivity increases drastically [89]. Increasing the electrical conductivity of

alumina increases its technological applications due to the fact that complex shapes can be made through electro-discharge machining (EDM) if resistivity is ≤100cm or electrical conductivity is ≥1 S/m [32, 90].

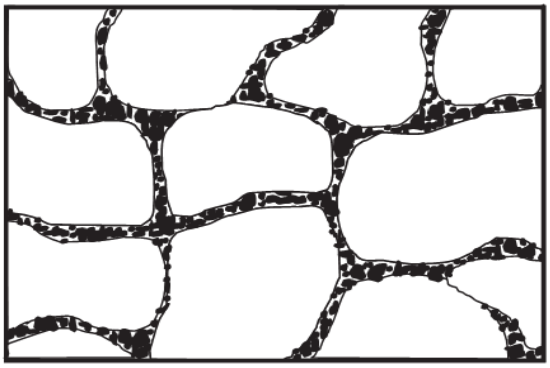

Figure 7. Percolation network of semiconductor reinforcement (SiC) in matrix [91]

M. Parchoviansky et al [32] reported the effect of different particle sizes and content of reinforcement on electrical properties of Al_2O_3-SiC nanocomposites. Fine SiC particles of 40nm and coarse particles of 200nm were reinforced in alumina and hot pressed at 1740°C. Electrical conductivity of Al_2O_3-SiC nanocomposites is shown in Figure 8. Electrical conductivity of pure alumina was reported to be $7.8x10^{-6}$ S/m. No appreciable increase in electrical conductivity was observed initially (SiC vol. fraction <5%). He concluded that continuous network of conducting SiC reinforcement has not achieved yet. However, as SiC crosses 5vol.%, sudden increase in electrical conductivity was observed which was attributed to the establishment of continuous conducting network of SiC reinforcement within alumina matrix grain boundaries, showing the percolation limit to be between 5-10vol.% of SiC. The value of electrical conductivity kept increasing with increase in SiC content and reached a maximum value of $4.05x10^{-2}$ S/m for Al_2O_3-20vol.%SiC nanocomposite with coarse SiC.

A. Borell et al [90] reported the electrical conductivity of Al_2O_3-17vol.%SiC nanocomposites with different particles sizes of alumina and SiC sintered at varying SPS temperatures. He reported range of values between $2.7x10^{-7}$-3.2 S/m for electrical conductivity. He attributed the increase in electrical conductivity to formation of continuous network of conducting SiC at grain boundaries.

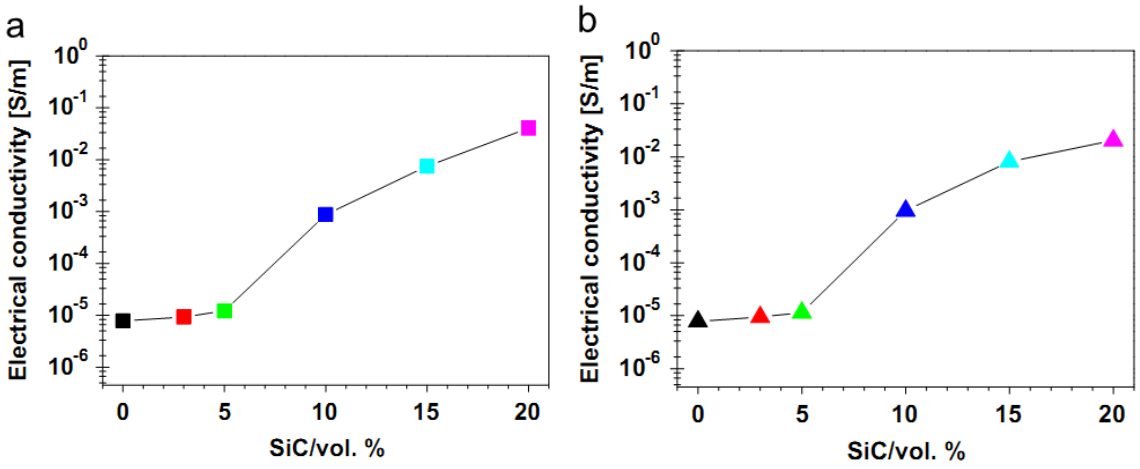

Figure 8. Electrical conductivity of Al_2O_3-SiC nanocomposites with (a) coarse SiC (b) fine SiC [32]

2.6 Al_2O_3-MWCNT Nanocomposites

2.6.1 Densification, Microstructural and Mechanical Properties

Reinforcement of CNTs in alumina matrix not only enhances the fracture toughness but also strength and hardness. Carbon nanotubes, due to their exceptional mechanical, thermal and electrical properties, are one of the best reinforcement materials. Uniform dispersion of CNT into the matrix and interfacial strength between the matrix and reinforcement, are two most important factors which determine the properties of final composite. Different processing routes have been used for preparing Al_2O_3-CNT

nanocomposite powders such as powder processing, colloidal processing, sol-gel processing and electrophoretic dispersion [49]. Then the nanocomposite powders are consolidated using different consolidation techniques such as conventional sintering, hot pressing, spark plasma sintering etc. [37, 45-48].

In Al_2O_3-CNT nanocomposites, presence of carbon nanotubes at grain boundaries of alumina matrix decreases the density of nanocomposite, but at the same time, it also restricts the grain growth of alumina matrix during sintering which results in grain refining [92]. Some of the toughening mechanisms which are proposed to be responsible for increase in mechanical properties are; CNT-pull out from grains of alumina matrix, crack deflection and crack bridging due to presence of CNT's [49, 93]. Some of the reported literature related to microstructural and mechanical properties of Al_2O_3-MWCNT nanocomposites is given in Table 7.

Large amount of work has been done to explore the enhanced microstructural and mechanical properties of Al_2O_3-CNT nanocomposites [13, 29, 49, 94]. Song Bi et al [36] used two powder processing routes, ball milling and hydrothermal crystallization, prior to hot pressing for preparing Al_2O_3-5wt.% CNT nanocomposites. He reported 61.1% and 17.2% increase in fracture toughness and flexural strength of nanocomposites prepared through ball milling and the prominent mechanism responsible for enhancements was found to be pinning effect of carbon nanotubes. While 80.3% and 24.6% increase in fracture toughness and flexural strength was observed in nanocomposites prepared through hydrothermal crystallization and prominent phenomenon responsible for enhancements was found to be pull-out effect of carbon nanotubes.

Table 7. Microstructural and mechanical properties of Al_2O_3-MWCNT nanocomposites

Matrix size (μm)	CNTs wt.%	Sintering process and parameters	Relative Density (%TD)	Matrix grain size (μm)	Hardness (GPa)	Fracture toughness ($MPa.m^{1/2}$)	Ref.
Al_2O_3	1	SPS:1400°C,10min, 60MPa, 100°C/min	99.5	---	24	4.3	[45]
	2		97.3		22.5	4.2	
	3		95		13	3.9	
Al_2O_3 (0.3)	5.7*	SPS: 1150°C, 3min, 50MPa	100	0.2	20	7.9	[57]
	10*		100	0.2	16.1	9.7	
Al_2O_3	2	HP: 60min, 1600°C, 40MPa	99.1	0.4	18	6.8	[46]
	5		96.2	0.3	15	5.8	
Al_2O_3 (0.5)	1	CS. Cold pressing 310MPa, 1500°C, 2hr	99	---	22.3	4.1	[47]
	3		96.5		17.9	3.5	
	5		91.7		12.6	3.6	
Al_2O_3	4*	HP: 60min, 40MPa, 1600°C,	99.2	0.45	18	6.7	[37]
	10*		96.3	0.37	16	5.8	

* CNTs are in vol.%

I. Ahmad et al [37] reported an increase of 94%, 13% and 6.4% in fracture toughness, hardness and strength of Al_2O_3-4vol.% CNT nanocomposites, respectively. He also reported decrease in densification with increasing in the content of CNT. J. Fan et al [48] reported a fracture toughness of 5.5 MPa.$m^{1/2}$ for Al_2O_3-12vol.% CNT nanocomposites, which is 1.8 times higher than monolithic alumina ceramic. K. Ahmad [25] reported 39% increase in fracture toughness for Al_2O_3-5vol.% CNT nanocomposites as compared to monolithic alumina.

2.6.2 Thermal Properties

Because of extraordinary thermal properties of carbon nanotubes, as shown in Table 1, it was expected that reinforcement of CNT in alumina matrix will result in significant enhancements in thermal conductivity of alumina matrix. However, enhancements observed so far in thermal conductivity of Al_2O_3-CNT nanocomposites are far lower than expected [13]. No proper justification is available for this behavior. Few researchers reported marginal increase in thermal properties with CNT reinforcement while some reported decrease in thermal properties as shown in Table 8. Some of the reasons proposed for this behavior were interfacial thermal resistance, agglomeration of CNTs, presence of porosity, defects etc [25, 38, 57, 74].

Guo-Dong et al [57] reported the thermal conductivity and diffusivity for spark plasma sintered nanocomposites containing 10% and 15% CNT's in alumina matrix. Thermal conductivity was found to be decreasing with increase in CNT's content. Thermal diffusivity was found to be decreasing only in traverse direction with increasing CNT's content while no change was observed within in-plane diffusivity. This anisotropic nature

Table 8. Thermal properties of spark plasma sintered Al_2O_3-CNT nanocomposites at room temperature

Al_2O_3-wt.% CNT nanocomposites	SPS parameters	Relative Density (% TD)	Thermal conductivity (W/mK)	Thermal Diffusivity (cm^2/s)	Ref.
Al_2O_3-10% CNT	1200°C/3min	99	11.4	0.04	[57]
Al_2O_3-15% CNT	1150°C/3min	99	7.3	0.02	
Al_2O_3-5% CNT	1450°C/50MPa	98	30.01	0.1	[25]
Al_2O_3-10% CNT	1450°C/50MPa	98	24.03	0.082	
Al_2O_3-1.1% CNT	1400°C, 3min, 50MPa	98.5	27	---	[74]
Al_2O_3-6.4% CNT		95.1	20		
Al_2O_3-10.4%CNT		92	16		

was due to the alignment of CNT ropes at particular angle within nanocomposite. It was proposed that decrease in thermal properties may be due to the presence of large thermal resistive interfaces which causes additional phonon scattering. Another proposed reason for decreased thermal properties was strong tube-tube coupling within nanocomposite which was previously suggested to be responsible for enhancement in mechanical properties. Figure 9 shows the measured thermal diffusivity for pure alumina and

alumina-CNT nanocomposites as a function of temperature. Thermal diffusivity was found to be decreasing with temperature for all the samples.

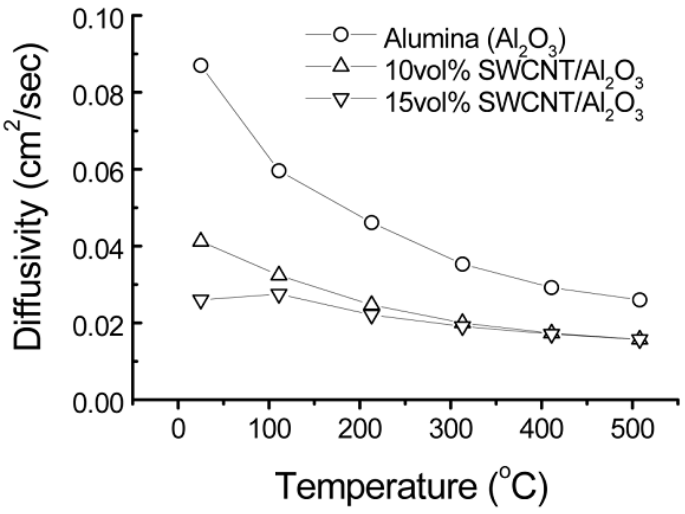

Figure 9. Thermal diffusivity for Al_2O_3 ceramic and Al_2O_3-CNT nanocomposite at different temperatures [57]

L. Kumari et al [38] reported the thermal conductivity, heat capacity and diffusivity of spark plasma sintered alumina-CNT nanocomposite. Figure 10 shows thermal diffusivity, thermal conductivity and heat capacity of various sintered samples at room and elevated temperatures. Thermal diffusivity was found to be dependent on density of nanocomposites. Those nanocomposites having high density (i-e 7.39% CNT sintered at 1550°C and 1450°C have relative densities 82.5% and 79.1%) showed better thermal diffusivity than pure alumina and other lower dense samples. In general, thermal diffusivity was found to be decreasing with increase in CNT content, as it reduces the density. Heat capacity of all the CNT-reinforced composites was found to be higher than pure alumina. This heat capacity was proposed to be dependent on sintering temperature, CNT content and density of samples. However, the exact mechanism responsible for this

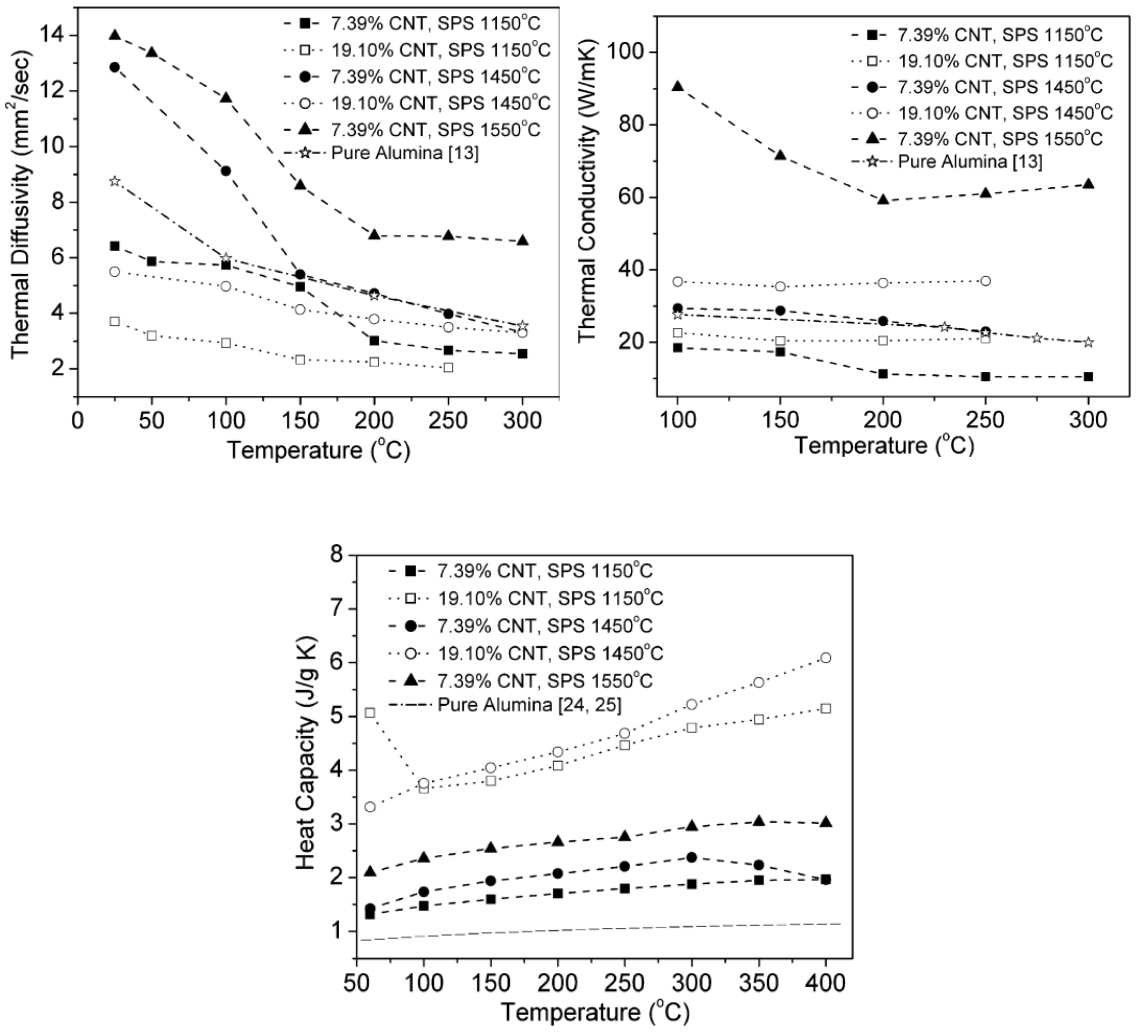

Figure 10. In-plane thermal diffusivity, thermal conductivity and heat capacity of alumina-CNT nanocomposites at different temperatures [38]

increase in heat capacity was unknown. Thermal conductivity of samples having high density was found to be increasing and maximum 90W/mK was observed for 7.39% CNT-alumina nanocomposite sintered at 1550°C and this increase was attributed to homogenous dispersion of CNTs in alumina matrix. It was proposed that high thermal resistance between CNT/CNT and CNT/matrix interfaces may be the reason for lower thermal conductivity.

Kaleem Ahmed et al [74] studied the densification and thermal conductivity of various alumina-CNT nanocomposites. It was observed that the density of nanocomposites decreases with increase in CNT content. Figure 11 shows the thermal conductivity of alumina-CNT nanocomposite having different percentage of CNT content over a range of temperature. Thermal conductivity was also found to be decreasing with increase in CNT content. Some of the reasons proposed for this decrease in thermal conductivity with increase in CNT content are; agglomeration of CNT's, interfacial resistance, inherent defects within carbon nanotubes and defects which are induced in carbon nanotubes during sintering.

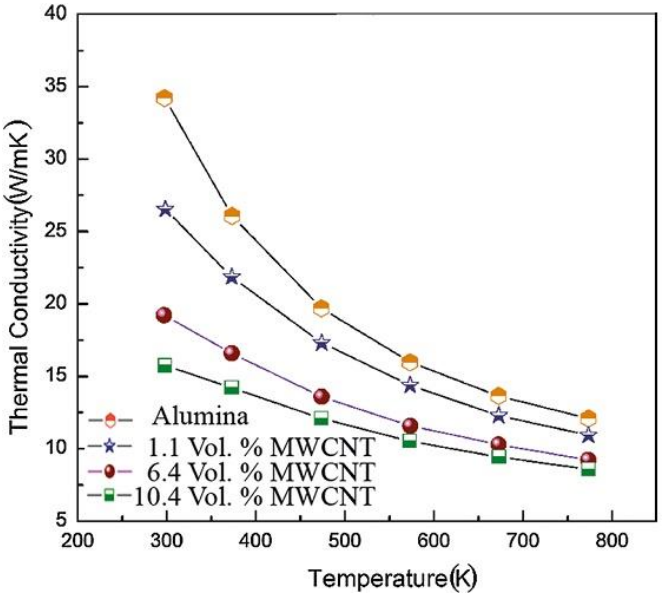

Figure 11. Thermal conductivity of alumina-CNT nanocomposites with varying temperature [74]

2.6.3 Electrical Conductivity

Electrical conductivity values of alumina and carbon nanotubes are presented in Table 1. Researchers have tried to improve the electrical conductivity of alumina by reinforcing it with different content of CNTs. It was observed that electrical conductivity of Al_2O_3-CNT nanocomposites increased drastically when the concentration of CNT reinforcement exceeds certain limit called percolation threshold [13]. This drastic increase in electrical conductivity was due to the formation of continuous network of conducting CNTs within grain boundaries of alumina matrix.

Different researchers have reported different levels of improvement in electrical conductivity as shown in Table 9. K. Ahmad et al [95] reported the effect of addition of different content (0.3-6wt.%) of CNT into alumina matrix using SPS. Author reported the percolation limit of reinforcement to be around 0.45wt.%CNT, after which electrical conductivity of Al_2O_3-CNT nanocomposites showed dramatic increase. The value of electrical conductivity kept on increasing and reached to a maximum value of 3 S/m for Al_2O_3-6wt.%CNT nanocomposite. K. Ahmad et al [77], in another study, reported the percolation limit of CNT reinforcement in alumina matrix to be 0.79vol.%. He found the electrical conductivity to be increasing with increase in CNT content, as shown in Figure 12. Zhan et al [57] reported increase in electrical conductivity of spark plasma sintered Al_2O_3-SWCNT nanocomposites with increase in SWCNT content. With reinforcement of 15vol.% SWCNT, the value of electrical conductivity reached to 3345 S/m. This increase in electrical conductivity was attributed to high quality SWCNTs used, which form a continuous conducting path on the grain boundaries of alumina. Figure 13 shows the comparison of Al_2O_3-CNT nanocomposites with other materials on electrical

conductivity scale. Transition of alumina can be seen, from being electrically insulator to semiconductor, just by reinforcing 15vol.% of SWCNTs.

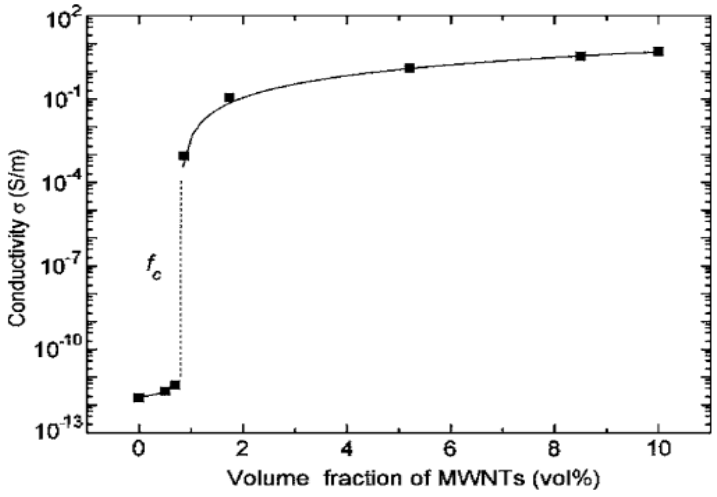

Figure 12. Electrical conductivity of Al_2O_3-CNT nanocomposites with varying CNT content [77]

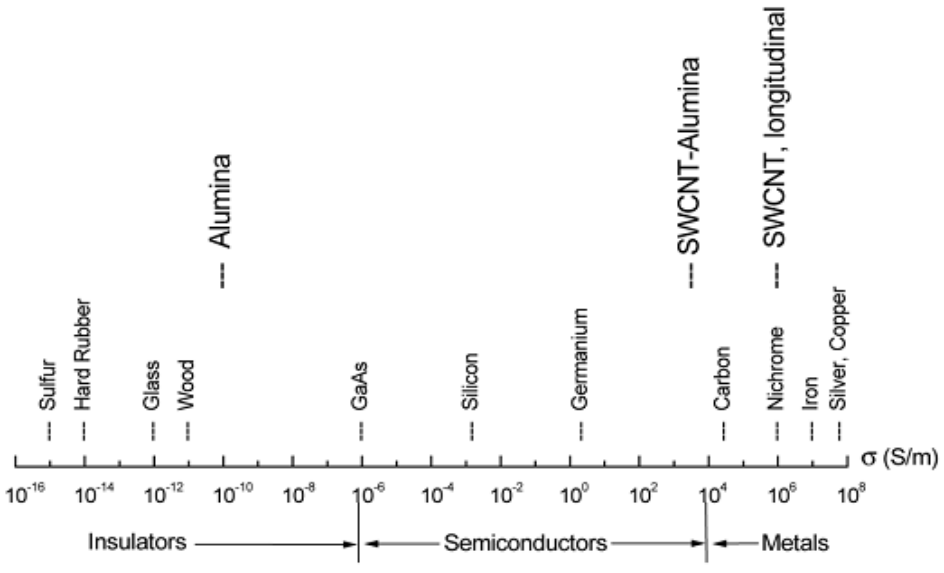

Figure 13. Electrical conductivity of Al_2O_3-15vol.% SWCNT nanocomposite in comparison with various materials [57]

Table 9. Electrical conductivity of Al_2O_3-CNT nanocomposites

Sintering Method	Reinforcement	Electrical Conductivity (S/m)	Ref.
SPS	0.9vol.% MWCNT	1.4	[75]
SPS	1wt.% MWCNT	10^{-1}	[95]
	2wt.% MWCNT	1	
	6wt.% MWCNT	3	
SPS	2vol.% MWCNT	10^{-1}	[77]
	10vol.% MWCNT	8	
SPS	5vol.% MWCNT	1.285	[25]
	10vol.% MWCNT	5	
SPS	2.48wt.% MWCNT	12.2	[96]
SPS	2wt.% MWCNT	125	[56]
	5wt.% MWCNT	576	
SPS	7.39wt.% MWCNT	705	[26]
	19.1wt.% MWCNT	3336	

2.7 Al_2O_3-based Hybrid Nanocomposites

2.7.1 Densification and Mechanical Properties

With the advancement in technology and demand to get better and better materials, researchers have moved from nanocomposites towards hybrid nanocomposites. Hybrid nanocomposites; is a new class of materials in which two reinforcing materials are added to a matrix, in order to get combination of properties of all the constituents. Alumina ceramic due to its high strength, low density, high rigidity, high temperature stability and chemical inertness provides a comparative advantage for being used as a matrix [97]. These alumina based hybrid nanocomposites are supposed to have potential applications in aerospace industry, defense industry, body parts in railway trains, space facilities, automotive fuel lines in automotive industry etc [98].

Kaleem et al [39] used the hybrid microstructure design by reinforcing alumina with SiC and multi walled CNTs in order to enhance the properties of alumina ceramic. He reported that using hybrid design increased the fracture toughness and flexure strength without affecting the hardness. The schematic representation of hybrid design presented is shown in Figure 14, where it is shown that reinforcing SiC nanoparticles are present on the grain boundaries and within the grains while multi walled CNTs are present at the grain boundaries. 117% improvement in fracture toughness and 44% improvement in bending strength were reported. Some of the toughening mechanisms proposed for this hybrid microstructure are; toughening due to thermal mismatch between alumina and SiC, strengthening and toughening of grain boundaries and matrix by SiC nanoparticles, strengthening due to removal of undesirable residual stresses from grain boundaries due to SiC nanoparticles, fiber toughening mechanism by dispersion of multi walled CNTs.

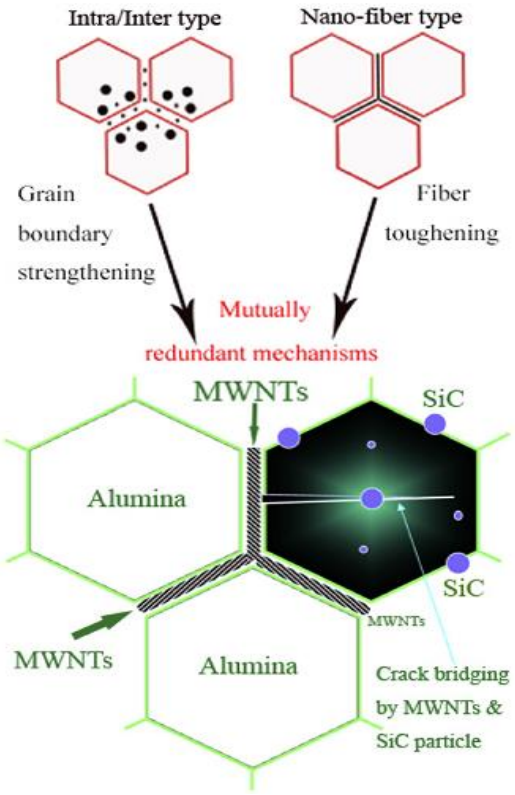

Figure 14. Schematic of hybrid microstructural design for Al_2O_3-SiC-MWCNT hybrid nanocomposites [39]

Table 10 shows some of the reported literature on alumina based hybrid nanocomposites. One advantage of using hybrid design mentioned by each author was; no significant reductions in hardness were observed along with enhancements in fracture toughness and flexure strength, which is in contrast with simple alumina based nanocomposites, where fracture toughness increases on the cost of hardness [39, 98-100].

Table 10. Densification and mechanical properties of alumina based hybrid nanocomposites

Reinforcements in Al_2O_3 matrix (vol %)	Sintering process	Relative density (%)	Hardness (GPa)	Fracture toughness ($MPa.m^{1/2}$)	Flexure strength (MPa)	Ref.
0	SPS 1550°C, 50MPa	99.5	17	3.3	350	[39]
5%CNT+1%SiC		98.2	16.5	6.5	480	
7%CNT+1%SiC		97.2	16	7	460	
10%CNT+1%SiC		95.1	15	5.5	455	
1%SiC+5%CNT	SPS 1550°C, 50MPa	98	16.5	6.5	500	[98]
3%SiC+5%CNT		96.46	16	6.2	450	
5%SiC+5%CNT		96.40	16	6	450	
0	HP 1750°C 1hr,30MPa	100	17.7	2.5	450	[99]
0.1%CNT+25%SiC*		99.8	20.5	4.3	720	
0.5%CNT+25%SiC*		99.3	20.3	4	680	
1%CNT+25%SiC*		99.2	19.8	3.5	650	

*SiC is in whiskers form

Table 10. (Continued)

Reinforcements in Al_2O_3 matrix (vol %)	Sintering process	Relative density (%)	Hardness (GPa)	Fracture toughness ($MPa.m^{1/2}$)	Flexure strength (MPa)	Ref.
0	SPS 50MPa, 1500°C, 3min	100	18.04	3.41	400	[100]
1%SiC+0.38%GPL*		99.03	21.34	4.77	572	
3%SiC+0.38%GPL		98.85	24.68	5.03	520	
5%SiC+0.38%GPL		97.35	21.58	4.94	535	

*GPL is for graphene platelets

D. Y Lee et al [99] prepared the hybrid nanocomposites by reinforcing alumina with 25wt.% SiC whiskers and varying content (0.1, 0.5 and 1wt.%) of MWCNT using hot pressing. He reported densification greater than 99% for all the compositions. Enhancements of greater than 60% in fracture toughness and flexural strength were observed in all Al_2O_3-SiCw-CNT hybrid nanocomposites. N. Saheb et al [41] prepared different Al_2O_3-SiC-CNT hybrid nanocomposites using spark plasma sintering. A density of greater than 98% was reported for all compositions. Improvements of upto 93.95% in fracture toughness and 12.12% in hardness were reported. J. Liu et al [100] reported enhancements of 36% in hardness, 40% in flexural strength and 50% in fracture toughness by preparing the hybrid nanocomposites of Al_2O_3-SiC-GPL (graphene platelets) through spark plasma sintering. He reported that crack bridging, carbon

nanotubes pullout and deflection of crack by reinforcements were responsible for enhancements in hybrid nanocomposites.

2.7.2 Thermal Properties

Thermal properties of alumina based hybrid nanocomposites, in spite of their importance, have not yet been explored by researchers. These alumina based hybrid nanocomposites are developed for high temperature and extreme condition applications, where the thermal behavior of these nanocomposites become as much important as mechanical behavior. However, not enough literature is available on thermal properties of alumina reinforced hybrid nanomaterials.

Kaleem et al [98] reported the thermal conductivity behavior of Al_2O_3 based hybrid nanocomposites reinforced with multi-walled CNTs and SiC nanoparticles. The density was found to be decreasing with increase in content of reinforcement. The thermal conductivity of hybrid composites was lower than pure alumina ceramic at all the temperatures as shown in Figure 15. Some of the reasons proposed for this lower conductivity in hybrid nanocomposites are; low thermal conductivity of multi walled CNT ropes as the thermal resistance between two nanotubes decreases the thermal conductivity drastically, interfacial thermal resistance between matrix and reinforcements, Kapitza resistance produced due to extra scattering of phonons because of multi walled CNT/SiC reinforcements.

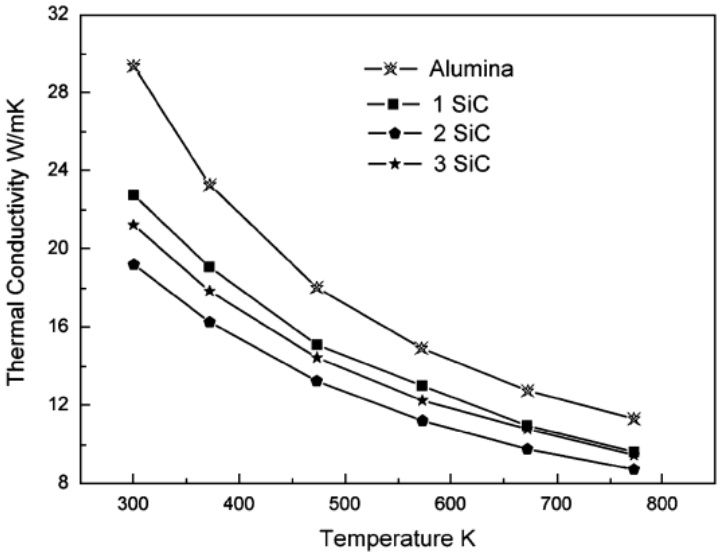

Figure 15. Thermal conductivity of alumina based hybrid nanocomposite reinforced with 5% multi walled CNTs along with varying amount (1, 2, 3%) of SiC nanoparticles [98]

2.7.3 Electrical Conductivity

Researchers have tried to improve the mechanical properties of alumina ceramic using hybrid filler but not enough work is available on electrical properties of alumina reinforced with hybrid filler. K. Ahmad et al [98] studied the electrical properties of alumina when reinforced with 5vol.% CNTs along with varying content (1, 2, 3vol.%) of SiC, prepared using SPS. He observed the dramatic increase in electrical conductivity of alumina with increase in reinforcement content, reaching the maximum value of 9 S/m for Al_2O_3-3vol.%SiC-5vol.%CNT nanocomposite. Figure 16 shows the variation in electrical conductivity of Al_2O_3-SiC-CNT hybrid nanocomposites with varying CNT content. He attributed this increase in electrical conductivity to interconnected continuous conductive path formed between the alumina grains by both CNTs and SiC.

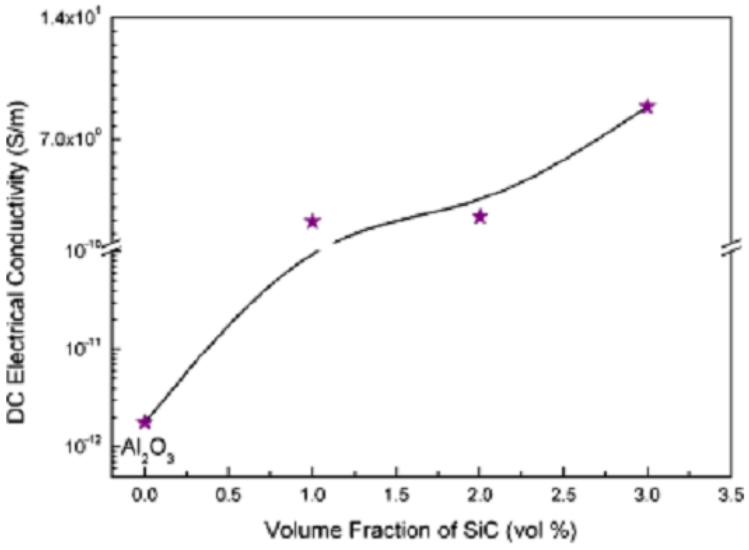

Figure 16. Electrical conductivity variation of Al_2O_3-SiC-CNT hybrid nanocomposites with varying SiC content while CNTs are 5vol.% [98]

CHAPTER 3

MATERIALS AND EXPERIMENTAL PROCEDURE

3.1 Introduction

This chapter contains the detailed information about materials, equipment and the experimental procedure used in this research. Magnetic stirring, ultrasonication and ball milling were used to ensure homogeneous dispersion. SPS parameters were optimized using alumina ceramic. Those optimized parameters were then used for sintering of hybrid nanocomposites. Microstructural analysis was done using FE-SEM and TEM. XRD was used for crystallite size calculation. Thermal properties were determined by Thermal Constants Analyser.

3.2 Materials

α-Al_2O_3 powder having an average particle size of 150nm (99.85% purity) supplied by ChemPUR Germany and β-SiC powder having particle size of 45-55nm, having 97.5% purity and supplied by Nanostructured and Amorphous Materials were used in this investigation. Locally synthesized functionalized CNTs were also used.

CNTs are usually in form of agglomerated bundles and difficult to disperse. Functionalizing the CNTs changes the surface chemistry of CNTs, resulting in impurities

removal such as catalytic remnants, addition of hydroxyl (-OH) or carboxyl (-COOH) group for bonding with matrix and significantly high level of dispersion in water [53]. This addition of oxygen-containing species on the surface of CNTs promotes their solubility in aqueous or organic solvents and decreases the van der Waals associations between different CNTs, enhancing the dissociation of nanotube bundles into individual tubes.

3.3 Experimental Procedure

3.3.1 Powder Preparation

Four different compositions of nanocomposite powders used in this study are; Al_2O_3-5wt.%SiC-1wt.%CNT, Al_2O_3-5wt.%SiC-2wt.%CNT, Al_2O_3-10wt.%SiC-1wt.%CNT and Al_2O_3-10wt.%SiC-2wt.%CNT designated as Al_2O_3-5SiC-1CNT, Al_2O_3-5SiC-2CNT, Al_2O_3-10SiC-1CNT and Al_2O_3-10SiC-2CNT, respectively. These nanocomposite powders were prepared through magnetic stirring, sonication and ball milling. The experimental procedure adopted for preparation of powders is shown in Figure 17.

To prepare each nanocomposite powder, the required amount of alumina and SiC powders were added to deionized water and magnetically stirred for 15 minutes. The slurry was then further ultrasonicated for 2 hours using high energy probe sonicator. The sonicated slurry was charged into cylindrical alumina vials (250ml in volume) along with alumina balls (10mm in diameter). A ball-to-powder weight ratio used was 4:1. A planetary ball mill (Fritsch Pulverisette Equipment P5, Germany) was used to mill the mixture for 2 hours. The milling experiments were done at room temperature, at a speed of 100 rpm. Then, required amount of functionalized CNTs, separately ultrasonicated for

15mins, were added to the ball-milled slurry and further sonicated for 2 hours using a high energy probe sonicator. The mixture was then dried in an oven at 120ºC for 15 hours.

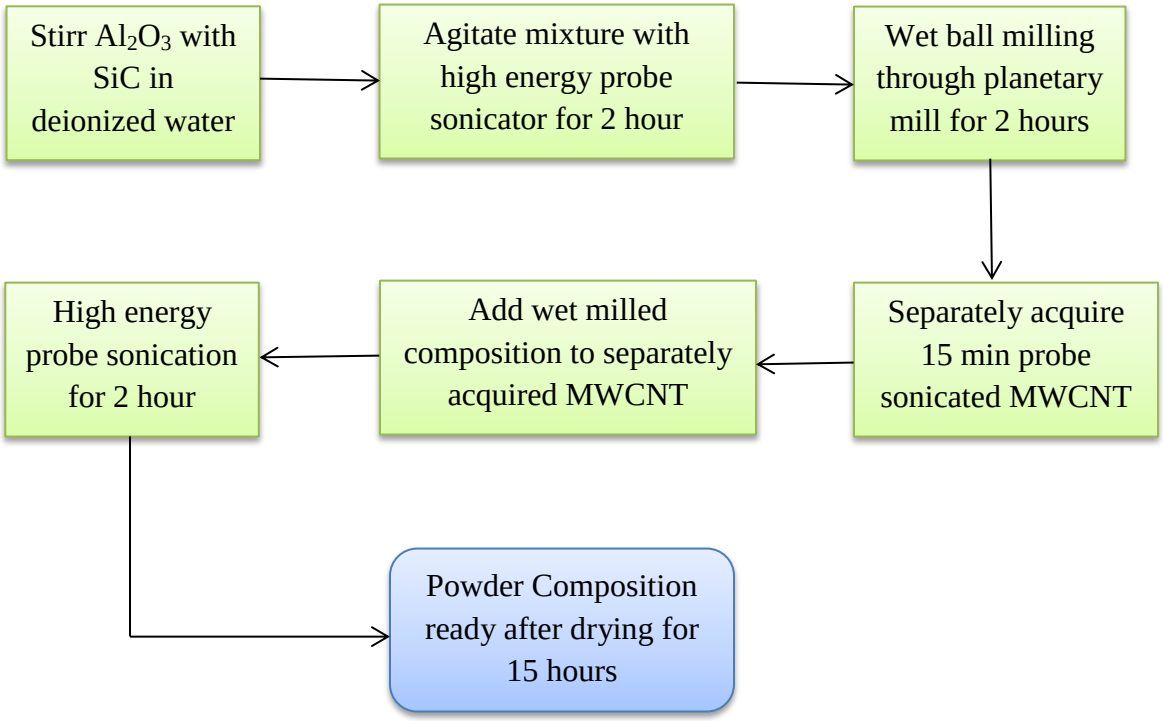

Figure 17. Flow chart showing powder preparation steps

3.3.2 Consolidation of Powders through Spark Plasma Sintering

In this thesis work, consolidation of powders was done in two steps. First, the SPS parameters were optimized using monolithic alumina. Then, those optimized parameters were used for the consolidation of hybrid nanocomposite powders.

Alumina powders were directly loaded into 30mm graphite die. Fully automated spark plasma sintering equipment (FCT system, Model HDP 5, Germany) was used. The pressure during the sintering process (i-e during heating and holding time) was kept at 50MPa and heating rate at 100℃/min. Samples were sintered in vacuum using

temperature range of 1000℃-1400°C, for varying holding times of 1-10 minutes. A thermocouple, which was inserted in the graphite die through a drilled hole, was used to measure sintering temperature. In order to reduce the friction between die and powders and to make the ejection of sample after sintering easy, a graphite sheet was used.

Almost full densification was achieved at 1400℃ and 10 minutes for alumina ceramic. However, as the addition of reinforcement reduces the densification of matrix, so a higher temperature of 1500℃ was selected for hybrid nanocomposite powders. The other parameters i-e pressure 50MPa, heating rate 100℃/min and time 10 minutes were kept constant in case of hybrid nanocomposites. For comparison, monolithic alumina was also sintered at the same sintering conditions as that of hybrid nanocomposites.

3.3.3 Density Measurement

Density of spark plasma sintered samples was measured using Metler Toledo balance density determination KIT model AG285 which uses Archimedes principle. This method for density measurement is used when porosity of samples is lower [9], i-e density>92%. However, if porosity of samples is high, then the density can be measured by measuring the mass of sample and dividing that mass with volume of sample. Some monolithic alumina samples sintered at lower temperatures showed high porosity, so this method of mass divided by volume was used for their density determination.

Theoretical density of 3.97g/cm^3 for alumina, 3.21g/cm^3 for SiC and 2g/cm^3 for CNTs was used. In case of hybrid nanocomposites, theoretical density was calculated using rule of mixtures. The relative density was determined by dividing measured density by theoretical density.

3.3.4 XRD Analysis

A high resolution X-ray Diffractometer (Model Bruker D8, USA, having a wavelength λ = 0.15405 nm) was used for recording XRD patterns of the milled powders and sintered samples. XRD was also used to analyze the powders in order to detect any possible new undesirable phase formed during sintering. The crystallite size of the monolithic alumina powder and sintered samples was calculated using the Scherrer equation [101]:

$$t = \frac{0.94\,\lambda}{\mathrm{B}\cos\theta} \tag{3.1}$$

Where t is the crystallite size, λ = 0.15405 nm for XRD, B is the peak broadening which is measured from XRD diffraction pattern, θ is angle at which peak appeared.

3.3.5 Field Emission Scanning Electron Microscopy (FE-SEM)

A Tescan Lyra-3 Field Emission Scanning Electron Microscope (FE-SEM) having Energy Dispersive X-ray Spectroscopy (EDS) facility was used for characterization of the powders and bulk samples. The microstructures of powders and sintered samples were studied using FE-SEM. EDS analysis was done to confirm that no new phase formed during the sintering process. X-ray mapping was used to confirm the homogeneous dispersion of reinforcements in matrix.

Prior to FE-SEM analysis, samples were gold plated for 30 seconds, in order to eliminate the possibility of charging effects during FE-SEM analysis.

3.3.6 Transmission Electron Microscopy (TEM)

Transmission electron microscopy (TEM) of the as-received powders was done using TEM (Machine Model: JEM-2100F, JEOL company, Japan).

3.3.7 Thermal Constants Analyzer

Thermal constants analyser (Hotdisk TPS 2500S) was used to measure the thermal conductivity, diffusivity and heat capacity of alumina powder, sintered alumina and sintered hybrid nanocomposites at room temperature and at elevated temperatures upto 250℃. This equipment uses transient plane source theory for measurement of properties and is in accordance with ISO 22007-2 standard.

Samples of disc shape, having 30mm dia. and 6-8mm thickness, were used for measurement of thermal properties. Each value of reported thermal conductivity, thermal diffusivity and heat capacity is an average of 5 readings.

3.3.8 Electrical Conductivity

Electrical conductivity was measured using two point technique as demonstrated by M.B. Heaney et al [102]. Samples were cut into rectangular shape of length 'l', width 'w' and height 'h'. Ammeter and voltmeter were connected with samples as shown in Figure 18. By applying voltage and measuring current or by applying current and measuring voltage, electrical resistivity was determined using following formula.

$$\rho = \frac{Vwh}{Il} \tag{3.2}$$

where ρ is the electrical resistivity, V is the voltage and I is the current. Electrical conductivity 'σ' can be determined by taking inverse of electrical resistivity as.

$$\sigma = \frac{1}{\rho} \tag{3.3}$$

In case of alumina, 1000volts were applied using calibrator WAVETEK 9105 across the sample and respective current was measured using high resolution digital multimeter Agilent 3458A. However in case of hybrid samples, 1.02mA current was supplied across samples using calibrator WAVETEK 9105 and respective voltages were measured using high resolution digital multimeter Agilent 3458A. These voltages and currents, along with the sample dimensions were used for calculation of electrical conductivity. 10 readings were taken for each sample and average value of electrical conductivity was reported.

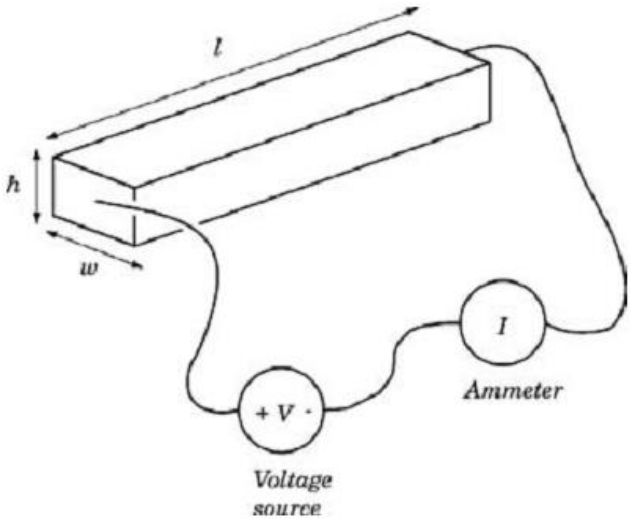

Figure 18. Schematic of two point technique used for measuring electrical conductivity [102]

CHAPTER 4

RESULTS AND DISCUSSION

4.1 Introduction

This chapter contains the results and detailed discussion on characterization of alumina and Al_2O_3-SiC-CNT hybrid nanocomposites. In case of monolithic alumina, characterization results of as-received alumina powder and SPS sintered alumina samples are presented. Effect of different sintering parameters on densification, microstructure and thermal properties of sintered alumina are also discussed in detail. In case of Al_2O_3-SiC-CNT hybrid nanocomposites, characterization results of as-received powders, processed Al_2O_3-SiC-CNT nanocomposite powders, as well as SPS sintered Al_2O_3-SiC-CNT hybrid nanocomposites are presented. Densification, microstructural analysis using FE-SEM and XRD, thermal properties and electrical conductivity of Al_2O_3-SiC-CNT hybrid nanocomposites are also discussed in detail in this chapter.

4.2 Monolithic Alumina

4.2.1 Powder Characterization

4.2.1.1 Microstructure

Figure 19 shows the FE-SEM and TEM images of as-received alumina powder. From the images, we can see that the average grain size of alumina is around 150nm as provided by the Supplier. Figure 20 shows the XRD pattern of as-received powder. Different peaks

of α-alumina are shown in the figure. The crystallite size (sub-grain size) of alumina was calculated using Scherrer Equation and came out to be 27.5nm.

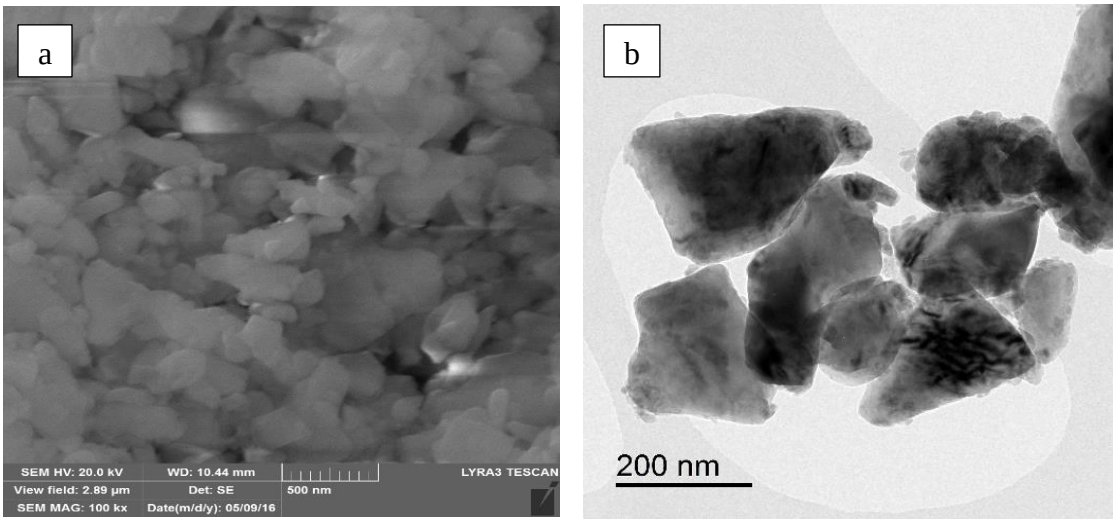

Figure 19. (a) FE-SEM (b) TEM image of as-received alumina powder

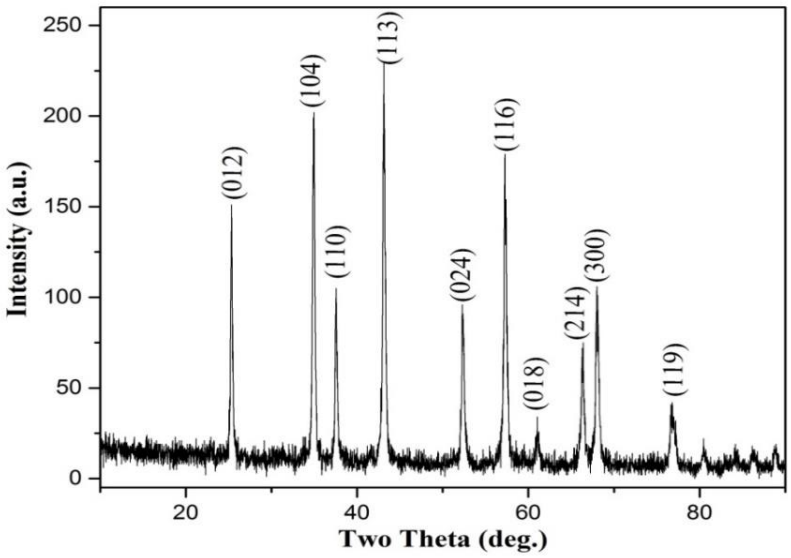

Figure 20. XRD pattern of as-received alumina powder

4.2.1.2 Thermal Properties

The thermal properties of alumina powder, measured using Thermal Constants Analyser at room temperature and elevated temperatures, are shown in Figure 21. Alumina powder showed very low thermal conductivity, diffusivity and heat capacity of 0.153W/mK, 0.15mm^2/s and 1.03 J/gK, respectively, at room temperature.

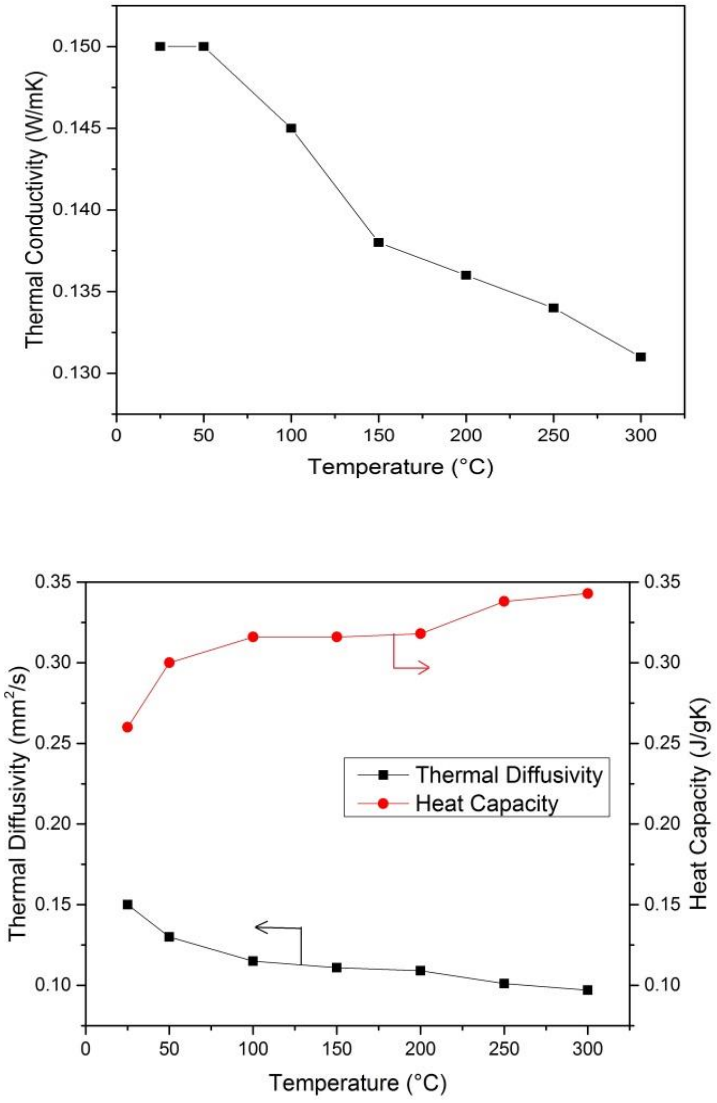

Figure 21. Thermal conductivity, diffusivity and heat capacity of monolithic alumina powder

These lower values for thermal properties are attributed to the presence of large amount of porosity in alumina powder and absence of bonding between powder particles. Thermal conductivity of ceramics is mainly due to the lattice vibrations called phonons. These phonons are scattered by defects and porosity, resulting in lower thermal conductivity. In case of alumina powder, where a large amount of porosity is present, the phonons undergo large scatterings which resulted in such lower thermal conductivity value. Thermal conductivity of powder was found to be decreasing with increase in temperature and reached a value of 0.13W/mK at 300℃.

Thermal diffusivity of powder was also affected by these pores and showed a conventional decreasing trend with increase in temperature, reaching to a very low value of 0.096mm^2/s at 300℃. Heat capacity was found to be increased from 1.03J/gK at 25℃ to 1.37J/gK at 300℃.

4.2.2 Spark Plasma Sintered Alumina

Table 11 shows the densification, crystallite size and thermal properties of spark plasma sintered alumina at different sintering conditions. Thermal properties reported in Table 11 were measured at room temperature.

Table 11. Densification, crystallite size and thermal properties of spark plasma sintered alumina

SPS Conditions		Relative Density (% TD)	Average crystallite size (nm)	Thermal Characterization (room temp.)		
Temp. (°C)	Time (min)			Thermal Conductivity (W/mK)	Thermal Diffusivity (mm^2/s)	Heat Capacity (J/gK)
1000	1	60.5	69	5.29	2.6	0.84
1000	5	62.5	72.74	6	2.95	0.83
1000	10	66.5	66.2	7.24	3.15	0.87
1300	1	98.5	84	30.6	7.18	1.13
1300	5	99	115	31.37	7.32	1.14
1300	10	99.1	98	31.72	7.52	1.15
1400	1	99.2	122.5	32.23	7.56	1.15
1400	5	99.3	127.3	33.84	7.59	1.20
1400	10	99.6	119.3	34.44	7.62	1.22

4.2.3 Densification

Figure 22 shows the density of spark plasma sintered alumina at different sintering temperatures and at different holding times. The relative densities of sintered specimen were found to be increasing with increase in sintering temperature and holding time. At 1000°C, 60.5% relative density was observed which increased upto 66.5% with the increase in holding time upto 10 minutes. When the temperature was increased to 1300°C, even at 1 minute, almost fully dense specimen (98.5% relative density) was achieved. Higher sintering temperatures and larger holding times enhance the grain boundary diffusion, which results in higher relative densities. Further increase in sintering temperature or holding time resulted in very small increase in density and the highest relative density of 99.6% was achieved at 1400°C for 10min holding time.

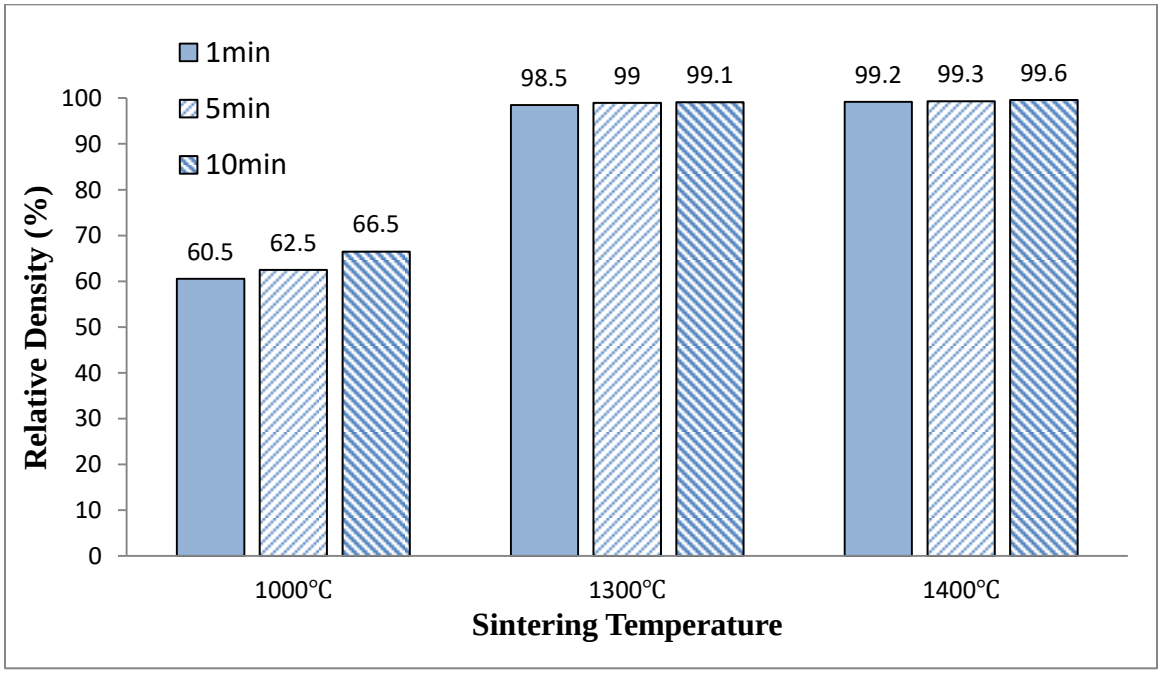

Figure 22. Relative density of alumina at varying sintering temperatures and holding times

It was observed that the rate of densification was faster initially, i-e relative density increased from 60.5% to 66.5% at 1000℃, when the holding time increased from 1 to 10 minutes. However, this rate of increase in relative density became significantly less at 1300℃ and 1400℃, as the relative density increased from 98.5% (at 1300℃, 1min) to 99.6% (at 1400℃, 10min). This is due to the fact that during initial stages of sintering at relatively lower temperatures, grain growth mechanisms are not fully active and hence densification progresses only by closing the pores present between alumina particles by the process of necking. Because of presence of large pores in powder, rate of densification is relatively fast in initial stages. However, during later stage at higher temperatures, when the necking process reaches its maximum point, different grain growth mechanisms like grain boundary diffusion and grain boundary migration becomes active and become rate determining phenomenon for the densification. That's why in our case, after 1300℃ and 1 minute which resulted in relative density of 98.5%, the rate of increase of densification became lower because after that, densification was due to grain boundary diffusion and migration.

J. Gurt et al [9] also reported two different densification regimes which occur during sintering; densification without grain growth and densification with grain growth. He showed the similar results of increasing relative density of alumina with increase in sintering temperature. He reported that fully dense specimen can be obtained even at lower temperature of 1100°C using SPS at a very fast heating rate and at higher pressures. He also proposed that holding time can be used to control the porosity within the sample. Z. Shen et al [10], S. Meng et al [11] and A. Kasperski et al [70] also

reported the same trend of increase in densification with increase in sintering temperature and holding time.

4.2.4 Microstructure

Crystallite sizes of sintered specimen were calculated from XRD diffraction pattern using Scherrer equation. Figure 23 shows the variation in crystallite size with sintering temperature and holding times. Crystallite size increased with increase in temperature from 69nm at 1000℃ to 84nm at 1300℃, and to 122.5nm at 1400℃ for the holding time of 1 minute. Similarly, at 1000℃, crystallite size increased from 69nm to 72.74nm when the holding time increased from 1 to 5 minutes.

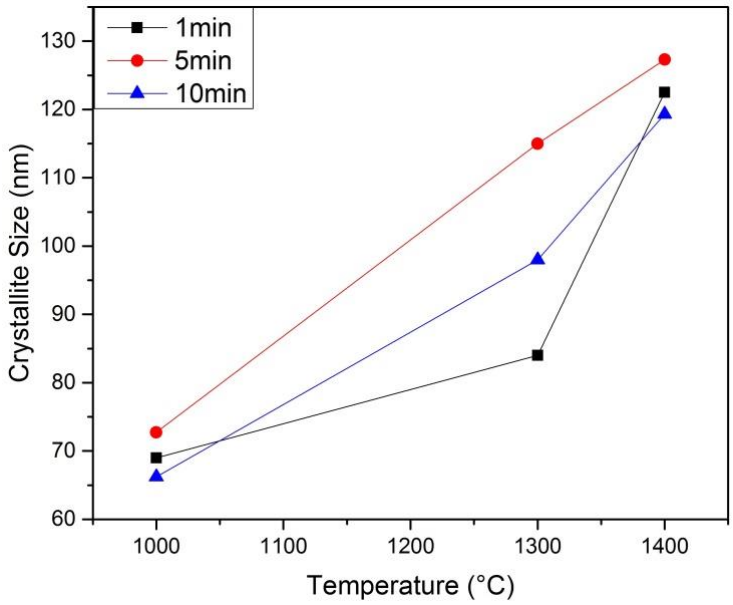

Figure 23. Crystallite sizes of SPS sintered alumina as a function of sintering temperature

For samples sintered at holding time of 1min and 5min, crystallite size showed an increase with increasing temperature and holding time. This behavior is exactly normal as the grain boundary diffusion and migration increases with sintering temperature and time,

which results in higher densification and larger grain growth. However, the samples which were sintered at 10min holding time showed lesser grain growth at all the temperatures as compared to samples sintered at 1min and 5min, but this difference in grain growth is not too large. This may be due to the fact that grain growth is strongly temperature dependent instead of holding time. Therefore it is possible that, at same sintering temperature, increasing holding time may or may not result in grain growth. This can be the possible reason of less grain growth in case of samples sintered for 10 minute holding time at all sintering temperatures.

J. Gurt et al [9] presented somehow similar results in which holding time (when increased from 0 to 5min) did not affect the grain growth, although the densification was increased from 90.8 to 96.8%. He also reported similar results in low densification regime where density increased from 64.4% to 86.1% with increase in holding time from 0 upto 60 minutes, but the grain size remained same. He, therefore, proposed that holding time can be used to control the porosity within samples instead of grain growth. Zhijian et al [10] proposed that grain boundary migration and grain boundary diffusion, which are responsible for grain growth during sintering, are largely dependent on sintering temperature. However, too large holding time may also result in grain growth.

Figure 24 shows the SEM microstructure of fractured surfaces of alumina samples sintered at 1000℃, 1300℃ and 1400℃ for holding time of 10 minutes. Figure 24a shows that at 1000℃, alumina is not fully sintered. Neck regions and pores between the particles can be seen. However, almost fully densified alumina at 1300℃ and 1400℃ can be seen in Figure 24b and 24c. It can also be observed that with increase in sintering temperature, there is an increase in grain size. This increase in grain size is due to the

enhanced grain boundary diffusion and grain boundary migration at higher temperatures, which resulted in grain growth.

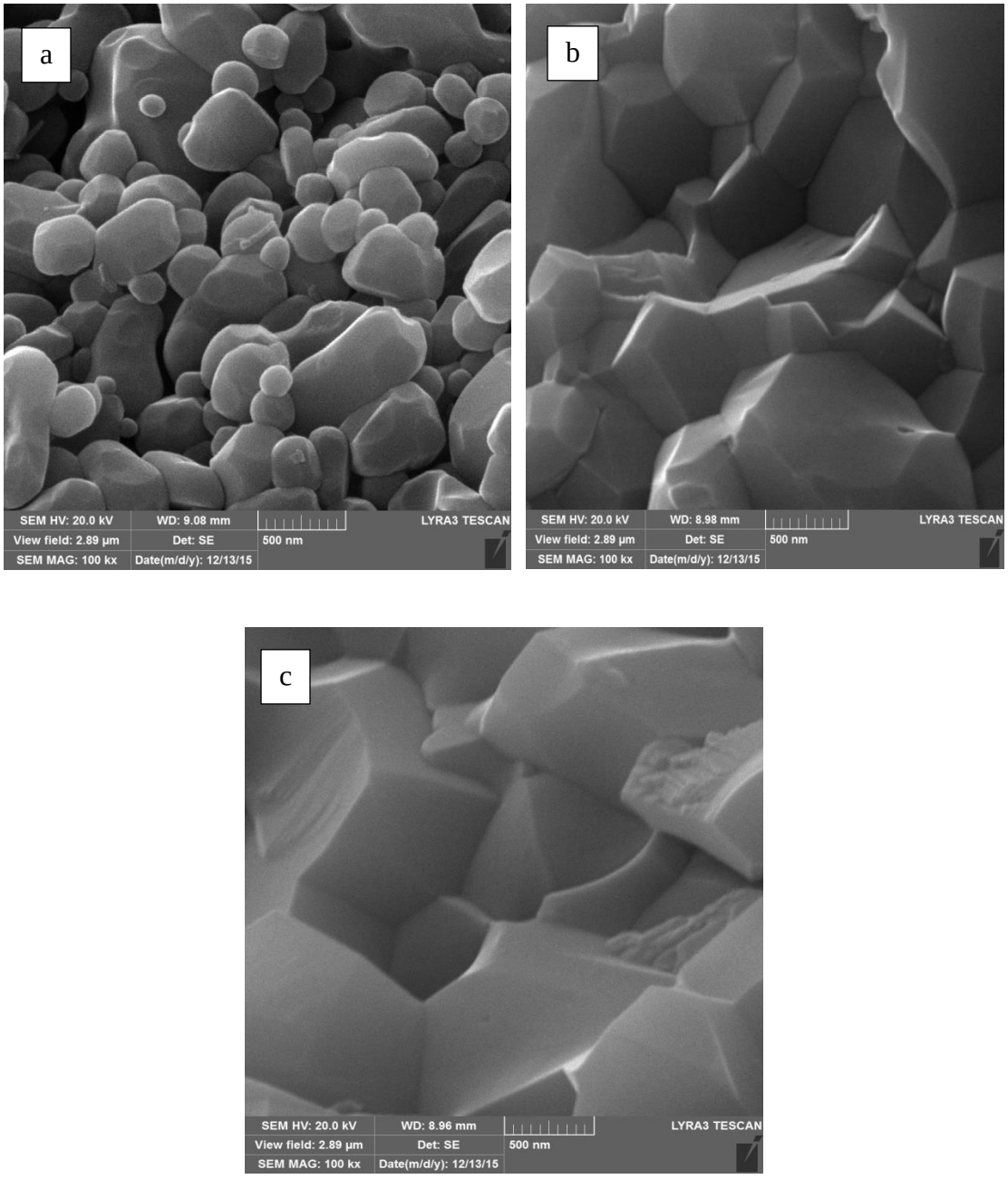

Figure 24. Fractured surfaces of SPS sintered alumina samples for 10 minutes and at (a) 1000°C, (b) 1300°C, (c) 1400°C

4.2.5 Thermal Properties

Thermal properties at room temperature for SPS sintered alumina are presented in Table 11. Detailed discussion on various thermal properties, i-e thermal conductivity, thermal diffusivity and heat capacity is given below.

4.2.5.1 Thermal Conductivity

Figure 25 shows the thermal conductivity of sintered alumina at varying sintering conditions at room temperature. Alumina sintered at 1000℃ for 1 minute holding time showed a very small thermal conductivity value of 5.29 W/mK. However, with the increase in holding time to 10 minutes, this value increased to 7.24 W/mK. When the sintering temperature further increased to 1300℃, this value of thermal conductivity reached to a relatively higher value of 30.6 W/mK for holding time of 1 minute. Increasing the holding time at 1300℃ from 5 to 10 minutes resulted in increase in thermal conductivity from 31.37 to 31.72 W/mK, respectively. This value of thermal conductivity kept on increasing with increasing sintering temperature and sintering time and reached to the highest value of 34.43 W/mK at 1400℃ for holding time of 10 minutes.

Thermal conduction in ceramics is mostly due to lattice vibrations called phonons. These phonons interact with pores, internal defects and scatter in different directions. The scattering of these phonons determine the thermal conductivity of the material. If phonon scattering is high, thermal conductivity of that material will be low and vice versa. Also, the presence of pores within material increases the thermal grain boundary resistance of

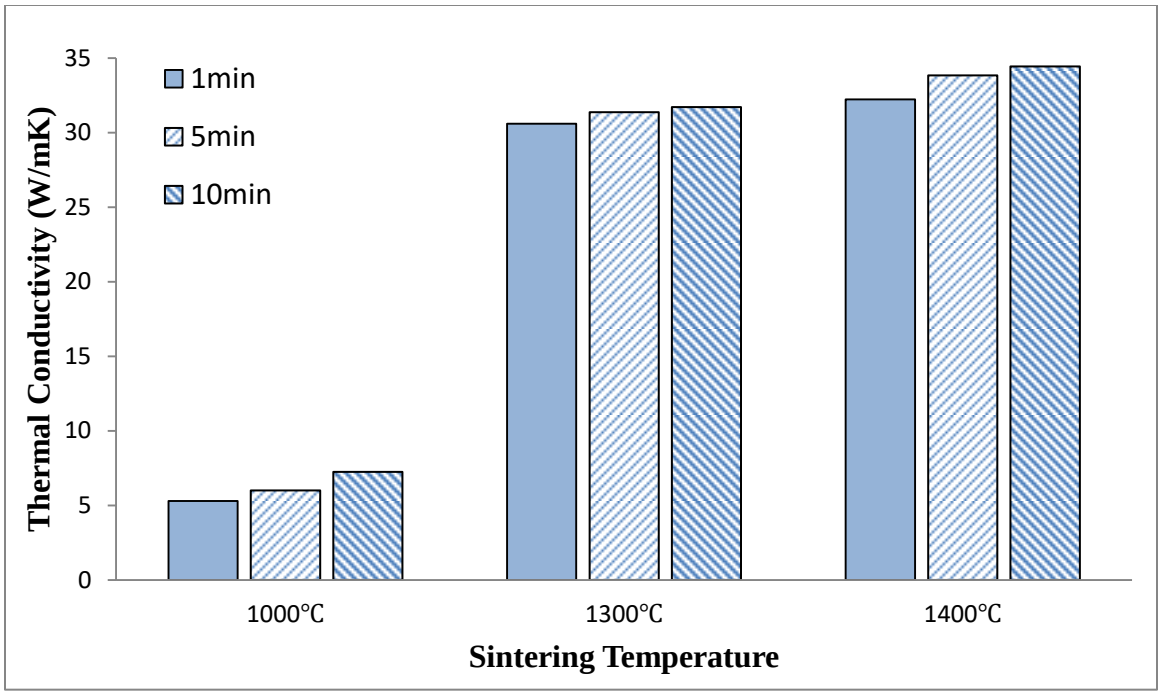

Figure 25. Room temperature thermal conductivity of alumina sintered at different SPS parameters

that material, which induces extra phonons scattering and results in further reduction in thermal conductivity.

The lower thermal conductivity of less dense samples sintered at 1000°C may be due to the extra scattering of phonons induced due to interaction with pores and other interfacial defects present due to impurities. Also, this decrease can also be due to the high thermal grain boundary resistance due to the presence of large porosity (as relative density is in range of 60.5% to 66.5%). David et al [103] calculated and showed that thermal grain boundary resistance in porous alumina materials is larger than in dense alumina materials. He calculated thermal grain boundary resistance value of 1.3×10^{-8} $m^2.K.W^{-1}$ for fully dense alumina and 2.2×10^{-8} $m^2.K.W^{-1}$ for alumina sample having porosity volume fraction of 0.3. He proposed that this increase in thermal grain boundary

resistance in materials having porosity is due to decrease in effective thermal conduction cross-section. This increased thermal boundary resistance in porous materials decreases the thermal conductivity. However, with the increase in density of samples sintered at 1000℃ for 1, 5 and 10 minutes, thermal conductivity was also found to be increasing.

The thermal conductivity of sample sintered at 1300°C, having relative density of 98.5%, reached upto 30.6W/mK. This increase in thermal conductivity can be attributed to higher relative density or less porosity which caused less phonon scattering as compared to lower density samples. The presence of even small amount of porosity affects the phonons scattering, which in turn affects the thermal conductivity. As the sample sintered above 1300°C and 1400°C at various holding times are almost fully dense (>98%) and have very small difference in relative density, yet it affected the thermal conductivity. The phonons scattering is quite sensitive to internal defects and porosity. No significant contribution was observed from crystallite size on thermal conductivity which may be due to fact that the change in crystallite size at different sintering conditions was not so large.

F. R Charvat et al [104] studied the effect of porosity and microstructure on thermal conductivity of single phase ceramic materials. He showed that small amount of porosity and impurities can reduce the thermal conductivity significantly. However, he observed no effect of microstructure of samples on thermal conductivity. He studied dense alumina samples having average grain size of 9 and 12μm, but observed no change in thermal conductivity. Different researchers [57, 74, 105] also reported similar values of thermal conductivity for fully dense samples.

Figure 26 shows the thermal conductivity of spark plasma sintered alumina at different temperatures between 25℃ to 250℃. For all the samples, thermal conductivity was found to be decreasing with increase in temperature. For sample sintered at 1400℃ for 10 minutes, thermal conductivity decreased from 30.44 W/mK at 25℃ to 18.3 W/mK at 250℃. This decrease in thermal conductivity may be due to increased crystal lattice vibrations of atoms at higher temperature, which leads to extra phonon scatterings and resulted in decrease in thermal conductivity.

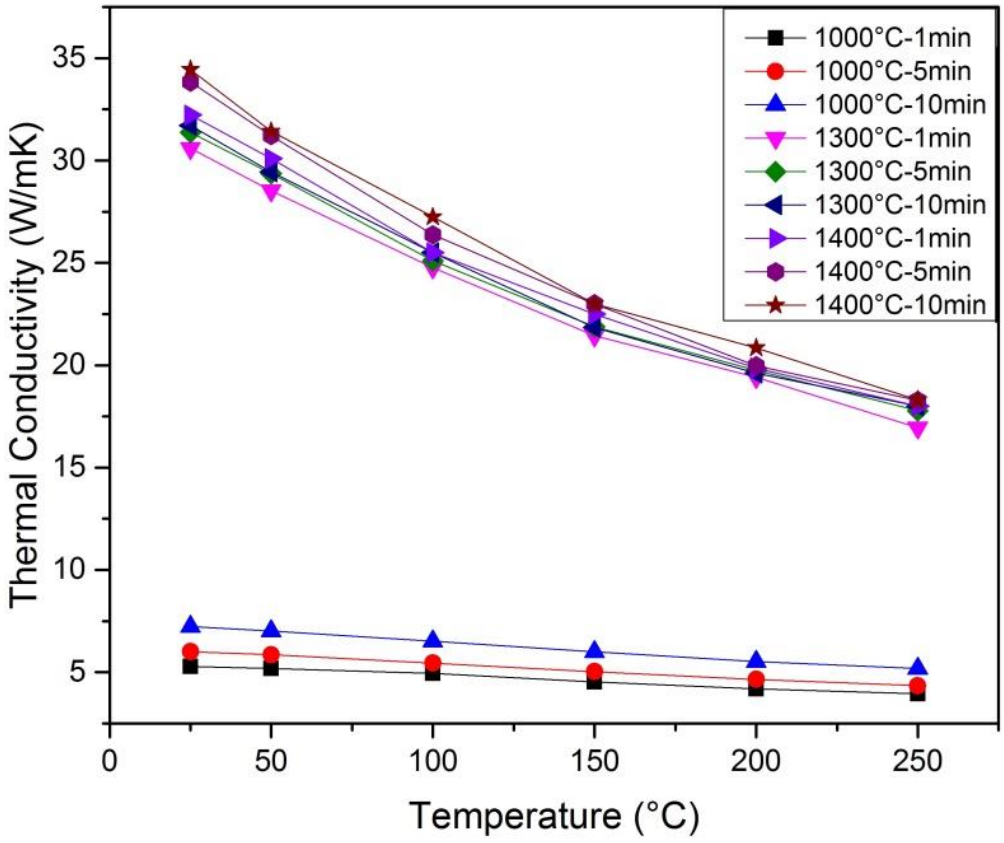

Figure 26. Thermal Conductivity of alumina sintered at different SPS parameters at elevated temperatures

4.2.5.2 Thermal Diffusivity

Room temperature thermal diffusivity of alumina sintered at different sintering temperatures and holding times is shown in Figure 27. Very low thermal diffusivity of 2.6mm^2/s was observed at sintering temperature of 1000℃ for 1 minute holding time. However, with the increase in holding time to 5 and 10 minutes at same 1000℃, thermal diffusivity increased from 2.95 to 3.15mm^2/s, respectively. Increasing the temperature to 1300℃ increased this value to 7.18mm^2/s at the holding time of 1 minute. This value kept on increasing with increase in sintering temperature and holding time, and reached to the maximum value of 7.62mm^2/s at 1400℃ for holding time of 10 minutes.

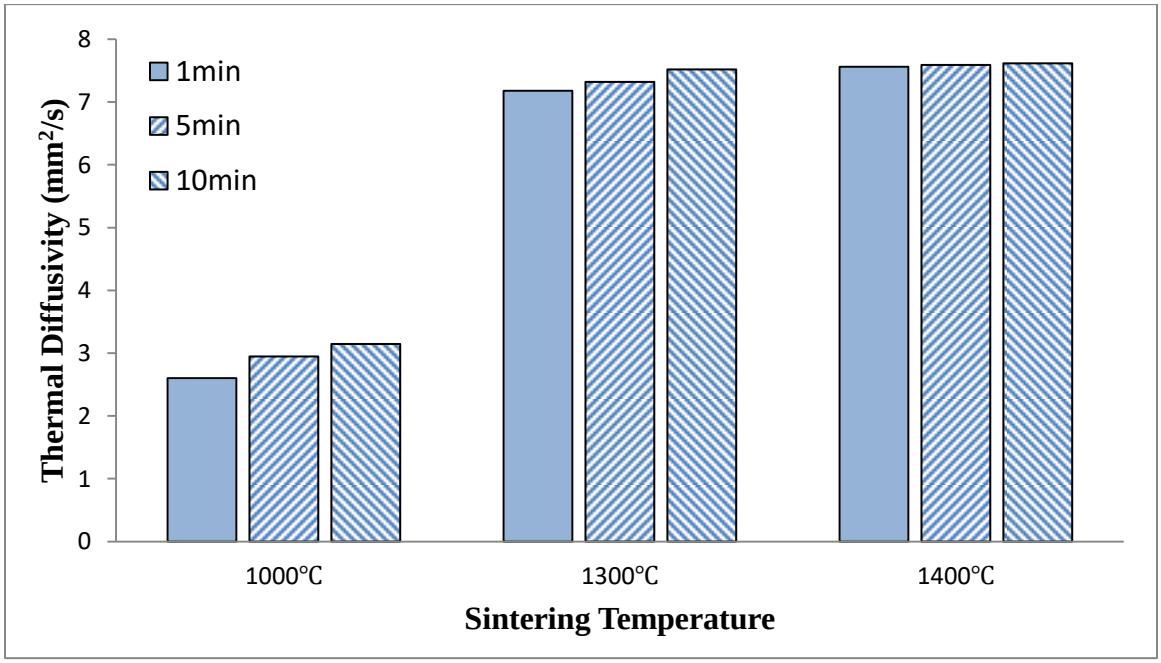

Figure 27. Room temperature thermal diffusivity of alumina sintered at different SPS parameters

Thermal diffusivity defines the rate at which heat travels within the material. Greater the thermal diffusivity, faster will be the heat conduction through materials. Thermal diffusivity is related to thermal conductivity and heat capacity by equation $\alpha = k/\rho C_p$, where α is thermal diffusivity, k is thermal conductivity, ρ is density and C_p is the specific heat capacity. Thermal diffusivity, like thermal conductivity, is dependent on lattice vibrations called phonons in case of ceramic materials. Scattering of the phonons determine the thermal diffusivity. Greater the phonon scattering within the material, lower will be the thermal diffusivity of that material.

The thermal diffusivity of samples sintered at 1000°C was lower than those sintered at higher temperature, i-e at 1300°C and 1400°C. This decrease may be due to the low relative density of samples or due to the presence of high porosity. Presence of large porosity enhanced the scattering of phonons, which resulted in lower thermal diffusivity. As the density kept on increasing from 60.5% to 66.5% with increase in holding time from 1 to 10 minutes at 1000°C, thermal diffusivity also kept on increasing. Similarly, the samples sintered at high sintering temperatures showed higher densities and consequently, higher values of thermal diffusivity. The behavior of thermal diffusivity appears to be same like thermal conductivity. The higher diffusivity of samples sintered at higher sintering temperatures and larger holding times can be attributed to the higher relative densities of these samples and presence of less porosity. L. Kumari et al [38] reported similar values for thermal diffusivity for sintered alumina. He, also, reported the changes in thermal diffusivity to be mainly dependent on density of sintered samples.

Thermal diffusivities were also measured at higher temperatures between 25℃ to 250℃ for all the alumina samples sintered at different SPS conditions and are shown in Figure 28. Decreasing trend of thermal diffusivity with increase in temperature can be observed. Higher temperatures accelerate the crystal lattice vibrations, resulting in enhanced scattering of phonons, which in turn results in decrease in thermal diffusivity. For alumina sintered at 1400℃ for 10 minutes, thermal diffusivity decreased from 7.62mm^2/s to 2.98mm^2/s with increase in temperature from 25 to 250℃, respectively. L Kumari et al [38] also reported the decrease in thermal diffusivity with increase in temperature.

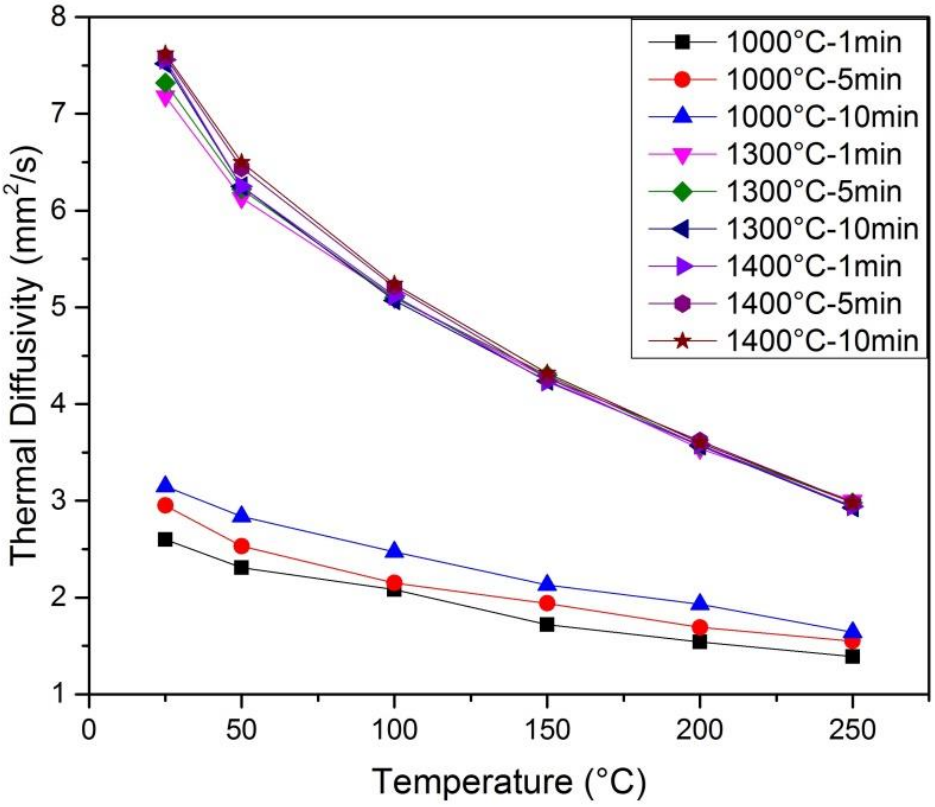

Figure 28. Thermal Diffusivity of alumina sintered at different SPS parameters at elevated temperatures

4.2.5.3 Specific Heat Capacity

Specific heat capacities of alumina samples sintered at varying SPS conditions are shown in Figure 29 at room temperature. At sintering temperature of 1000℃, alumina showed a small value of 0.84J/gK for the sample having holding time of 1 minute. However, increase in holding time resulted in increase in specific heat and the value reaches to 0.87J/gK for sample having holding time of 10 minutes at 1000℃. Increase in temperature to 1300℃ caused the specific heat value to increase upto 1.13J/gK for sample having holding time of 1 minute. This specific heat value kept on increasing, with increase in sintering temperature and holding time, until it reached a maximum value of 1.22J/gK for sample sintered at 1400℃ for 10 minutes. Heat capacity seems to be dependent on various factors like sintering temperature, holding time, density of sample and at the measuring temperature. However, the exact mechanism responsible for this increase in specific heat is still unknown, as stated by L. Kumari et al [38] as well. He, also, reported similar values of heat capacity for fully sintered alumina samples.

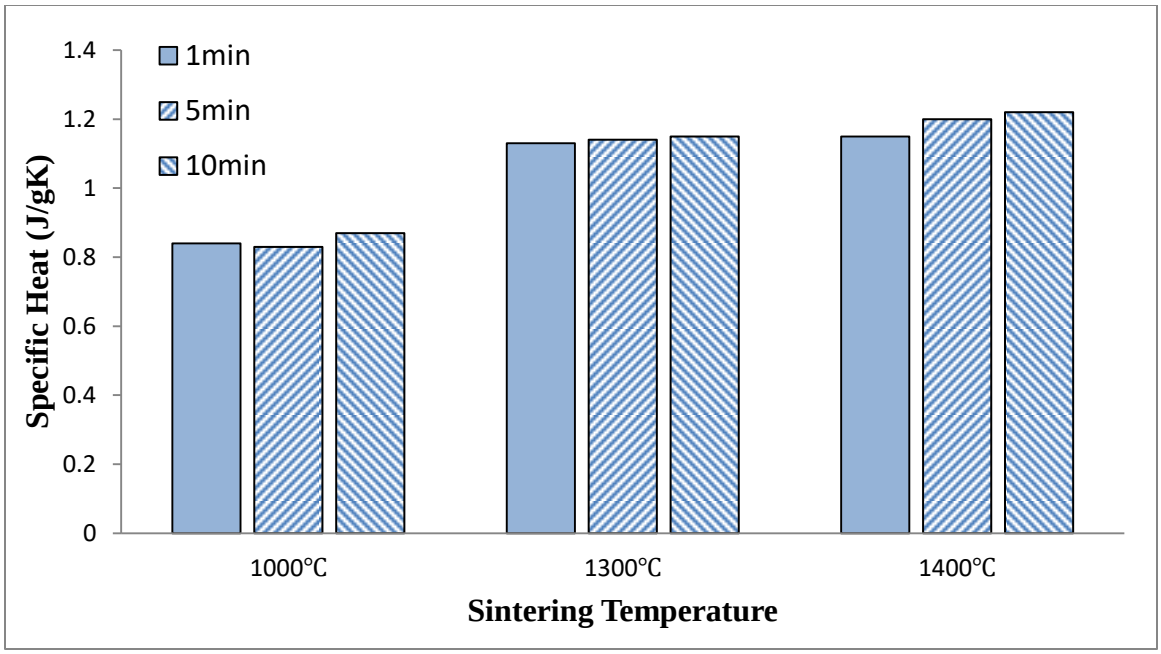

Figure 29. Room temperature specific heat capacity of alumina sintered at different SPS parameters

The behavior of heat capacity is exactly opposite to that of thermal conductivity and thermal diffusivity at elevated temperatures, as shown in Figure 30. Specific heat capacity was found to be increasing with increase in temperature from 25℃ to 250℃ for all the alumina samples sintered at different SPS conditions. For sample sintered at 1000℃ for 1 minute holding time, specific heat capacity increased from 0.84 to 1.13J/gK when temperature increased from 25℃ to 250℃. Similarly, for sample sintered at 1400℃ for 10 minute holding time, specific heat value increased from 1.22 to 1.55J/gK with increase in temperature from 25℃ to 250℃, respectively. L. Kumari et al [38] reported the similar trend of increasing values of heat capacity with increase in temperature.

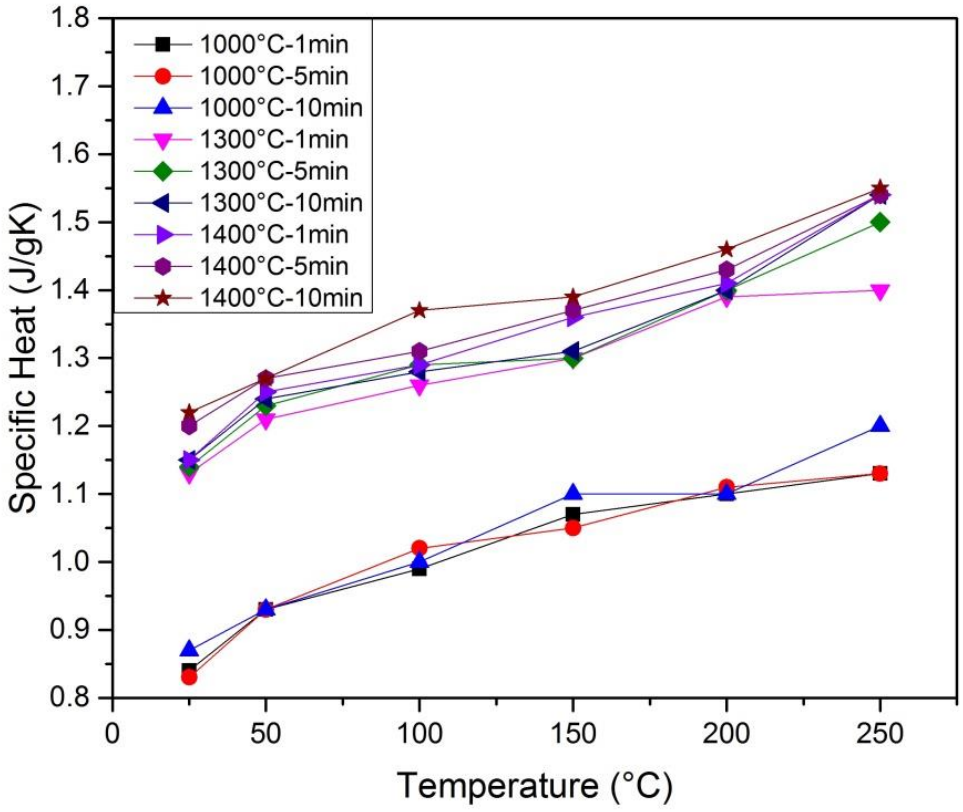

Figure 30. Specific heat capacity of alumina sintered at different SPS parameters at elevated temperatures

4.3 Al_2O_3-SiC-CNT Hybrid Nanocomposites

4.3.1 Powders Characterization

4.3.1.1 SiC and CNT Powders

Characterization details of alumina powder are already discussed in Section 4.2.1. Figure 31a and 31b shows the FE-SEM and TEM images of as-received SiC. The average particle size is 45-55nm, as provided by Supplier, can also be seen in SEM and TEM images. Figure 31c shows the TEM image of functionalized as-received multi-walled CNTs. The reasons for selection of functionalized CNT is their good dispersion and less

agglomeration ability because of presence of –COOH bonds on the surface [53] which reduces the Van Der Waal forces between CNT.

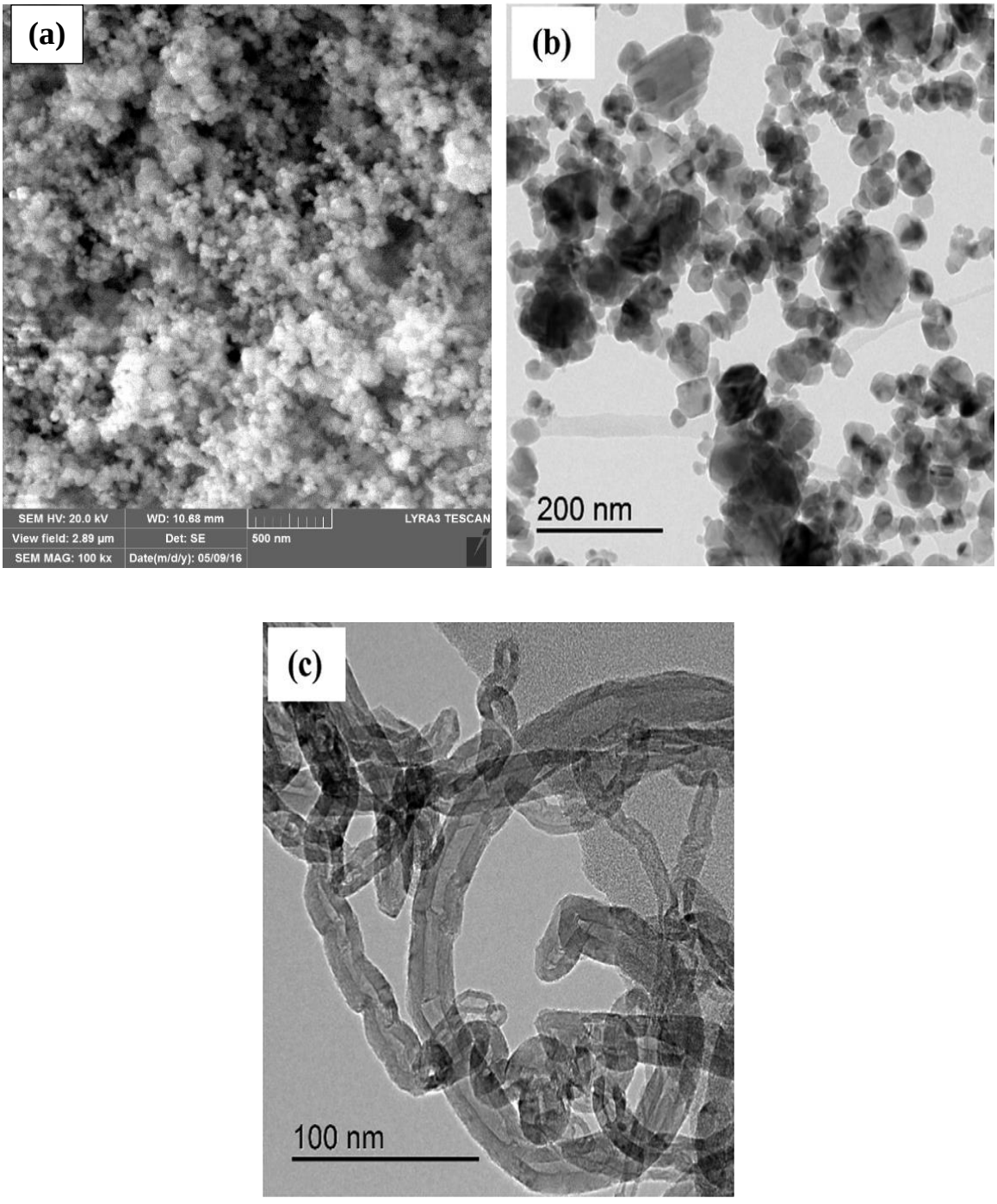

Figure 31. (a) FE-SEM image of as-received SiC, TEM images of as-received (b) SiC, (c) CNTs

4.3.1.2 XRD of Nanocomposite Powders

Figure 32 shows the XRD patterns of as-received alumina and SiC powders, as well as processed hybrid nanocomposite powders. In case of Al_2O_3-5SiC-1CNT and Al_2O_3-5SiC-2CNT hybrid nanocomposite powders, only one silicon carbide peak was detected in XRD pattern, while all other peaks belonged to alumina. This is due to the fact that silicon carbide was present in very small proportion as compared to alumina. No peak related to carbon nanotubes was observed in XRD pattern. This is also due to the presence of CNT in very small amount that is beyond the detection limit of XRD.

In case of Al_2O_3-10SiC-1CNT and Al_2O_3-10SiC-2CNT hybrid nanocomposite powders, two silicon carbide peaks were observed in XRD pattern, while all other peaks belonged to alumina. SiC was present in a very small proportion in comparison with alumina, that's why very few SiC peaks were observed in XRD pattern. The presence of CNTs was not detected here in XRD pattern, same like in case of Al_2O_3-5SiC-1CNT and Al_2O_3-5SiC-2CNT hybrid nanocomposite powders. No other peak related to any contamination was observed in XRD which indicates that either there was no contamination during the processing of hybrid nanocomposite powders or its proportion was so small that XRD was not able detect it.

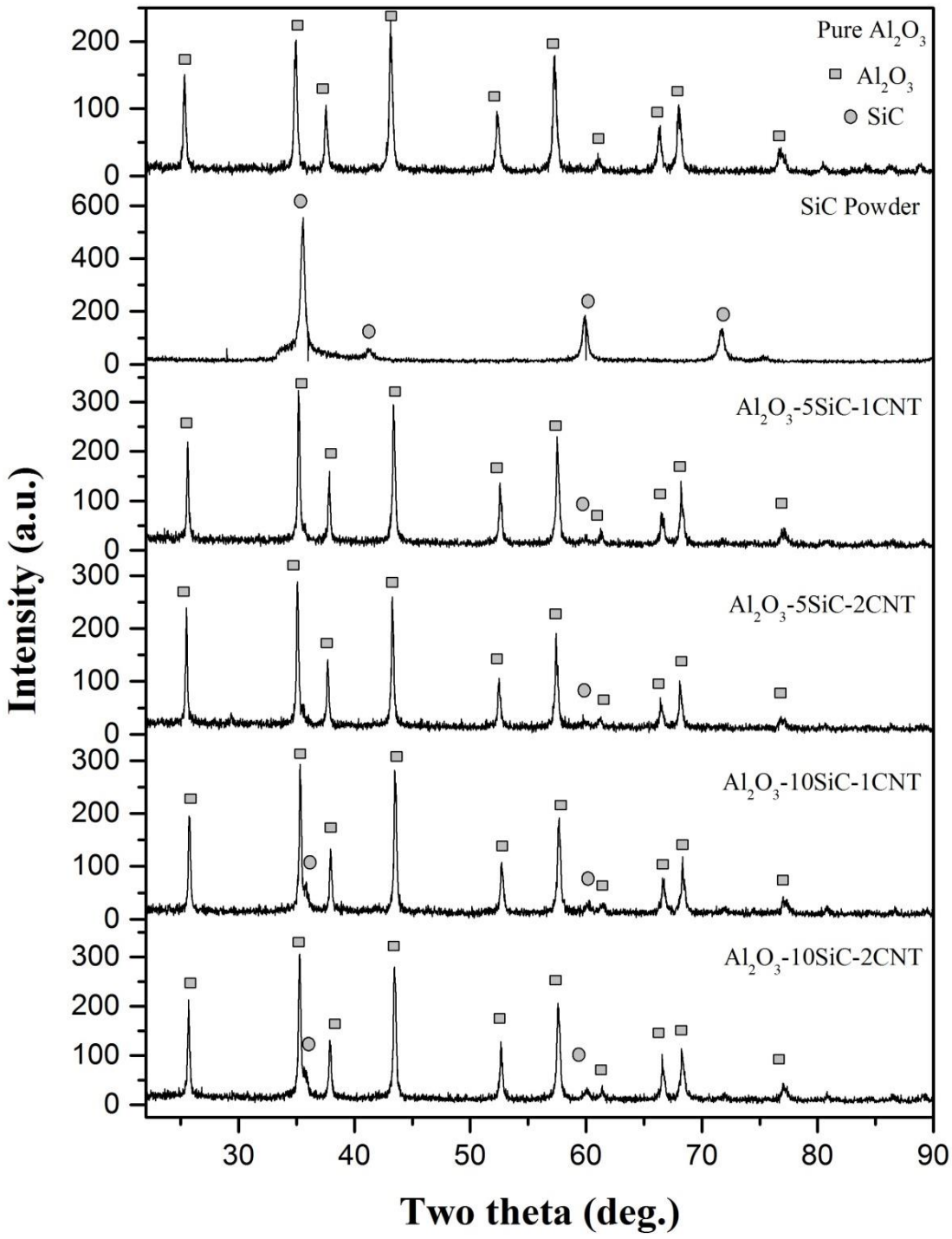

Figure 32. XRD spectra of as-received Al_2O_3, SiC powders along with processed Al_2O_3-5SiC-1CNT, Al_2O_3-5SiC-2CNT, Al_2O_3-10SiC-1CNT and Al_2O_3-10SiC-2CNT hybrid nanocomposite powders

4.3.2 Spark Plasma Sintered Hybrid Nanocomposites

SPS parameters were optimized using pure alumina in Section 4.2. At 1400℃, alumina showed 99.6% relative density which can be considered as full densification. As it is understood that the addition of reinforcements reduces the densification of matrix, hence a slightly higher temperature (i-e 1500℃) was selected for hybrid nanocomposites. As a reference, pure alumina was also sintered at the same sintering conditions. Table 12 shows the densification, matrix crystallite size and thermal properties at room temperature of spark plasma sintered pure alumina and different hybrid nanocomposites.

Table 12. Densification, crystallite size and room temperature thermal properties of SPS sintered hybrid nanocomposites

Nature of samples	Relative Density (%TD)	Crystallite Size (nm)	Thermal Conductivity (W/mK)	Thermal Diffusivity (mm^2/s)	Heat Capacity (J/gK)
Pure Al_2O_3	99.85	125	34.44	7.62	1.24
Al_2O_3-5SiC-1CNT	97.7	98	21.2	6.64	0.87
Al_2O_3-5SiC-2CNT	97.2	93	20.4	6.43	0.84
Al_2O_3-10SiC-1CNT	95.43	88	17.71	5.98	0.80
Al_2O_3-10SiC-2CNT	95.40	85	17.83	6.01	0.807

4.3.3 Densification

Figure 33 shows the densification of spark plasma sintered pure alumina and alumina based hybrid nanocomposites. Relative density of pure alumina was found to be 99.8%. The addition of reinforcements in alumina resulted in decrease in density of pure alumina. For instance, in Al_2O_3-5SiC-1CNT nanocomposite, relative density dropped down to 97.7%. Further addition of CNT to 2wt.% caused the relative density to decrease to 97.2%, in Al_2O_3-5SiC-2CNT nanocomposite. When the SiC content was increased to 10wt.%, in Al_2O_3-10SiC-1CNT nanocomposite, relative density significantly dropped down to 95.43%. Further addition of CNTs upto 2wt.%, in Al_2O_3-5SiC-2CNT nanocomposite, caused a very small drop in density which reached to a value of 95.40%. The amount of reinforcements showed a strong effect on densification reduction. SiC was added in larger proportion in alumina as compared to CNTs, hence it effect on densification reduction was more prominent.

It is well understood that addition of reinforcements causes the reduction in density. In case of pure alumina, dominant densification mechanisms are plastic flow during initial stage and diffusion during the final stage of sintering [106, 107]. Diffusion in alumina usually occurs by grain boundary diffusion and grain boundary migration [10]. When SiC is added as reinforcement in alumina, it is believed that these SiC particles are located on the grain boundaries as well as within the grains of alumina matrix. However, CNTs are present on the grain boundaries of alumina matrix [26, 39]. During densification, the presence of CNTs on the grain boundaries and SiC particles on the grain boundaries and within grains, cause the diffusion path to become longer. This decreases the diffusion of atoms and vacancies along the interfaces, which results in decrease in densification. Also,

SiC and CNT reinforcements which are present on the grain boundaries restrict the motion of grain boundaries, causing decrease in densification. Hence, decrease in grain boundary diffusivity, lattice diffusivity and grain boundary mobility, as a result of addition of reinforcements are some of causes of decrease in densification in nanocomposites.

K. Ahmad et al [39] also reported the decrease in densification of Al_2O_3-SiC-CNT hybrid nanocomposites, prepared using SPS at 1550℃, with increase in reinforcement content. 100% relative density was achieved for pure alumina. However, when the alumina was reinforced with 1vol.% SiC in combination with varying MWCNT content of 5, 7 and 10vol.%, the relative densities of respective Al_2O_3-SiC-CNT hybrid composites were reduced to 98.2%, 97.2% and 95.1%, respectively.

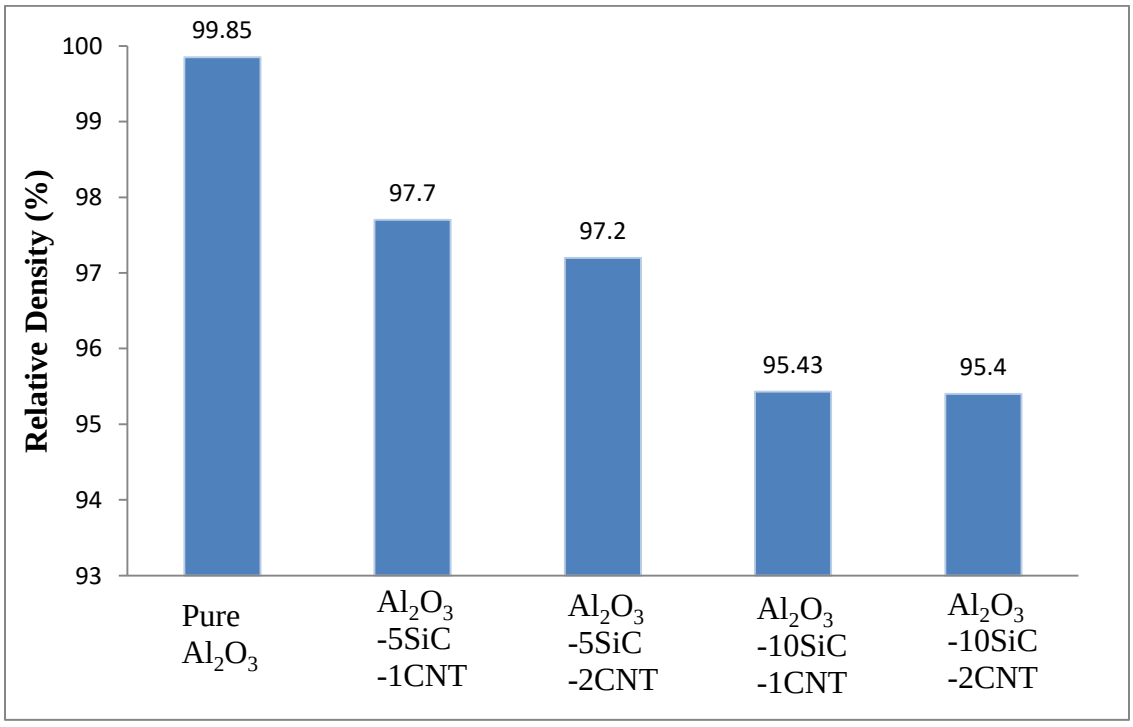

Figure 33. Relative density of Al_2O_3-SiC-CNT hybrid nanocomposites

In another study, K. Ahmad et al [98] reinforced alumina with 5vol.% MWCNT along with varying content (1, 2, 3vol.%) of SiC using SPS at 1550℃. They reported 100% relative density for pure alumina. However, when this alumina was reinforced with 5vol.% MWCNT along with 1, 2 and 3vol.% of SiC, relative densities of resulting hybrid nanocomposites were reduced to 98%, 96.46% and 96.40%, respectively. Similarly, K. Mohammad et al [40] also reported reduction in densification to 91.65% for Al_2O_3-5SiC-1CNT hybrid nanocomposite prepared using molecular level mixing and SPS at 1500℃ while that of pure alumina was 99.3%. J. Liu et al [100] also reported decrease in densification with increase in reinforcement content while studying Al_2O_3-SiC-GPL (graphene platelets) nanocomposites.

Even in the case of simple nanocomposites with single reinforcement, reduction in density with increase in reinforcement content was observed by many researchers. S. Ghadami et al [42] reported decrease in relative density from 99.4% to 94% when SiC content increased from 0 to 10vol.%, respectively, for Al_2O_3-SiC nanocomposites prepared through conventional sintering at 1740℃. X. L Shi et al [30] also reported decrease in densification of pure alumina from 99.3% to 95.8%, when reinforced with 20wt.% SiC using hot pressing at 1635℃. However, increase in temperature to 1735℃ resulted in increase in the densities of Al_2O_3-SiC nanocomposites to 100%. L. Kumari et al [26] reported that relative density of alumina decreased from 98.2% to 59.7%, when MWCNT content increased to 19.1wt.% in Al_2O_3-CNT nanocomposites prepared through SPS at 1450℃. I. Ahmad et al [37, 46], N. Bakhsh et al [45], J. Fan et al [48] and L. Kumari et al [38] also reported the same trend of decrease in densification of alumina with increasing CNT content in Al_2O_3-CNT nanocomposites.

However, there are few conflicting reports of increase in densification with addition of reinforcements. N. Saheb et al [41] reported relative density value of 99.3% for pure alumina, sintered using SPS at 1500℃, which increased to 99.76% and 99.36% for Al_2O_3-5wt.%SiC and Al_2O_3-5wt.%SiC-1wt.% CNT nanocomposites, respectively. He claimed that the discharge produced and plasma generated during SPS may be responsible for this increase in density of nanocomposites. M. Parchoviansky et al [31] also reported higher densification values for Al_2O_3-SiC nanocomposites as compared to monolithic alumina, prepared using hot pressing at 1740℃. 98.3% relative density was reported for pure alumina, however, when reinforced with 5, 10, 15 and 20vol.% coarse SiC, relative density greater than 99% was reported in all nanocomposites. He attributed this high densification of nanocomposites, as compared to monolithic alumina, to fine dispersion, high temperature and pressure used during hot pressing. G. D. Zhan et al [57] reported 100% densification for monolithic alumina and alumina reinforced with 5.7vol.% and 10vol.% SWCNT, using SPS at 1150℃. The relative density remained at 100% in spite of addition of 5.7vol.% and 10vol.% SWCNT in alumina

4.3.4 Microstructure

Figure 34 shows the variation in crystallite sizes (sub-grains) when alumina was reinforced with hybrid reinforcements. These crystallite sizes were measured from XRD patterns using Scherrer Equation. Crystallite size of pure alumina was 125nm. When alumina was reinforced with 5wt.% SiC and 1wt.% CNTs, crystallite size of alumina matrix reduced to 98nm. Increasing the CNT content to 2wt.% while keeping the SiC content constant at 5wt.% in alumina further reduced the crystallite size of alumina matrix to 93nm. When the SiC content increased to 10wt.% in Al_2O_3-10SiC-1CNT and

Al_2O_3-10SiC-2CNT hybrid nanocomposites, crystallite size became 88nm and 85nm, respectively. Crystallite size of alumina matrix was found to be decreasing with increase in reinforcements.

It is well known that in pure alumina, like densification, grain growth or crystallite size increase is also due to the grain boundary diffusion and grain boundary mobility [10, 44]. Addition of reinforcements reduces the grain boundary mobility of alumina matrix during sintering, resulting in less grain growth as compared to pure alumina. In case of Al_2O_3-SiC-CNT hybrid nanocomposites, presence of CNTs on the grain boundaries and SiC on the grain boundaries and within the grains [39] reduces the grain boundary mobility by pinning effect during sintering, which results in less grain growth in all nanocomposites as compared to monolithic alumina [37, 100].

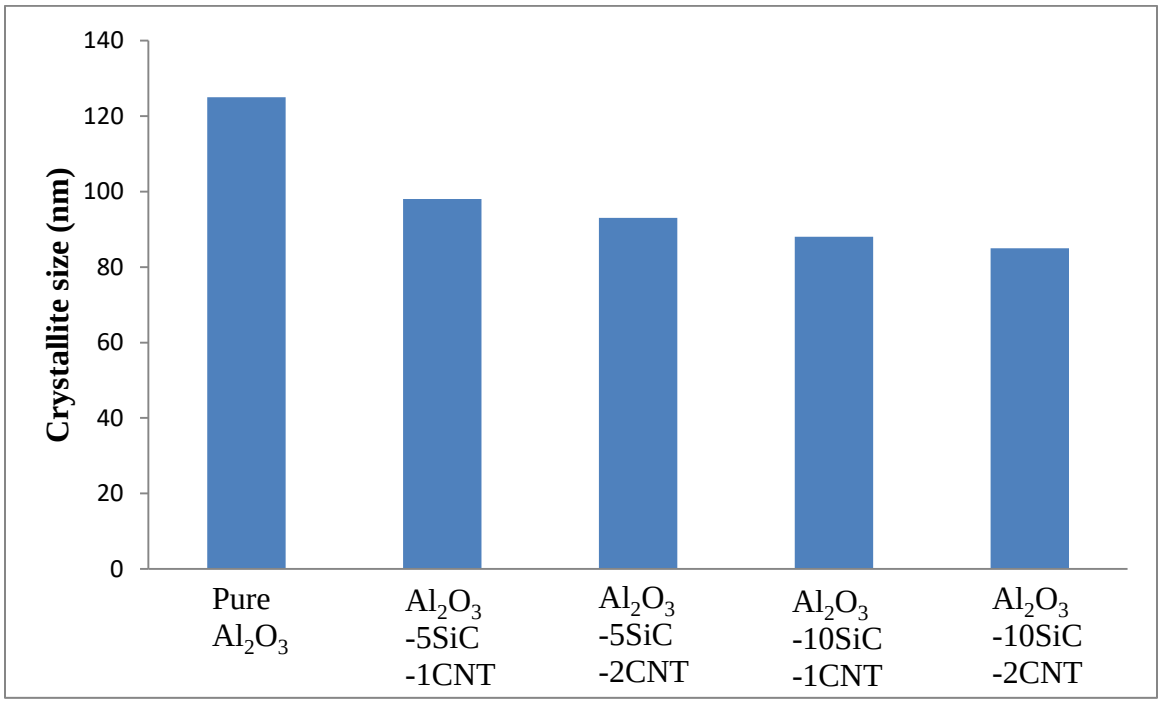

Figure 34. Crystallite size variation in Al_2O_3-SiC-CNT hybrid nanocomposites

Different researchers have reported the same trend of decrease in grain size of alumina matrix, when reinforced with different reinforcements, as compared to pure alumina. N. Saheb et al [41] showed decrease in grain size of Al_2O_3-SiC-CNT hybrid nanocomposites sintered using SPS at 1500℃, containing different fractions of CNTs and SiC reinforcements, as compared to monolithic alumina. J. Liu et al [100] et al also reported a continuous decrease in grain size of alumina matrix with increase in content of reinforcements in Al_2O_3-SiC-GPL (graphene platelets) hybrid nanocomposites, using SPS at 1500℃. Grain size of pure alumina was reported to be 4.68µm. Addition of 0.38vol.% graphene platelets along with 1, 3 and 5vol% SiC resulted in decrease in grain size to 3.67, 2.66 and 2.33µm, respectively. This decrease in grain size of Al_2O_3-SiC-GPL hybrid nanocomposites with increase in SiC content was attributed to pinning effect of SiC and graphene platelets.

S. Ghadami et al [42] reported continuous decrease in grain size of alumina prepared using hot pressing at 1750℃, with increase in SiC content, from 11.04µm for pure alumina to 3.80µm for Al_2O_3-20vol.%SiC nanocomposite. X. L Shi et al [30], M. Parchoviansky et al [31] and Z. Y. Deng et al [82] also reported the same trend of decrease in grain size of alumina matrix with increase in SiC content in Al_2O_3-SiC nanocomposites. I. Ahmad et al [37] reported 66% and 75% reduction in grain size of alumina matrix, when reinforced with 4 and 10vol.% of CNTs respectively, using hot pressing at 1600℃. This decrease in grain size was attributed to pinning effect of CNTs during sintering. D. Y. Lee et al [99] also reported decrease in grain size of alumina matrix, prepared using hot pressing at 1450℃, when reinforced with different fractions of MWCNTs. Grain size reported for pure alumina was 8.37µm which reduced to 3.31, 2.33

and 1.87μm with the addition of 0.1, 0.5 and 1wt.% MWCNTs, respectively. Grain size was reported to be decreasing continuously with increase in reinforcement content. S. C. Zhang et al [47], I. Ahmad et al [46], and G. D. Zhan et al [57] also reported similar trends of decrease in grain size of alumina matrix with increase in content of CNTs in Al_2O_3-CNT nanocomposites.

Figure 35 shows the FE-SEM images of fractured surfaces of alumina sintered at 1500℃. Intergranular mode of fracture can be seen easily. Figure 36-39 shows the FE-SEM images of fractured surfaces, EDX analysis and X-ray mapping of Al_2O_3-5SiC-1CNT, Al_2O_3-5SiC-2CNT, Al_2O_3-10SiC-1CNT and Al_2O_3-10SiC-2CNT hybrid nanocomposites. Rod-like CNTs can be observed in FE-SEM images of fractured surfaces of nanocomposites. Mode of fracture changed to mixture of intergranular and transgranular in case of hyrbrid nanocomposites. Also, grain refining effect by addition of reinforcements can be observed from FE-SEM images. This microstructural refinement is due to the pinning effect of reinforcements and is one of the reasons of enhanced mechanical properties of hybrid nanocomposites. However, there is no clear contrast between alumina matrix and SiC particles in FE-SEM images. This is due to the fact that Al and Si have atomic numbers very close to each other (13 and 14), due to which FE-SEM was not able to produce clear contrast between alumina and SiC. That is why, X-ray mapping was done to check the dispersion of reinforcements within matrix. X-ray mapping confirmed that the reinforcements are almost uniformly distributed within matrix in case of all hybrid nanocomposites. EDX analysis of all the hybrid nanocomposites showed that no new phase formation took place due to reaction of

reinforcements during sintering. Gold peak present in EDX analysis came from the gold coating which was done to avoid charging effects during SEM.

Figure 40 shows the XRD patterns of SPS sintered hybrid nanocomposites along with reference alumina. As can be seen in case of hybrid nanocomposites, few SiC peaks were identified. This is due to very small presence of SiC as compared to alumina. In case of Al_2O_3-5SiC-1CNT and Al_2O_3-5SiC-2CNT nanocomposites, only one SiC peak was identified. However, when content of SiC was increased i-e in case of Al_2O_3-10SiC-1CNT and Al_2O_3-10SiC-2CNT nanocomposites, number of identified SiC peaks increased to three. No peak related to CNTs was present in case of all hybrid nanocomposites because of the very small fraction of CNTs present within nanocomposites. Along with this, no extra peak was present in XRD pattern of hybrid nanocomposites to indicate some sort of contamination or reaction of reinforcements.

Also, in XRD patterns of hybrid nanocomposites, peak shifting towards right or higher two theta values was observed. This shift kept increasing with increase in reinforcement content, with maximum shift in case of Al_2O_3-10SiC-2CNT hybrid nanocomposite. This peak shifting towards right or higher two theta values is because of accumulation of compressive strain within matrix of hybrid nanocomposites. Accumulation of compressive strain causes the decrease in d-spacing of atoms, which results in diffraction at higher angles as stated by Bragg's law, $\sin\theta=\lambda/2d$, where θ is the diffraction angle, λ is wavelength of x-rays and d is the d-spacing.

The presence of compressive stress within alumina matrix after reinforcing with SiC has also been reported by many researchers as well [30, 108]. The reason may be the

difference in coefficient of thermal expansion between matrix alumina and reinforcement SiC. As coefficient of thermal expansion of alumina ($8.6x10^{-6}K^{-1}$) is twice that of SiC ($4.5x10^{-6}K^{-1}$) [27], therefore alumina matrix becomes under compressive stress after cooling from sintering [30, 31, 42, 62]. This presence of compressive stress within alumina matrix caused shifting of XRD peaks towards higher two theta angles in hybrid nanocomposites. The presence of this stress due to thermal expansion coefficient mismatch between matrix and reinforcement is one of the toughening mechanisms in alumina based nanocomposites.

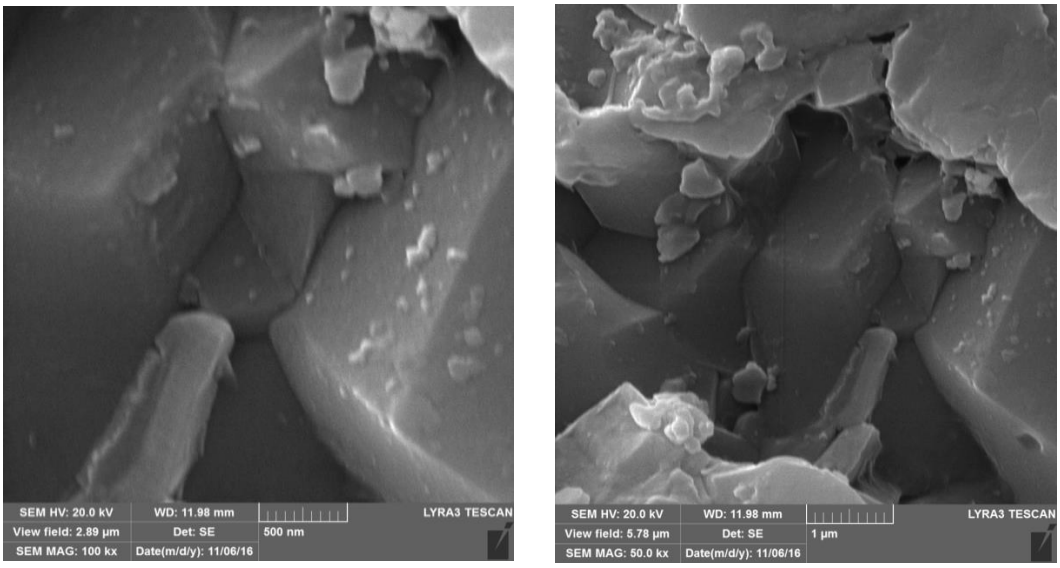

Figure 35. FE-SEM images of fractured surfaces of Al_2O_3 sintered at 1500°C at different magnifications

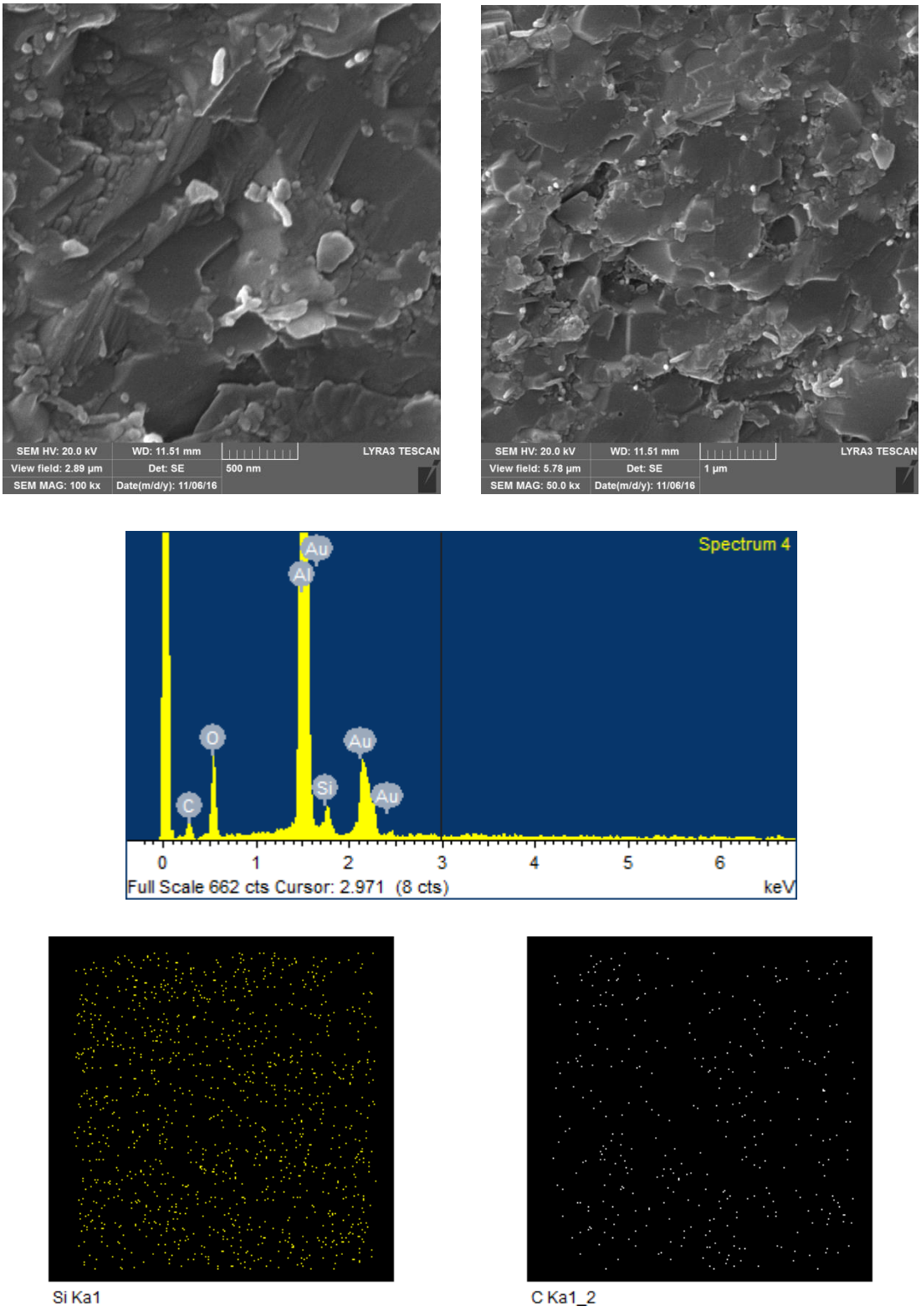

Figure 36. FE-SEM images of fractured surfaces, EDX analysis and X-ray mapping of Al_2O_3-5SiC-1CNT hybrid nanocomposite

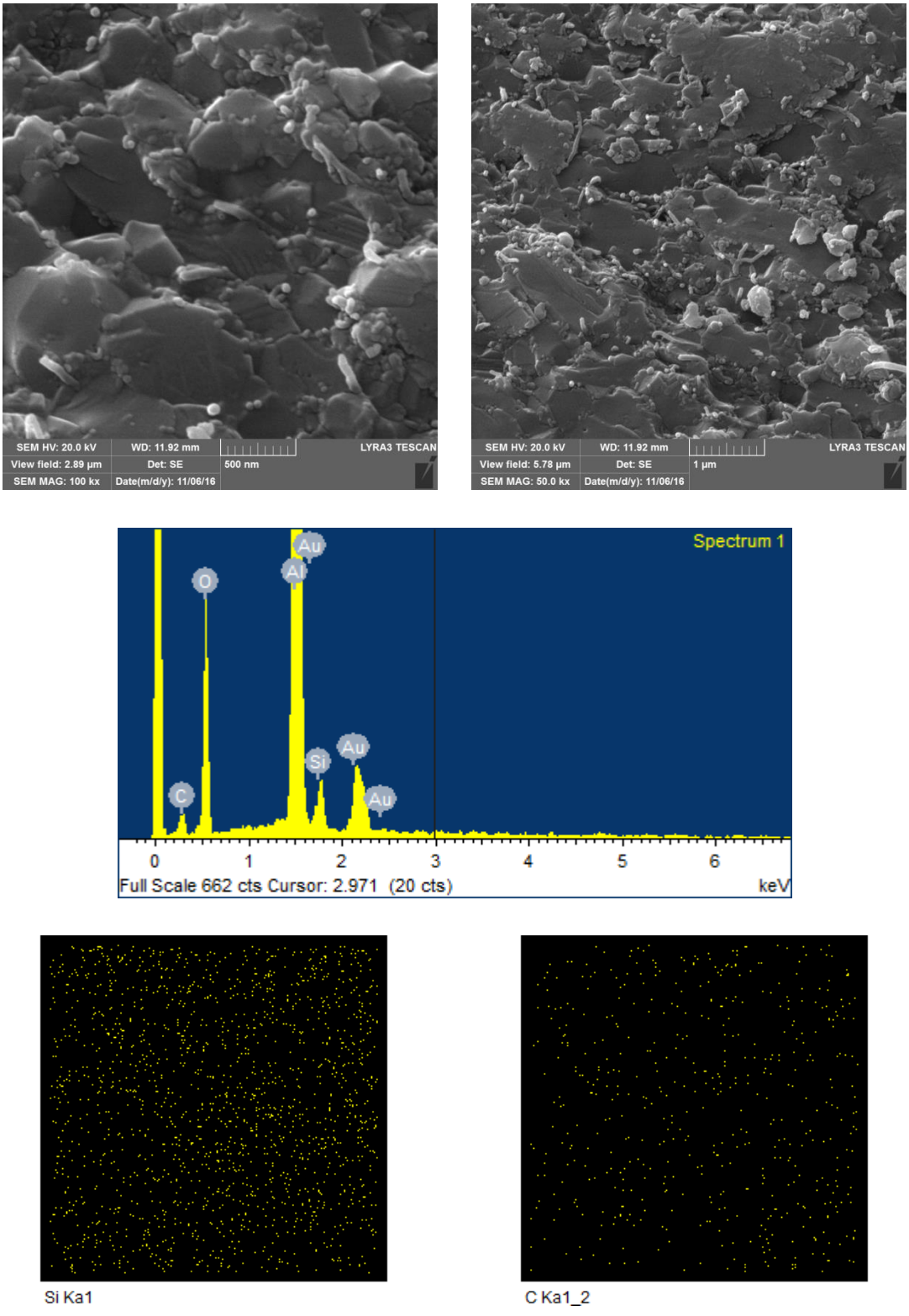

Figure 37. FE-SEM images of fractured surfaces, EDX analysis and X-ray mapping of Al_2O_3-5SiC-2CNT hybrid nanocomposite

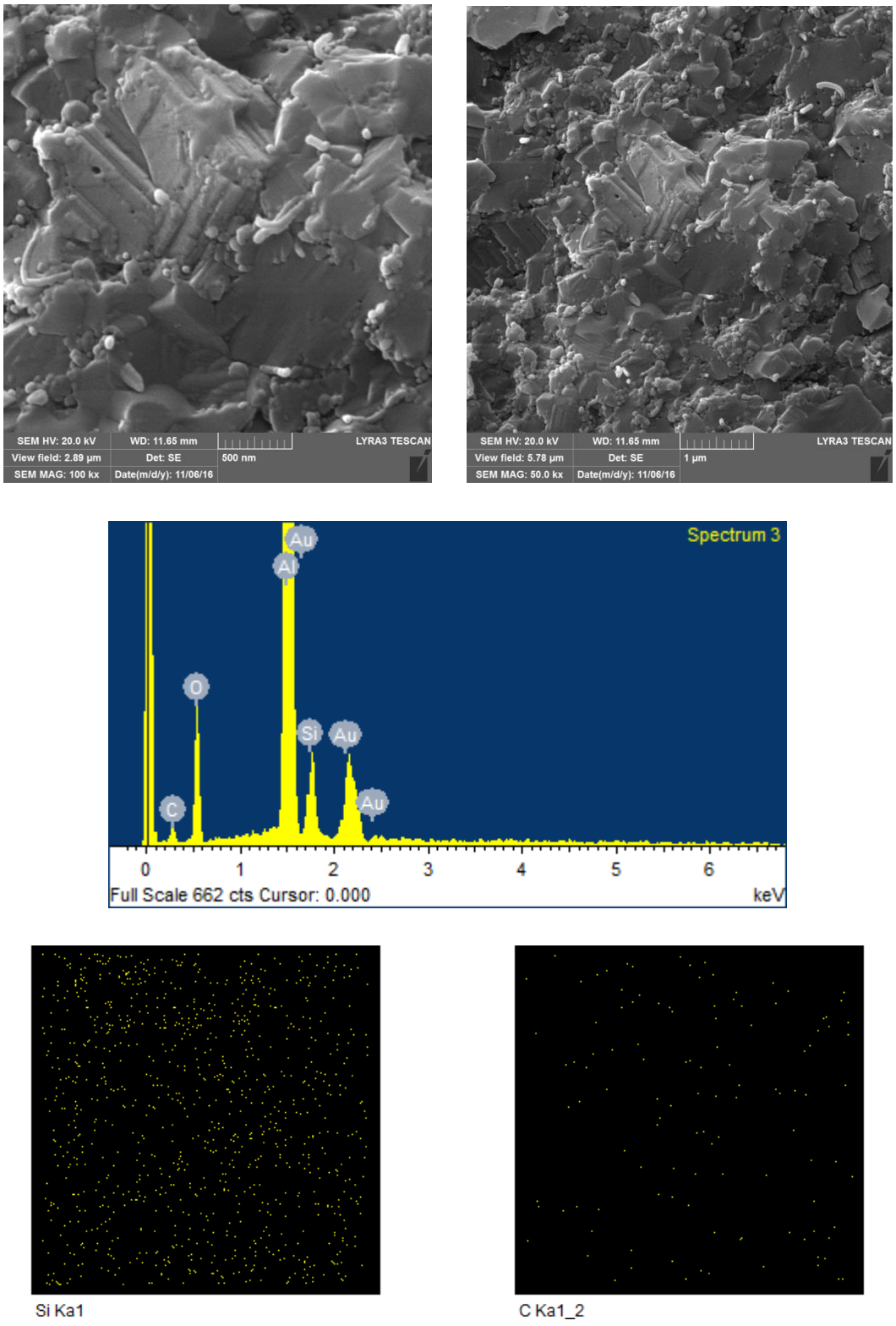

Figure 38. FE-SEM images of fractured surfaces, EDX analysis and X-ray mapping of Al_2O_3-10SiC-1CNT hybrid nanocomposite

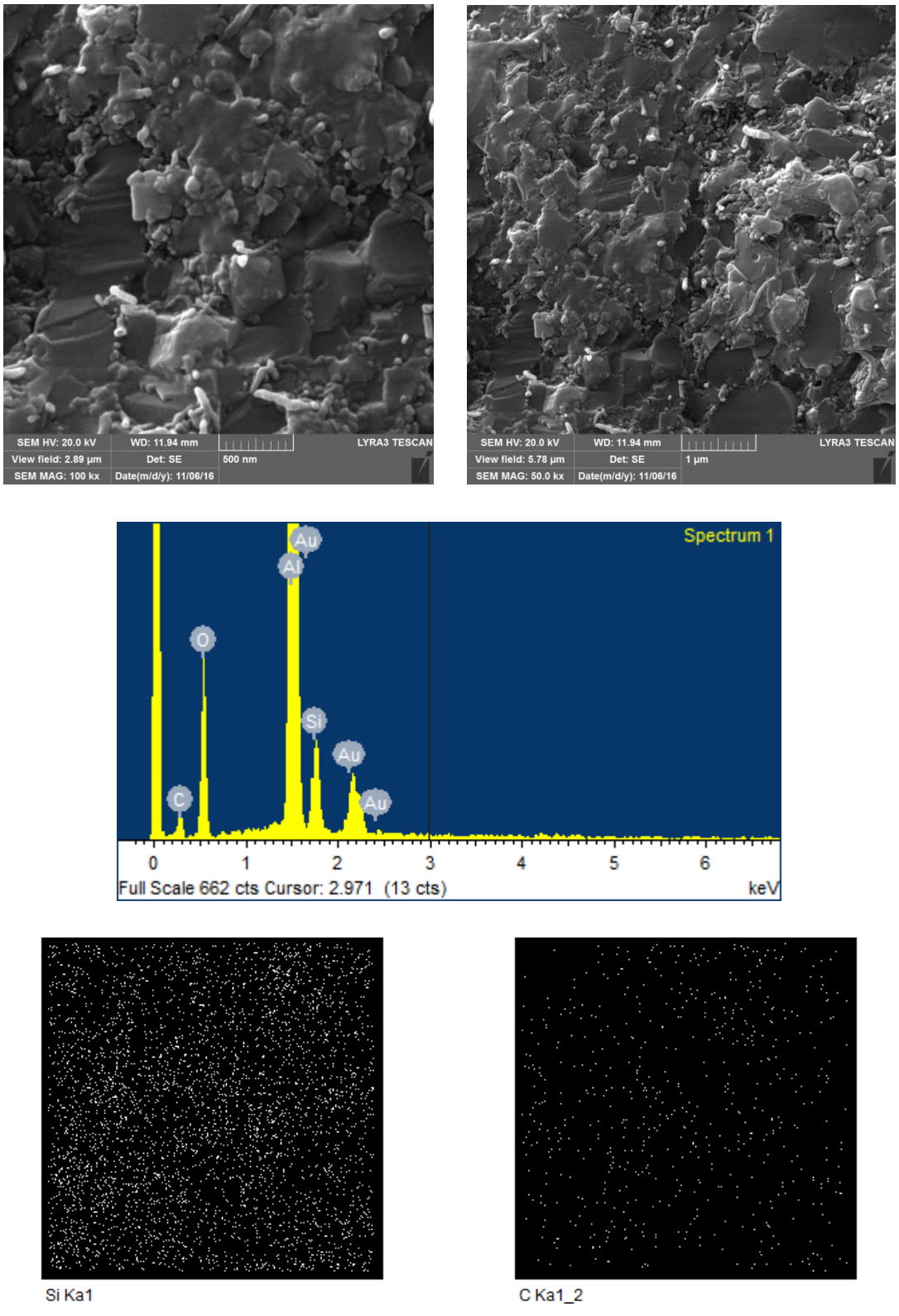

Figure 39. FE-SEM images of fractured surfaces, EDX analysis and X-ray mapping of Al_2O_3-10SiC-2CNT hybrid nanocomposite

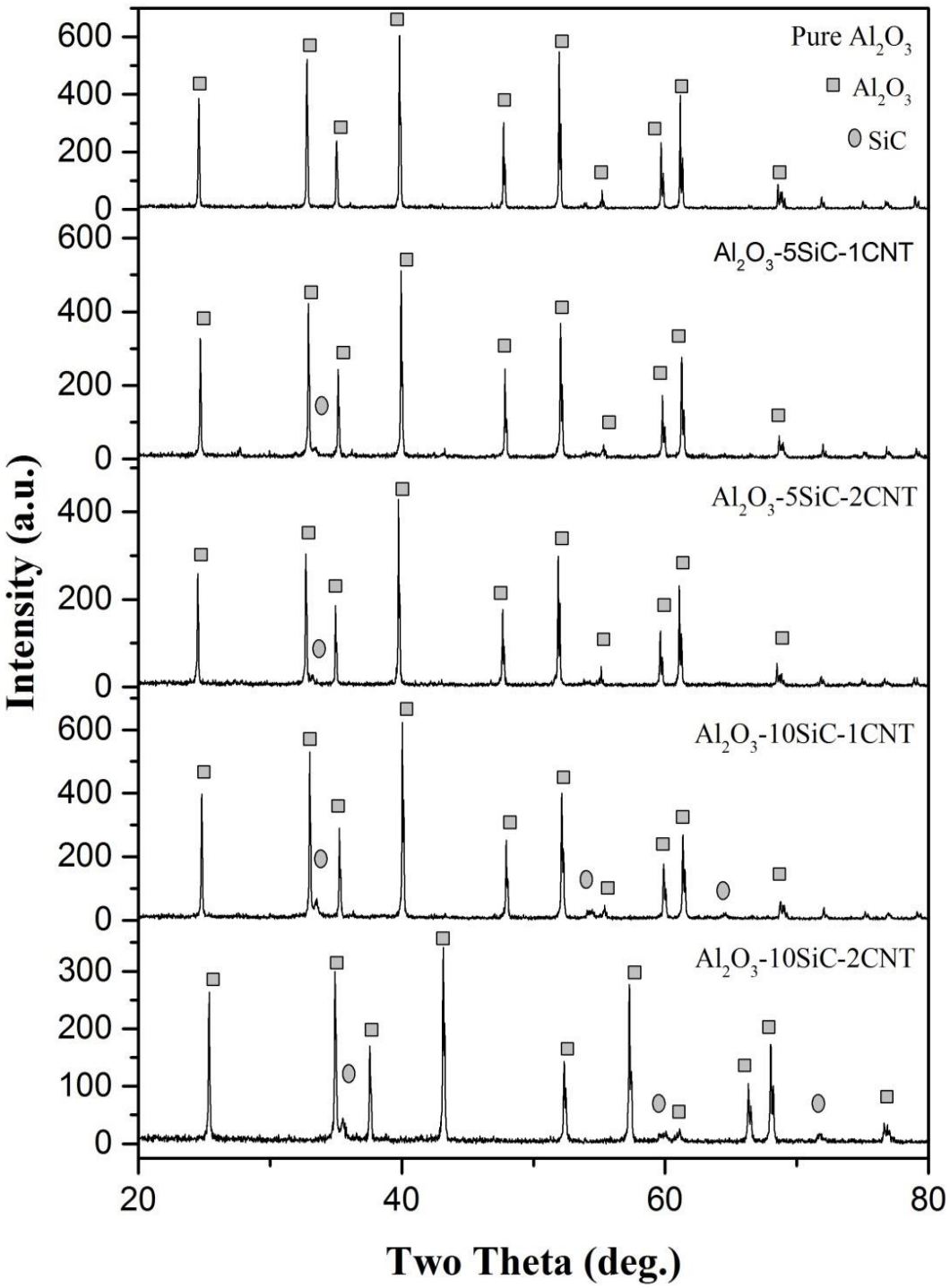

Figure 40. XRD patterns of SPS sintered alumina and Al_2O_3-SiC-CNT hybrid nanocomposites

4.3.5 Thermal Properties

Thermal conductivity, thermal diffusivity and heat capacity values at room temperature are shown in Table 12. Variation of thermal properties within hybrid nanocomposites is discussed below.

4.3.5.1 Thermal Conductivity

Figure 41 shows the room temperature thermal conductivity of alumina based hybrid nanocomposites. SiC and CNTs have higher thermal conductivity as compared to alumina as shown in Table 1, therefore it was expected that reinforcing alumina with SiC and CNTs will enhance the thermal conductivity. However, further decrease in thermal conductivity was observed when alumina was reinforced with SiC and CNTs. Pure alumina showed the thermal conductivity value of 34.44W/mK which decreased to 21.2W/mK when alumina was reinforced with 5wt.% SiC and 1wt.% CNTs. This value further decreased to 20.4 and 17.71W/mK for Al_2O_3-5SiC-2CNT and Al_2O_3-10SiC-1CNT hybrid nanocomposites, respectively. For Al_2O_3-10SiC-2CNT nanocomposite, thermal conductivity became 17.81W/mK which is a little bit higher than Al_2O_3-10SiC-1CNT nanocomposite, for which the value was 17.71W/mK.

Thermal conduction in ceramics is mainly due to lattice vibrations called phonons. These phonons interact with pores, internal defects and scatter in different directions. The scattering of these phonons determine the thermal conductivity of the material. If phonon scattering is high, thermal conductivity of that material will be low and vice versa. In case of Al_2O_3-SiC-CNT hybrid nanocomposites, thermal conductivity was found to be decreasing with increase in reinforcements. This decrease in thermal conductivity may be

due to increase in porosity, increase in interfacial thermal resistance because of reinforcements, CNT tube-tube interactions, interfacial imperfections induced because of reinforcements, internal defects generated due to reinforcements, increase in grain boundaries because of microstructure refinement, internal defects within SiC and CNTs, kinks or twists that appear in CNTs during sintering.

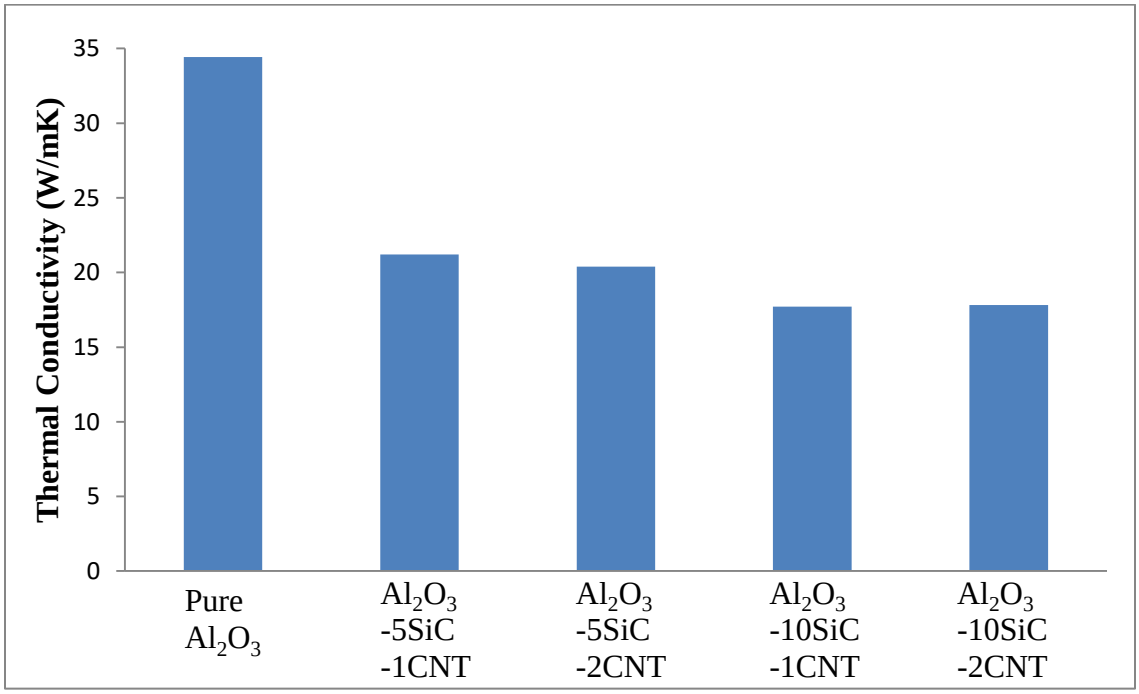

Figure 41. Room temperature thermal conductivity of Al_2O_3-SiC-CNT hybrid nanocomposites

Presence of porosity is one of the factors that increase the phonon scatterings. Interaction of phonons with pores causes them to scatter in different directions, resulting in decrease in thermal conductivity. In case of pure alumina, the sample was fully dense (relative density 99.85%), the presence of very low porosity resulted in very small phonon scatterings, hence giving a high value of thermal conductivity. However, in case of Al_2O_3-5SiC-1CNT hybrid nanocomposite, presence of 5wt.% SiC and 1wt.% CNTs

reduced the densification to 97.7% by pinning the grain boundaries during sintering. This increase in porosity level increased the phonon scatterings, which resulted in decrease in thermal conductivity of Al_2O_3-5SiC-1CNT hybrid nanocomposite. Similarly in case of Al_2O_3-5SiC-2CNT and Al_2O_3-10SiC-1CNT hybrid nanocomposites, further reduction in relative density to 97.2% and 95.43% caused further decrease in thermal conductivity. However, a very small increase in thermal conductivity from 17.71W/mK for Al_2O_3-10SiC-1CNT nanocomposite to 17.83W/mK for Al_2O_3-10SiC-2CNT nanocomposite may be due to the fact that CNTs started playing their role, because both samples are almost at same porosity level.

Presence of this porosity also increases the thermal grain boundary resistance, causing extra phonons scatterings. D. S. Smith et al [103] calculated and reported thermal grain boundary resistance value of monolithic alumina with different porosity levels. He reported a value of $1.3x10^{-8}$ $m^2.K.W^{-1}$ for fully densified alumina and $2.2x10^{-8}$ $m^2.K.W^{-1}$ for alumina with 0.3 volume fraction of porosity. He concluded that high thermal grain boundary resistance due to increased porosity caused the decrease in thermal conductivity by decreasing the effective thermal conduction cross-section. P. Rutkowski et al [109] reported decrease in thermal conductivity when reinforced alumina with different fractions of graphene using SPS and HP. He reported highest value of 33.6W/mK for alumina and values between 16.1 to 28.1W/mK for different alumina-graphene nanocomposites. He concluded that decrease in densification is one of the major reasons of decrease in thermal conductivity. K. Ahmed et al [74] reported the increase in porosity, in case of Al_2O_3-CNT nanocomposites, as one of the reasons of decrease in thermal conductivity of nanocomposites as compared to monolithic alumina.

Interfacial thermal resistance between the reinforcements and matrix also increases the extra phonon scatterings, resulting in decrease in thermal conductivity from the expected value. SiC particles because of their Nano size and CNTs due to their higher aspect ratio, have very large surface area. When alumina was reinforced with these SiC and CNTs, interfacial thermal resistance became significantly higher because of very large interfacial area of reinforcements. This high interfacial thermal resistance caused extra phonon scatterings and consequently, thermal conductivity decreased in case of Al_2O_3-SiC-CNT hybrid nanocomposites. D. Hasselman et al [110] also reported that SiC with small particle size has large surface area, which in turn creates more interfacial thermal resistance and results in decrease in thermal conductivity of composite. He proposed that particle size of SiC should be as large as possible, in order for minimum interfacial thermal resistance and increase in thermal conductivity of composite material. R. Barea [73] calculated the value of interfacial thermal resistance for SiC platelets reinforced alumina to be 0.5×10^{-8} $m^2.K.W^{-1}$, with SiC platelets having 17µm diameter and 3µm thickness. M. Collin et al [87] proposed that because of thermal barrier between SiC reinforcement and alumina matrix, SiC cannot fully contribute to thermal conductivity, hence alumina-SiC nanocomposites have lower thermal conductivity. K. Ahmad et al [74] used the theoretical models along with experimental verifications to show that very high interfacial thermal resistance between MWCNT-alumina nanocomposites is the major cause of decrease in thermal conductivity. Decrease in thermal conductivity because of interfacial thermal resistance in CNT-ceramic nanocomposites has been reported by different researchers [25, 57, 111, 112]. In CNTs reinforced matrix, value reported for interfacial thermal resistance is 8.3×10^{-8} $m^2.K.W^{-1}$ [38].

CNT tube-tube interaction is another possible reason for decrease in thermal conductivity [38] in CNT-based nanocomposites. Due to Van Der Waal forces between CNTs, they tend to agglomerate. CNT agglomerates, in shapes of ropes and bundles, offer surprisingly low values of thermal conductivity, as bundling introduces inter-tube scatterings [113]. Although in this work, functionalized CNTs were used whose agglomeration ability is less because of presence of –COOH bonds on surface [53] and have a very good dispersion ability. Also, ultrasonication which has been proven as an effective method of dispersion of CNTs [54], was used in this work for uniform dispersion of CNTs. In spite of all this, still there could be some CNTs agglomerations, although very small, but may possibly have contributed in lowering thermal conductivity of Al_2O_3-SiC-CNT hybrid nanocomposites as compared to monolithic alumina.

Addition of reinforcements also induces the interfacial imperfections which increases the phonon scatterings and results in decrease in thermal conductivity. Interfacial imperfections caused by the difference in coefficient of thermal expansion between the SiC reinforcement and alumina matrix is one of the reasons of decrease in thermal conductivity [98]. These interfacial imperfections like residual stresses and dislocations also have been reported as a possible causes of decrease in thermal conductivity [114, 115]. K. Ahmad et al [39, 98] proposed the generation of dislocations around the SiC particles for relieving residual stresses in alumina matrix, thus providing the strengthening to Al_2O_3-SiC-CNT hybrid nanocomposite system. Although these dislocations contributed in increasing mechanical strength, however, they may also have contributed in decreasing the thermal conductivity. Presence of these dislocations at particle tips was also reported by many authors [4, 108]. Also, presence of residual

stresses in Al_2O_3-SiC nanocomposite was reported by different researchers [27, 30, 42-44], and is one of the important strengthening mechanism [108]. The presence of residual stresses within alumina matrix in this study was also confirmed from XRD patterns (Figure 40) of Al_2O_3-SiC-CNT hybrid nanocomposites, where peak shifting was observed. These interfacial imperfections might also have contributed in decreasing the thermal conductivity of Al_2O_3-SiC-CNT hybrid nanocomposites.

Internal defects in SiC and CNT reinforcements also act as scattering sites for phonons and results in decrease in thermal conductivity. Stacking disorder in SiC, as reported by H. Nakano [115], may also be the reason of decrease in thermal conductivity of Al_2O_3-SiC-CNT hybrid nanocomposites. Also, thermal conductivity of SiC itself varies widely with the impurity content as reported by G. Slack [116]. Impurities present within the SiC reinforcement act as phonon scattering sites and affect the thermal conductivity of the nanocomposite. SiC used in this study has 97.5% purity, so it is possible that impurities present within SiC reinforcement may have contributed in decreasing thermal conductivity of Al_2O_3-SiC-CNT hybrid nanocomposites. Also, kinks and twists in CNTs, which can produce during high pressure sintering, may also reduce the thermal conductivity of CNT-based nanocomposites [38]. These kinks or twists can block phonons travelling along the CNT, resulting in decrease in thermal conductivity. K. Yang et al [117] reported kinks, corrugation and collapse of side walls of muli-walled carbon nanotubes induced during SPS sintering.

Decrease in thermal conductivity was also reported by K. Ahmad et al [98]. SPS was used at 1550°C for reinforcing alumina with 5vol.% MWCNT along with varying content (1, 2, 3vol.%) of SiC to produce Al_2O_3-SiC-CNT hybrid nanocomposites. He reported a

thermal conductivity of 30W/mK for pure alumina which decreased to 23W/mK for Al_2O_3-5vol.%MWCNT-1vol.% SiC nanocomposite. Increasing the SiC content to 2vol.% further decreased thermal conductivity to 19.5W/mK. However, a small increase in thermal conductivity value to 21.5W/mK was observed for Al_2O_3-5vol.%MWCNT-3vol.% SiC hybrid nanocomposite. This overall decrease in thermal conductivity of hybrid nanocomposites, as compared to monolithic alumina, was attributed to interfacial thermal resistance, low thermal conductivity of MWCNT ropes as compared to individual MWCNT, interfacial imperfections like residual stresses and dislocations.

In Al_2O_3-CNT nanocomposites, decreasing trend of thermal conductivity with increase in CNT reinforcements was also reported by K. Ahmad et al [74]. Thermal conductivity of pure alumina decreased from 34W/mK to 27, 20 and 16W/mK when alumina was reinforced with 1.1, 6.4 and 10.4vol.% CNTs, respectively. This decrease in thermal conductivity was attributed to large interfacial thermal resistance between MWCNTs and alumina, porosity and CNTs agglomeration. In another study, K. Ahmad et al [25] reported the same decreasing trend from 31.16W/mK for pure alumina to 30.01 and 24.03W/mK for Al_2O_3-5vol.% MWCNT and Al_2O_3-10vol.% MWCNT nanocomposites, respectively. This decrease in thermal conductivity was attributed to interfacial thermal resistance, CNTs tube-tube interactions

There are some conflicting reports where researchers have reported an increase in thermal conductivity of alumina when reinforced with CNTs or SiC. L. Kumari et al [38] reported increase in thermal conductivity of alumina when reinforced with CNTs using SPS. The highest value of 90.44W/mK was reported for Al_2O_3-7.39wt.%CNT nanocomposites. Enhancements in thermal conductivity were attributed to weight fraction of CNTs,

densification and sintering conditions. M. Collin et al [87] reported a very high value of 49W/mK for Al_2O_3-30wt.% SiC whiskers composites. R. Barea et al [73] also reported enhancements in thermal conductivity of hot pressed Al_2O_3-SiC platelet composites. Thermal conductivity values increased from 29W/mK for pure alumina to 36, 39 and 49W/mK when alumina was reinforced with 12, 20 and 30vol.% of SiC platelets, respectively. Slight increase in thermal conductivity to 38W/mK for Al_2O_3-20vol.% SiC hot pressed nanocomposite was also reported by M. Parchoviansky [32]. He proposed that because of porosity, interfacial thermal resistance and interfacial imperfections, the expected enhancements in thermal conductivity of Al_2O_3-SiC nanocomposites were not achieved.

Figure 42 shows the thermal properties of Al_2O_3-SiC-CNT hybrid nanocomposites at elevated temperatures. Thermal conductivity was found to be decreasing with increase in temperature for all the samples. At high temperatures, atomic vibrations of alumina matrix become higher which interfere with phonon propagation waves and cause scattering of phonons, resulting in decrease in thermal conductivity [32]. For pure alumina, thermal conductivity decreased from 34.44W/mK at 25℃ to 18.32W/mK at 250℃. Similarly, for Al_2O_3-5SiC-1CNT and Al_2O_3-5SiC-2CNT hybrid nanocomposites, thermal conductivity decreased from 21.2 and 20.4W/mK at 25℃ to 13.73 and 13.55W/mK at 250℃, respectively. For Al_2O_3-10SiC-1CNT and Al_2O_3-10SiC-2CNT hybrid nanocomposites, thermal conductivity values decreased from 17.71 and 17.83W/mK at 25℃ to 12.19 and 12.34W/mK at 250℃, respectively. Similar decreasing trend of thermal conductivity for Al_2O_3-SiC-CNT hybrid nanocomposites was also reported by K. Ahmad et al [98]. Different other researchers have also reported decrease

in thermal conductivity for Al_2O_3-SiC nanocomposites [32, 73] and Al_2O_3-CNT nanocomposites [38, 74, 118] with increase in temperature.

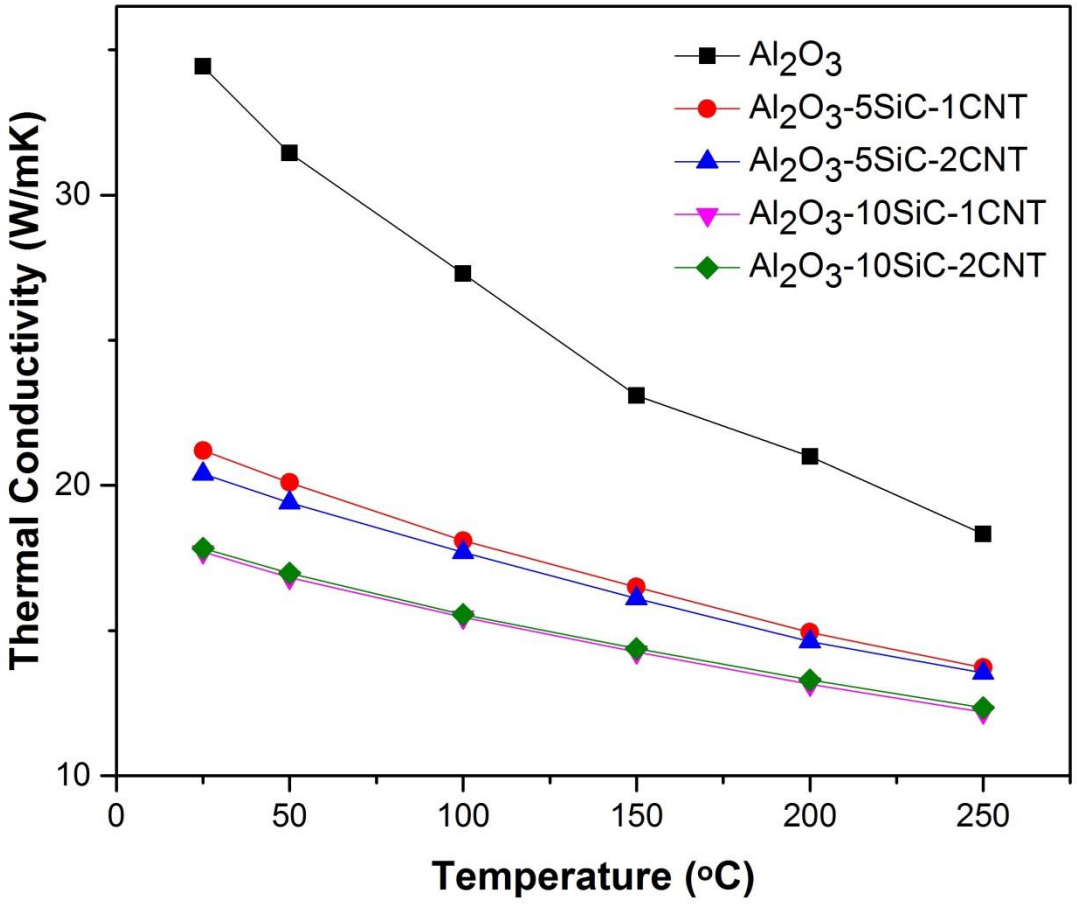

Figure 42. Thermal conductivity of Al_2O_3-SiC-CNT hybrid nanocomposites at elevated temperature

4.3.5.2 Thermal Diffusivity

Thermal diffusivity of Al_2O_3-SiC-CNT hybrid nanocomposites at room temperature is shown in Figure 43. Pure alumina showed the highest value of 7.62mm^2/s for thermal diffusivity. This value of thermal diffusivity decreased to 6.64mm^2/s when alumina was reinforced with 5wt.% SiC along with 1wt.% CNTs. This thermal diffusivity value kept

on decreasing to 6.43 and 5.98mm^2/s for Al_2O_3-5SiC-2CNT and Al_2O_3-10SiC-1CNT hybrid nanocomposites. However, for Al_2O_3-10SiC-2CNT nanocomposite, this value showed a slight increase and reached 6.01mm^2/s. Thermal diffusivity showed a decreasing trend with increase in SiC and CNTs reinforcements. Thermal diffusivity for all the Al_2O_3-SiC-CNT hybrid nanocomposites was lower than pure alumina.

Thermal diffusivity basically determines the rate of conduction of heat. Higher thermal diffusivity means faster heat conduction within material. Thermal diffusivity is related to thermal conductivity and heat capacity by equation $\alpha = k/\rho C_p$, where α is thermal diffusivity, k is thermal conductivity, ρ is density and C_p is specific heat capacity. Thermal diffusivity in ceramics, like thermal conductivity, also depends on lattice vibrations called phonons. Scattering of phonons determine the thermal diffusivity of material. Larger phonon scatterings decrease the thermal diffusivity of material. In case of Al_2O_3-SiC-CNT hybrid nanocomposites, decrease in thermal diffusivity was also due to the increased phonons scatterings induced due to SiC and CNT reinforcements. This decrease in thermal diffusivity, in case of Al_2O_3-SiC-CNT hybrid nanocomposites, may be due to increased porosity, interfacial thermal resistance, interfacial defects like residual stresses and dislocations, CNT agglomerations, CNT tube-tube interactions and due to increased grain boundaries because of microstructure refinements in hybrid nanocomposites.

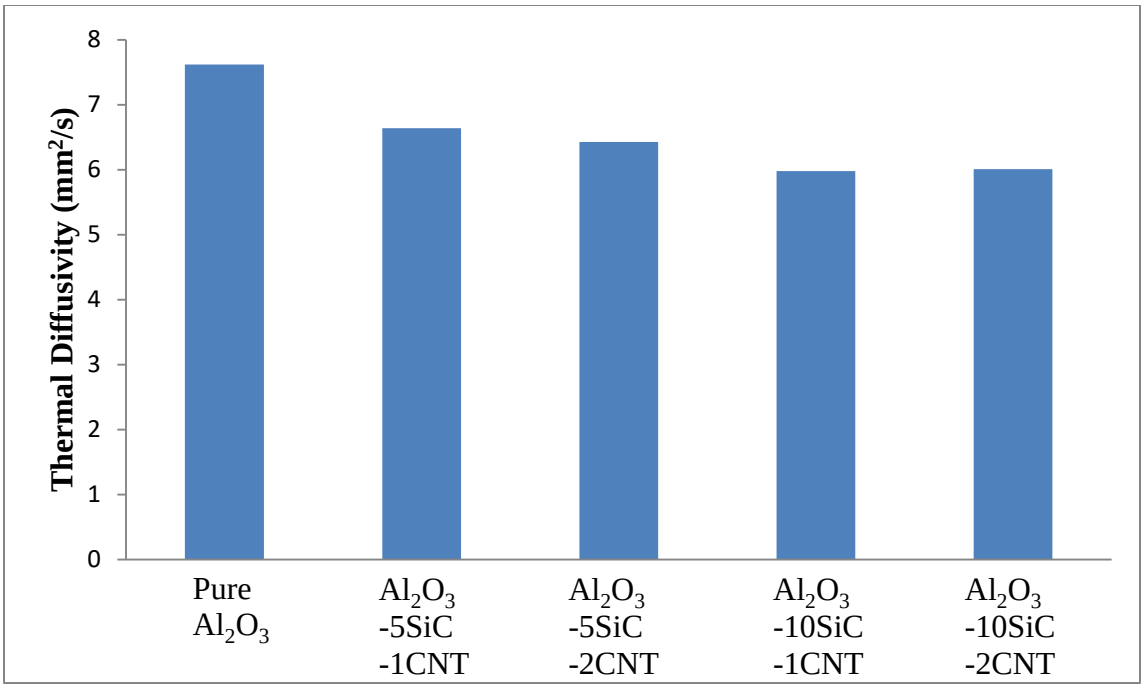

Figure 43. Room temperature thermal diffusivity of Al_2O_3-SiC-CNT hybrid nanocomposites

L. Kumari et al [38] also reported decrease in thermal diffusivity from 9mm^2/s for pure alumina to 6.5 and 5.5mm^2/s for Al_2O_3-7.39wt.%CNT and Al_2O_3-19.10wt.%CNT nanocomposites when sintered at SPS temperature of 1450℃. This decrease in thermal diffusivity was attributed to decreased density of samples. However, when high density samples were prepared using higher SPS temperature of 1550℃, thermal diffusivity values became higher than pure alumina. Similarly, in case of Al_2O_3-SiC-CNT hybrid nanocomposites, increased porosity with increase in reinforcements caused higher phonon scatterings, resulting in reduction in thermal diffusivity. Pure alumina sample was almost fully densified with 99.85% relative density. However, addition of CNTs and SiC reduced the densification during sintering by pinning the grain boundaries of alumina

matrix. Decreased densification in Al_2O_3-SiC-CNT hybrid nanocomposites caused more phonon scatterings by pores and thus low value of thermal diffusivity was observed.

However, there can be many other reasons for decrease in thermal diffusivity, apart from porosity. Very high surface area of SiC and CNT reinforcements because of their Nano size resulted in very large interfacial surface area in alumina matrix, which increased the interfacial thermal resistance. This increased thermal interfacial resistance caused extra phonon scatterings in Al_2O_3-SiC-CNT hybrid nanocomposites, causing the thermal diffusivity to decrease. Also, CNT tube-tube interactions because of CNT agglomerations may also have contributed in lowering the thermal diffusivity because it is impossible to avoid the agglomeration at all. Additionally, interfacial defects like residual stresses and dislocations produced due to difference in coefficient of thermal expansion between alumina matrix and SiC, CNT reinforcements might also have contributed in lowering the thermal diffusivity value. Decrease in thermal diffusivity was also reported by G. D. Zhan et al [57] for Al_2O_3-SWCNT nanocomposites. He reported decrease in thermal diffusivity from $9mm^2/s$ for pure alumina to 4 and $2.5mm^2/s$ when reinforced with 10 and 15vol.% SWCNTs. He also attributed this decrease in thermal diffusivity to interfacial thermal resistance, CNT tube-tube interaction, CNT agglomeration, bending and twisting of CNTs during sintering. K. Ahmed et al [25] also reported decrease in thermal diffusivity when reinforced alumina with increasing content of MWCNTs.

On contrary to this work, few researchers have reported increase in thermal diffusivity of alumina when reinforced with SiC of different shapes. For instance, R. Barea et al [73] reported that thermal diffusivity increased with increasing SiC platelets content in alumina. Value of thermal diffusivity increased from $9mm^2/s$ for pure alumina to 12, 13

and 15.3mm^2/s for alumina reinforced with 12, 20 and 30vol.% SiC platelets, respectively. Similarly, M. Parchoviansky et al [32] also reported slight enhancements in thermal diffusivity from 9.3mm^2/s for pure alumina to 13.5mm^2/s for Al_2O_3-20vol.%SiC particles. P. McCluskey et al [88] and M. Collin et al [87] also reported increase in thermal diffusivity of pure alumina with increase in SiC whiskers reinforcement.

Figure 44 shows the thermal diffusivity of Al_2O_3-SiC-CNT hybrid nanocomposites from room temperature upto 250℃. Thermal diffusivity was found to be decreasing with increase in temperature for all samples. Increase in temperature increases the atomic vibrations within alumina matrix which interfere with phonon waves and result in decrease in thermal diffusivity. Decreasing trend of thermal diffusivity for alumina-based composites with increase in temperature was reported by other researchers as well [25, 32, 38, 57, 73, 87, 88]. Decrease in thermal diffusivity with temperature in alumina was quite higher than Al_2O_3-SiC-CNT hybrid nanocomposites. From 125℃ onward, thermal diffusivity of Al_2O_3-SiC-CNT hybrid nanocomposites became higher than pure alumina. At 250℃, thermal diffusivity of pure alumina was 2.99mm^2/s while that for Al_2O_3-SiC-CNT hybrid nanocomposites was within range of 3.24 to 3.4mm^2/s. Similar behavior was also reported by L. Kumari et al [38] for Al_2O_3-7.39wt.%CNT nanocomposite. At room temperature, thermal diffusivity value of Al_2O_3-7.39wt.%CNT nanocomposite was lower than pure alumina. But decrease in thermal diffusivity with increase in temperature was lower in nanocomposite as compared to pure alumina, due to which thermal diffusivity of Al_2O_3-7.39wt.%CNT nanocomposite became equal to that of pure alumina after 100℃.

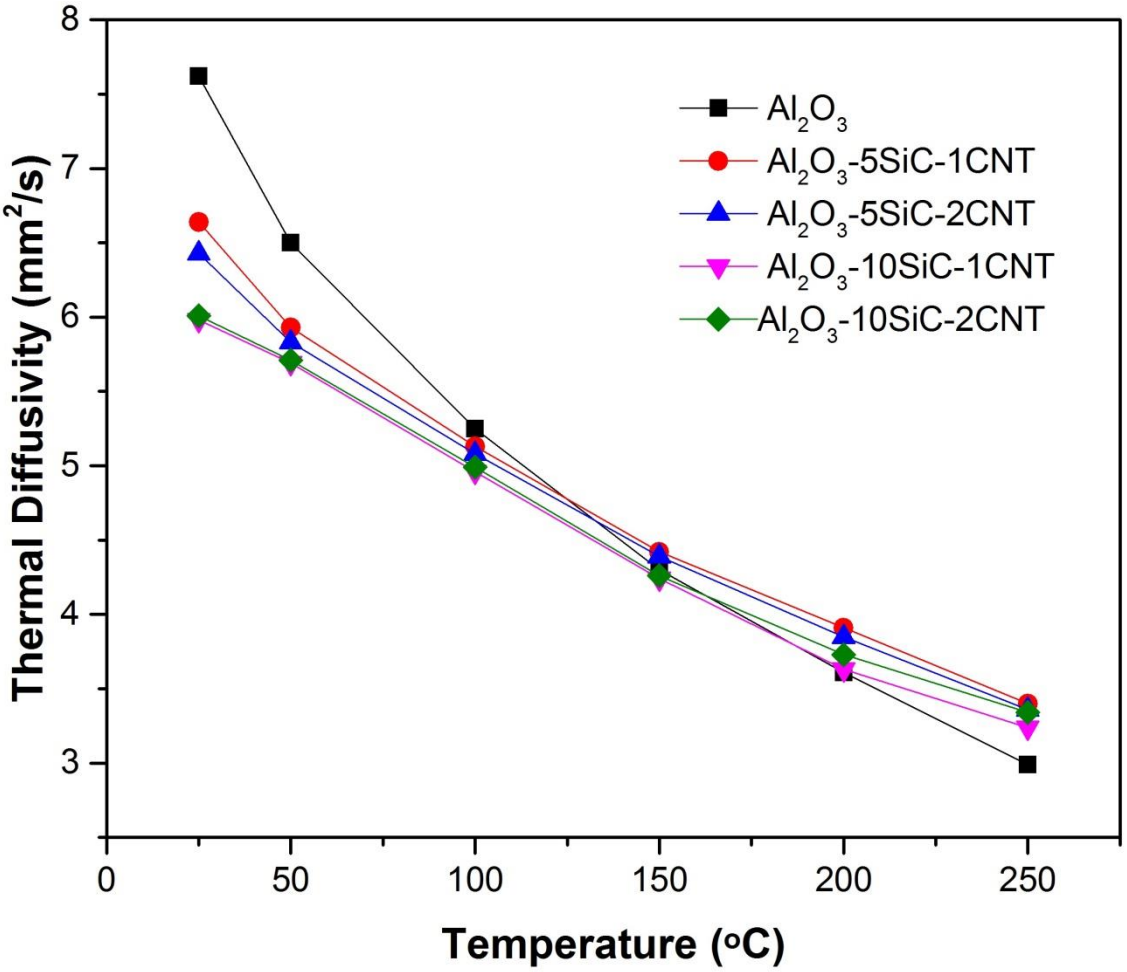

Figure 44. Thermal diffusivity of Al_2O_3-SiC-CNT hybrid nanocomposites at elevated temperatures

4.3.5.3 Specific Heat Capacity

Specific heat capacity of Al_2O_3-SiC-CNT hybrid nanocomposites at room temperature is shown in Figure 45. Decrease in specific heat capacity was observed when alumina was reinforced with SiC and CNTs. For pure alumina, specific heat capacity observed was 1.24J/gK which decreased down to 0.87J/gK when alumina was reinforced with 5wt.% SiC along with 1wt.% CNTs. This value kept on decreasing to 0.84, 0.80 and 0.807J/gK

for Al_2O_3-5SiC-2CNT, Al_2O_3-10SiC-1CNT and Al_2O_3-10SiC-2CNT hybrid nanocomposites, respectively.

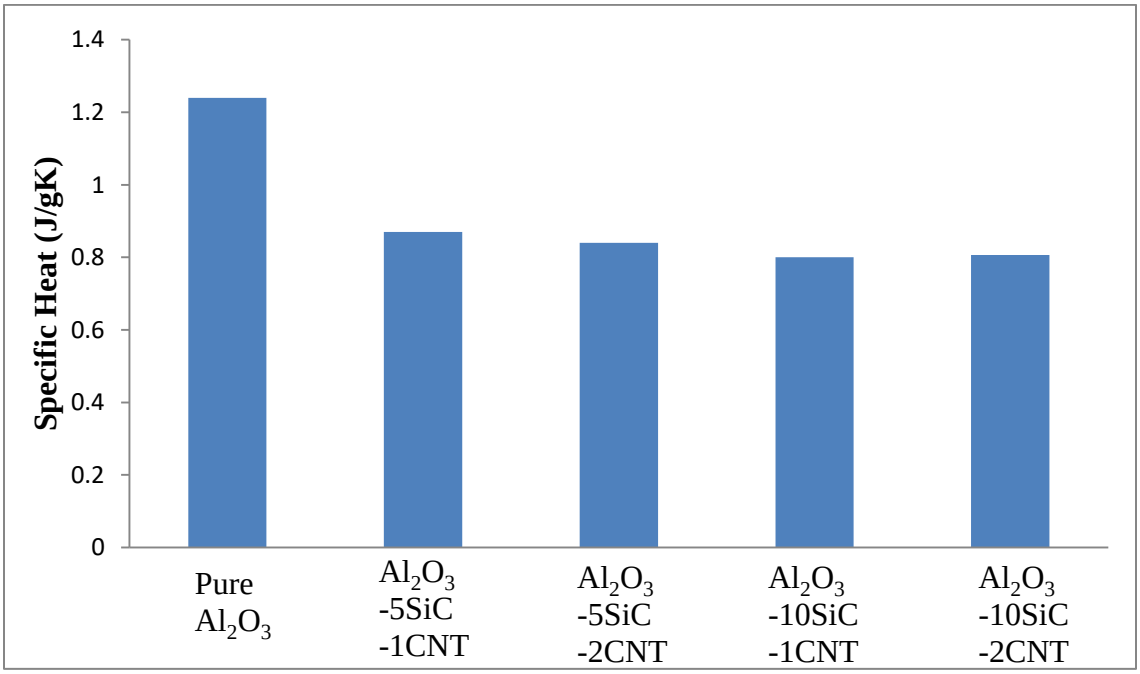

Figure 45. Room temperature specific heat capacity of Al_2O_3-SiC-CNT hybrid nanocomposites

Specific heat capacity by definition is amount of heat required to raise temperature of unit mass of body through 1℃. Specific heat capacity of all the Al_2O_3-SiC-CNT hybrid nanocomposites was lower than the pure alumina. Apparently, densification appears to be one of the reasons for this decrease in specific heat. Increase of porosity in Al_2O_3-SiC-CNT hybrid nanocomposites may have resulted in decrease in specific heat capacity as compared to pure alumina. However, the exact mechanism responsible for decrease in specific heat is unknown. Also, not enough literature is available to explain the mechanisms of heat capacity in nanocomposites. On contrary to this work, L. Kumari et al [38] reported an increase in heat capacity when alumina was reinforced with different

content of MWCNT. He reported a value of 0.82J/gK for pure alumina and maximum value of 5J/gK for Al_2O_3-19.10wt.%CNT nanocomposite. He also reported that exact mechanism of this heat capacity enhancement is unknown.

Figure 46 shows the specific heat capacity of Al_2O_3-SiC-CNT hybrid nanocomposites from room temperature upto 250℃. Unlike thermal conductivity and thermal diffusivity, specific heat capacity increased with increase in temperature. For pure alumina, specific heat capacity increased from 1.24J/gK at 25℃ to 1.57J/gK at 250℃. Similarly, the heat capacity values increased with increase in temperature for all Al_2O_3-SiC-CNT hybrid nanocomposites. For instance, for Al_2O_3-5SiC-1CNT hybrid nanocomposite, heat capacity value increased from 0.87J/gK at 25℃ to 1.06J/gK at 250℃. Same increasing trend of heat capacity for Al_2O_3-CNT nanocomposites was also reported by L. Kumari et al [38]. He reported an increase in specific heat value of pure alumina from 0.82J/gK at 50℃ to 1.05J/gK at 250℃. Munro et al [5] also reported specific heat capacity value of 0.75J/gK for pure alumina which increased with increase in temperature.

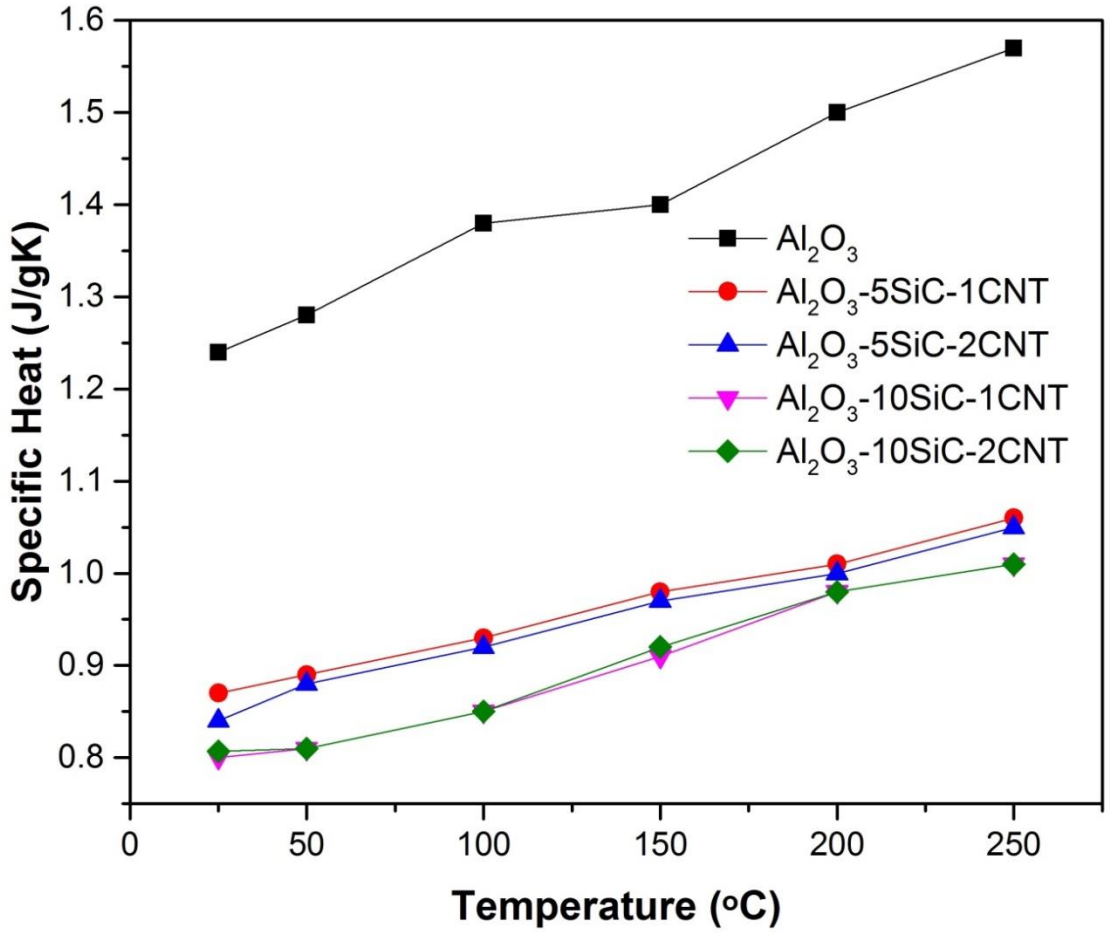

Figure 46. Specific heat capacity of Al_2O_3-SiC-CNT hybrid nanocomposites at elevated temperatures

4.3.6 Electrical Conductivity

Figure 47 shows the electrical conductivity of Al_2O_3-SiC-CNT hybrid nanocomposites. Alumina, being an electrical insulator, showed a very small value of 6.87×10^{-10} S/m for electrical conductivity. However, when this alumina was reinforced with 5wt.% SiC along with 1wt.% CNTs, drastic increase in value of electrical conductivity was observed and value reached to 4.28 S/m. Further increase in CNTs to 2wt.%, in Al_2O_3-5SiC-2CNT nanocomposite, caused the electrical conductivity to reach the highest value of 8.85 S/m.

However, when amount of SiC was increased to 10wt.%, in Al_2O_3-10SiC-1CNT and Al_2O_3-10SiC-2CNT hybrid nanocomposites, relatively lower values of 1.28 and 3.87 S/m were observed for electrical conductivity. All the hybrid nanocomposites showed improved electrical conductivity in range of semiconductors.

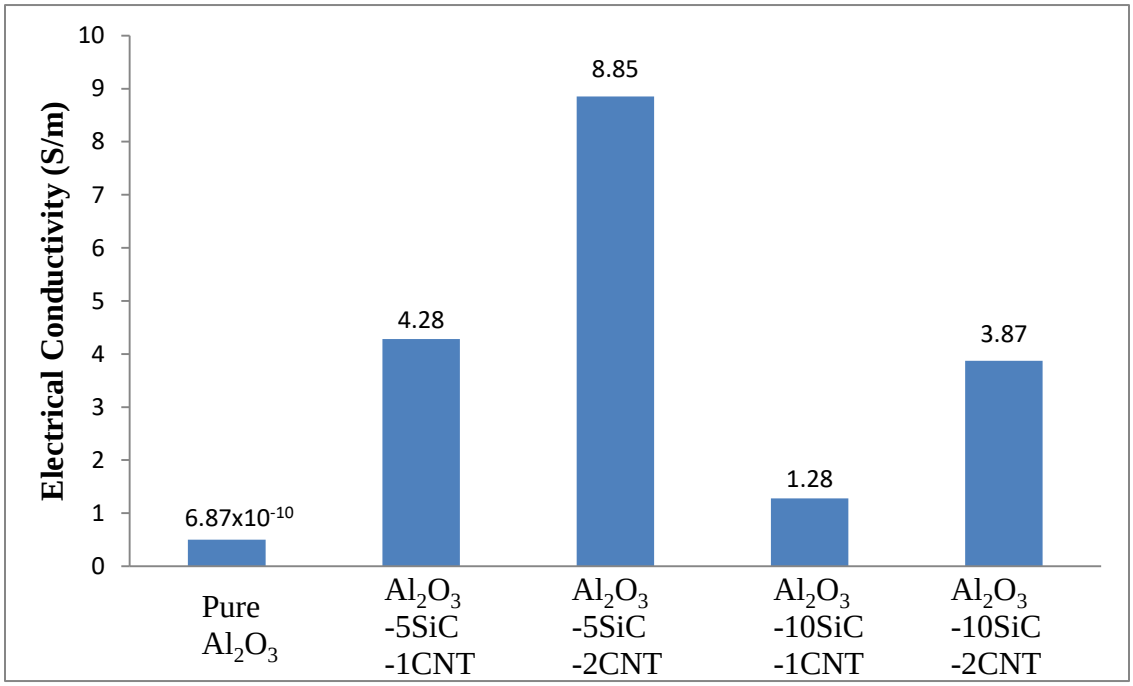

Figure 47. Electrical Conductivity of Al_2O_3-SiC-CNT hybrid nanocomposites

Electrical conduction mechanism in insulting ceramics is because of formation of interconnected continuous network of some conducting or semi-conducting phase within the grain boundaries. At particular concentration of this reinforcement in matrix, continuous network of conducting or semi-conducting reinforcement is established, called percolation threshold, beyond which electrical conductivity increases drastically [89]. One of the differences in electrical conductivity and thermal conductivity is that the electrical conduction occurs through network of conducting or semiconducting phase

present within the grain boundaries while in thermal conduction, dominant channel always involves the grains of matrix for the flow of heat [98].

Increase in electrical conductivity values observed in case of Al_2O_3-SiC-CNT hybrid nanocomposites was because of the formation of conducting network of CNTs and SiC reinforcements within the grain boundaries of alumina. Such high increase in electrical conductivity showed that the amount of reinforcement was well beyond percolation threshold. The electrical conductivity kept on increasing from Al_2O_3-5SiC-1CNT to Al_2O_3-5SiC-2CNT nanocomposites because increasing the CNT content improved the interconnected network between grain boundaries of alumina. However, in case of Al_2O_3-10SiC-1CNT and Al_2O_3-10SiC-2CNT hybrid nanocomposites, relatively low values may be due to increased porosity present within these samples which caused disruptions within interconnected continuous network of CNTs and SiC, causing the electrical conductivity to decrease. Also, the small amount of agglomerations present within Al_2O_3-10SiC-1CNT and Al_2O_3-10SiC-2CNT hybrid nanocomposites, as confirmed by FE-SEM analysis, might have caused disruptions in interconnected network and caused the electrical conductivity to decrease.

K. Ahmad et al [98] reported similar values of electrical conductivity for Al_2O_3-SiC-CNT hybrid nanocomposites with 5vol.% CNTs and varying content (1, 2, 3vol.%) of SiC. He reported highest value of 9 S/m for Al_2O_3-3vol.%SiC-5vol.%CNT hybrid nanocomposite. He attributed the increase in electrical conductivity to formation of continuous network of SiC and CNTs within grain boundaries of alumina. Very small electrical conductivity values for pure alumina in the range of 10^{-10}-10^{-12}S/m were also reported by different researchers [25, 26, 57, 75, 77-79]. M. Parchoviansky et al [32] studied the electrical

behavior of Al_2O_3-SiC nanocomposites with varying content (0-20vol.%) of SiC and reported the maximum value of electrical conductivity to be $4.05x10^{-2}$ S/m for Al_2O_3-20vol.%SiC nanocomposite. He observed the percolation threshold between 5-10vol.% SiC. A. Borell et al [90] reported the range of electrical conductivity values for Al_2O_3-17vol.%SiC nanocomposites between $2.7x10^{-7}$-3.2 S/m using different particle sizes of alumina matrix and SiC reinforcement along with different SPS parameters.

K. Ahmad et al [25] reported values of 1.285 S/m and 5 S/m for electrical conductivity of Al_2O_3-5vol.%CNT and Al_2O_3-10vol.%CNT nanocomposites, respectively. This increase in electrical conductivity was attributed to percolating conducting CNTs network within alumina grain boundaries. G. Yamamoto et al [75] reported a value of 1.4 S/m for electrical conductivity of Al_2O_3-0.9vol.%CNT nanocomposite. K. Ahmad et al [95] found the percolation limit of Al_2O_3-CNT nanocomposites to be 0.45wt.% CNTs, beyond this value electrical conductivity increased drastically and reached a maximum value of 3 S/m for Al_2O_3-6wt.%CNT nanocomposite. In another study, K. Ahmad et al [77] reported percolation limit to be 0.79vol.% CNTs for Al_2O_3-CNT nanocomposites with maximum electrical conductivity of 8 S/m for Al_2O_3-10vol.%CNT nanocomposite. M. Poorteman et al [78] found electrical conductivity of 2.5 S/m for Al_2O_3-0.5wt.%CNT nanocomposite while the percolation threshold reported was ≤0.6wt%CNT. K. Lee et al [96] reported electrical conductivity to be 12.2 S/m for Al_2O_3-2.48wt.%CNT nanocomposite.

There are few researchers who have reported very high values of electrical conductivity for Al_2O_3-CNT nanocomposites. For instance, L. Kumari et al [26] reported values of 288 and 705 S/m for Al_2O_3-7.39wt.%CNT nanocomposite, SPS sintered at 1150°C and 1450°C, respectively. Also, for Al_2O_3-19.1wt.%CNT nanocomposite, values of electrical

conductivity reported were 2460 and 3336 S/m for sintering temperature of 1150℃ and 1450℃, respectively. This increase was also attributed to conductive network of CNTs within alumina matrix. Furthermore, increase in electrical conductivity with increase in SPS temperature was attributed to higher densification at higher SPS temperature. F. Inam et al [56] reported the electrical conductivity values of 125 and 576 S/m for Al_2O_3-2wt.%CNT and Al_2O_3-5wt.%CNT nanocomposites, respectively. Zhan et al [57] also reported very high electrical conductivity values for Al_2O_3-SWCNT nanocomposites. He reported electrical conductivity values to be 1050, 1510 and 3345 S/m for Al_2O_3-5.7vol.%SWCNT, Al_2O_3-10vol.%SWCNT and Al_2O_3-15vol.%SWCNT nanocomposites, respectively.

Above discussion shows that the results of electrical conductivity enhancements found in this work follows the trend of most of the researchers. Reinforcing alumina with SiC and CNTs changed the electrical behavior of alumina from being insulator to semiconductor. This transition in electrical behavior can lead to usage of alumina in wide range of applications. With conductive behavior of alumina, complex shapes can be fabricated using electro-discharge machining (EDM), as electro-discharge machining is possible if resistivity is ≤100cm or electrical conductivity is ≥1 S/m [32, 90]. Some of the potential applications where electrically conductive alumina can be used are; heating elements, electromagnetic and antistatic shieldings of electronic components, electric igniters, electrodes for fuel cells, crucibles for vacuum induction furnaces etc. [77].

CHAPTER 5

CONCLUSIONS AND RECOMMENDATIONS

5.1 Conclusions

Homogenous Al_2O_3-SiC-CNTs nanocomposites were produced using ball-milling and spark plasma sintering methods. Temperature-dependent thermal properties of alumina were reported and the influence of SiC and CNTs on thermal properties and electrical conductivity of Al_2O_3-SiC-CNTs hybrid nanocomposites was investigated. The properties were correlated with the microstructure and possible transport mechanisms were discussed. The following conclusions are drawn:

1- The room temperature thermal conductivity of monolithic alumina was 34.44 W/mK. The thermal conductivity decreased to 21.2 and 20.4 W/mK for the Al_2O_3-5SiC-1CNT and Al_2O_3-5SiC-2CNT composites, respectively. The increase in SiC content to 10 wt.% led to further decrease in the thermal conductivity to reach 17.71 and 17.81 W/mK for Al_2O_3-10SiC-1CNT and Al_2O_3-10SiC-2CNT, respectively.

2- The room temperature thermal diffusivity of monolithic alumina was 7.62 mm^2/s. The thermal diffusivity decreased to 6.64 and 6.43 mm^2/s for the Al_2O_3-5SiC-1CNT and Al_2O_3-5SiC-2CNT composites, respectively. The increase in SiC content to 10 wt.% led to further decrease in the thermal diffusivity to reach 5.98 and 6.01 mm^2/s for Al_2O_3-10SiC-1CNT and Al_2O_3-10SiC-2CNT, respectively.

3- The room temperature specific heat of monolithic alumina was 1.24 J/gK. The specific heat decreased to 0.87 and 0.84 J/gK for the Al_2O_3-5SiC-1CNT and Al_2O_3-5SiC-2CNT composites, respectively. The increase in SiC content to 10 wt.% led to further decrease in the specific heat to reach 0.80 and 0.807 J/gK for Al_2O_3-10SiC-1CNT and Al_2O_3-10SiC-2CNT, respectively.

4- The increase in temperature decreased the thermal conductivity and thermal diffusivity, but increased the specific heat of the monolithic alumina and the hybrid nanocomposites.

5- The SiC and CNT reinforced alumina hybrid nanocomposites showed significant increase in room temperature electrical conductivity, which made them suitable for electrical discharge machining. This makes the hybrid composites suitable for EDM and allows for the manufacturing of low cost products that have intricate shapes, irrespective of their hardness or strength. The Al_2O_3-5SiC-2CNTs had a high electrical conductivity value of 8.85 S/m compared to a low value of 6.87 x 10^{-10} S/m for the monolithic alumina.

5.2 Recommendations

The SiC and CNT reinforced alumina nanocomposites had homogenous microstructure and showed significant increase in electrical conductivity, with respect to alumina, which made them suitable for electrical discharge machining. However, the hybrid composites showed reduced thermal properties compared with monolithic alumina.

Further investigation of the developed materials is recommended. This may include:

1- Optimization of sintering parameters to improve the densification.

2- Optimization of reinforcements' content to improve the thermal properties.

3- Sintering the composites using other non-conventional methods such as microwave sintering.

4- Investigation of the machining behaviour of the developed hybrid nanocomposites using electrical discharge machining (EDM).

REFERENCES

[1] A. G. Evans, "Perspective on the Development of High-Toughness Ceramics," *Journal of the American Ceramic Society,* vol. 73, pp. 187-206, 1990.

[2] T. Wei, Z. Fan, G. Luo, F. Wei, D. Zhao, and J. Fan, "The effect of carbon nanotubes microstructures on reinforcing properties of SWNTs/alumina composite," *Materials Research Bulletin,* vol. 43, pp. 2806-2809, 2008.

[3] K. Niihara, "New design concept of structural ceramics—ceramic nanocomposites," *Nippon seramikkusu kyokai gakujutsu ronbunshi,* vol. 99, pp. 974-982, 1991.

[4] P. H. C. Camargo, K. G. Satyanarayana, and F. Wypych, "Nanocomposites: synthesis, structure, properties and new application opportunities," *Materials Research,* vol. 12, pp. 1-39, 2009.

[5] M. MUNRO, "Evaluated Material Properties for a Sintered alpha-Alumina," *Journal of the American Ceramic Society,* vol. 80, pp. 1919-1928, 1997.

[6] O. L. Ighodaro and O. I. Okoli, "Fracture toughness enhancement for alumina systems: a review," *International Journal of Applied Ceramic Technology,* vol. 5, pp. 313-323, 2008.

[7] K.-Y. Lee, L. Cropsey, B. Tyszka, and E. Case, "Grain size, density, and mechanical properties of alumina batch-processed in a single-mode microwave cavity," *Materials research bulletin,* vol. 32, pp. 287-295, 1997.

[8] M. Demuynck, J.-P. Erauw, O. Van der Biest, F. Delannay, and F. Cambier, "Densification of alumina by SPS and HP: A comparative study," *Journal of the European Ceramic Society,* vol. 32, pp. 1957-1964, 2012.

[9] J. G. Santanach, A. Weibel, C. Estournès, Q. Yang, C. Laurent, and A. Peigney, "Spark plasma sintering of alumina: Study of parameters, formal sintering analysis and hypotheses on the mechanism (s) involved in densification and grain growth," *Acta Materialia,* vol. 59, pp. 1400-1408, 2011.

[10] Z. Shen, M. Johnsson, Z. Zhao, and M. Nygren, "Spark plasma sintering of alumina," *Journal of the American Ceramic Society,* vol. 85, pp. 1921-1927, 2002.

[11] M. Shan, G.-H. Zhou, and S.-W. Wang, "Fabrication of Sub-micron Alumina by Spark Plasma Sintering," *JOURNAL OF INORGANIC MATERIALS-BEIJING-,* vol. 23, pp. 1001-1004, 2008.

[12] S. Wang, L. Chen, and T. Hirai, "Densification of Al 2 O 3 powder using spark plasma sintering," *Journal of Materials Research,* vol. 15, pp. 982-987, 2000.

[13] S. Sarkar and P. K. Das, "Processing and properties of carbon nanotube/alumina nanocomposites: a review," *Rev. Adv. Mater. Sci,* vol. 37, pp. 53-82, 2014.

[14] D. Jack, "Ceramic cutting tool materials," *Materials & Design,* vol. 7, pp. 267-273, 1986.

[15] K. GERIC, "Ceramics tool materials with alumina matrix," *TiC*, vol. 200, pp. 310-410, 2010.

[16] B. North, "Ceramic cutting tools—A review," *International journal of high technology ceramics*, vol. 3, pp. 113-127, 1987.

[17] A. S. Kumar, A. R. Durai, and T. Sornakumar, "Machinability of hardened steel using alumina based ceramic cutting tools," *International Journal of Refractory Metals and Hard Materials*, vol. 21, pp. 109-117, 2003.

[18] Y. M. Ko, W. T. Kwon, and Y.-W. Kim, "Development of Al 2 O 3–SiC composite tool for machining application," *Ceramics international*, vol. 30, pp. 2081-2086, 2004.

[19] S. Sarkar, S. Sarkar, P. K. Das, S. Das, and S. Paul, "Performance of a newly developed multiwalled carbon nanotube reinforced alumina tool insert during turning of aisi 1060 steel," *Journal of the Association of Engineers, India*, vol. 86.

[20] X. Hong, "Wear behaviour and wear mechanism of ceramic tools in machining hardened alloy steel," *Wear*, vol. 139, pp. 439-451, 1990.

[21] A. Chakraborty, K. Ray, and S. Bhaduri, "Comparative wear behavior of ceramic and carbide tools during high speed machining of steel," *Materials and Manufacturing Processes*, vol. 15, pp. 269-300, 2000.

[22] R. Munro, "Material properties of a sintered α-SiC," *Journal of Physical and Chemical Reference Data*, vol. 26, pp. 1195-1203, 1997.

[23] S. Hayun, V. Paris, R. Mitrani, S. Kalabukhov, M. Dariel, E. Zaretsky, *et al.*, "Microstructure and mechanical properties of silicon carbide processed by Spark Plasma Sintering (SPS)," *Ceramics International*, vol. 38, pp. 6335-6340, 2012.

[24] M. Sternitzke, "Structural ceramic nanocomposites," *Journal of the European Ceramic Society*, vol. 17, pp. 1061-1082, 1997.

[25] K. Ahmad, W. Pan, and C. L. Wan, "Electro-Mechanical and Thermal Properties of Multiwalled Carbon Nanotube Reinforced Alumina Composites," in *Key Engineering Materials*, 2008, pp. 701-703.

[26] L. Kumari, T. Zhang, G. Du, W. Li, Q. Wang, A. Datye, *et al.*, "Synthesis, microstructure and electrical conductivity of carbon nanotube–alumina nanocomposites," *Ceramics International*, vol. 35, pp. 1775-1781, 2009.

[27] Y. Dong, F. Xu, X. Shi, C. Zhang, Z. Zhang, J. Yang, *et al.*, "Fabrication and mechanical properties of nano-/micro-sized Al 2 O 3/SiC composites," *Materials Science and Engineering: A*, vol. 504, pp. 49-54, 2009.

[28] L. L. Snead, T. Nozawa, Y. Katoh, T.-S. Byun, S. Kondo, and D. A. Petti, "Handbook of SiC properties for fuel performance modeling," *Journal of nuclear materials*, vol. 371, pp. 329-377, 2007.

[29] M. Tobi, A. Latif, and A. E. Ismail, "A review on carbon nanotubes reinforced ceramic composite," *Journal of Engineering and Applied Sciences*, 2015.

[30] X. Shi, F. Xu, Z. Zhang, Y. Dong, Y. Tan, L. Wang, *et al.*, "Mechanical properties of hot-pressed Al 2 O 3/SiC composites," *Materials Science and Engineering: A,* vol. 527, pp. 4646-4649, 2010.

[31] M. Parchovianský, D. Galusek, J. Sedláček, P. Švančárek, M. Kašiarová, J. Dusza, *et al.*, "Microstructure and mechanical properties of hot pressed Al 2 O 3/SiC nanocomposites," *Journal of the European Ceramic Society,* vol. 33, pp. 2291-2298, 2013.

[32] M. Parchovianský, D. Galusek, P. Švančárek, J. Sedláček, and P. Šajgalík, "Thermal behavior, electrical conductivity and microstructure of hot pressed Al 2 O 3/SiC nanocomposites," *Ceramics International,* vol. 40, pp. 14421-14429, 2014.

[33] S. Iijima, "Helical microtubules of graphitic carbon," *Nature,* vol. 354, pp. 56-58, 1991.

[34] C. Suryanarayana and N. Al-Aqeeli, "Mechanically alloyed nanocomposites," *Progress in Materials Science,* vol. 58, pp. 383-502, 2013.

[35] A. Javadi, S. Mirdamadi, M. Faghihisani, S. Shakhesi, and R. Soltani, "Fabrication of well-dispersed, multiwalled carbon nanotubes-reinforced aluminum matrix composites," *New Carbon Materials,* vol. 27, pp. 161-165, 2012.

[36] S. Bi, G. Hou, X. Su, Y. Zhang, and F. Guo, "Mechanical properties and oxidation resistance of α-alumina/multi-walled carbon nanotube composite ceramics," *Materials Science and Engineering: A,* vol. 528, pp. 1596-1601, 2011.

[37] I. Ahmad, H. Cao, H. Chen, H. Zhao, A. Kennedy, and Y. Q. Zhu, "Carbon nanotube toughened aluminium oxide nanocomposite," *Journal of the European Ceramic Society,* vol. 30, pp. 865-873, 2010.

[38] L. Kumari, T. Zhang, G. Du, W. Li, Q. Wang, A. Datye, *et al.*, "Thermal properties of CNT-Alumina nanocomposites," *Composites Science and Technology,* vol. 68, pp. 2178-2183, 2008.

[39] K. Ahmad and W. Pan, "Hybrid nanocomposites: a new route towards tougher alumina ceramics," *Composites Science and Technology,* vol. 68, pp. 1321-1327, 2008.

[40] K. Mohammad and N. Saheb, "Molecular level mixing: An approach for synthesis of homogenous hybrid ceramic nanocomposite powders," *Powder Technology,* vol. 291, pp. 121-130, 2016.

[41] N. Saheb and K. Mohammad, "Microstructure and mechanical properties of spark plasma sintered Al 2 O 3-SiC-CNTs hybrid nanocomposites," *Ceramics International,* 2016.

[42] S. Ghadami, H. Baharvandi, and F. Ghadami, "Influence of the vol% SiC on properties of pressureless Al2O3/SiC nanocomposites," *Journal of Composite Materials,* p. 0021998315591300, 2015.

[43] S. Gustafsson, L. K. Falk, E. Lidén, and E. Carlström, "Pressureless sintered Al 2 O 3–SiC nanocomposites," *Ceramics International*, vol. 34, pp. 1609-1615, 2008.

[44] J. H. Chae, K. H. Kim, Y. H. Choa, J.-i. Matsushita, J.-W. Yoon, and K. B. Shim, "Microstructural evolution of Al 2 O 3–SiC nanocomposites during spark plasma sintering," *Journal of alloys and compounds*, vol. 413, pp. 259-264, 2006.

[45] N. Bakhsh, F. A. Khalid, A. S. Hakeem, and T. Laoui, "Dispersion of Carbon Nanotubes in Alumina using a Novel Mixing Technique and Spark Plasma Sintering of the Nanocomposites with Improved Fracture Toughness," *Advances in Science & Technology*, vol. 89, 2014.

[46] I. Ahmad, M. Unwin, H. Cao, H. Chen, H. Zhao, A. Kennedy, *et al.*, "Multi-walled carbon nanotubes reinforced Al 2 O 3 nanocomposites: mechanical properties and interfacial investigations," *Composites Science and Technology*, vol. 70, pp. 1199-1206, 2010.

[47] S. C. Zhang, W. G. Fahrenholtz, G. E. Hilmas, and E. J. Yadlowsky, "Pressureless sintering of carbon nanotube–Al 2 O 3 composites," *Journal of the European Ceramic Society*, vol. 30, pp. 1373-1380, 2010.

[48] J. Fan, D. Zhao, M. Wu, Z. Xu, and J. Song, "Preparation and Microstructure of Multi-Wall Carbon Nanotubes-Toughened Al2O3 Composite," *Journal of the American Ceramic Society*, vol. 89, pp. 750-753, 2006.

[49] J. Cho, A. R. Boccaccini, and M. S. Shaffer, "Ceramic matrix composites containing carbon nanotubes," *Journal of Materials Science*, vol. 44, pp. 1934-1951, 2009.

[50] P. Palmero, "Structural ceramic nanocomposites: a review of properties and powders' synthesis methods," *Nanomaterials*, vol. 5, pp. 656-696, 2015.

[51] V. Viswanathan, T. Laha, K. Balani, A. Agarwal, and S. Seal, "Challenges and advances in nanocomposite processing techniques," *Materials Science and Engineering: R: Reports*, vol. 54, pp. 121-285, 2006.

[52] C. Suryanarayana, *Mechanical alloying and milling*: CRC Press, 2004.

[53] P.-C. Ma, N. A. Siddiqui, G. Marom, and J.-K. Kim, "Dispersion and functionalization of carbon nanotubes for polymer-based nanocomposites: a review," *Composites Part A: Applied Science and Manufacturing*, vol. 41, pp. 1345-1367, 2010.

[54] Q. Cheng, S. Debnath, E. Gregan, and H. J. Byrne, "Ultrasound-assisted SWNTs dispersion: effects of sonication parameters and solvent properties," *The Journal of Physical Chemistry C*, vol. 114, pp. 8821-8827, 2010.

[55] F. Inam, H. Yan, T. Peijs, and M. J. Reece, "The sintering and grain growth behaviour of ceramic–carbon nanotube nanocomposites," *Composites Science and Technology*, vol. 70, pp. 947-952, 2010.

[56] F. Inam, H. Yan, D. D. Jayaseelan, T. Peijs, and M. J. Reece, "Electrically conductive alumina–carbon nanocomposites prepared by spark plasma sintering," *Journal of the European Ceramic Society,* vol. 30, pp. 153-157, 2010.

[57] G. D. Zhan and A. K. Mukherjee, "Carbon Nanotube Reinforced Alumina-Based Ceramics with Novel Mechanical, Electrical, and Thermal Properties," *International Journal of Applied Ceramic Technology,* vol. 1, pp. 161-171, 2004.

[58] J. Sun, L. Gao, and X. Jin, "Reinforcement of alumina matrix with multi-walled carbon nanotubes," *Ceramics international,* vol. 31, pp. 893-896, 2005.

[59] J. Ning, J. Zhang, Y. Pan, and J. Guo, "Surfactants assisted processing of carbon nanotube-reinforced SiO 2 matrix composites," *Ceramics International,* vol. 30, pp. 63-67, 2004.

[60] G. Yamamoto, M. Omori, T. Hashida, and H. Kimura, "A novel structure for carbon nanotube reinforced alumina composites with improved mechanical properties," *Nanotechnology,* vol. 19, p. 315708, 2008.

[61] G. Yamamoto, M. Omori, and T. Hashida, "Preparation of Carbon Nanotube---Toughened Alumina Composites," in *Water Dynamics*, 2008, pp. 83-85.

[62] L. Gao, H. Wang, J. Hong, H. Miyamoto, K. Miyamoto, Y. Nishikawa, *et al.*, "Mechanical properties and microstructure of nano-SiC–Al 2 O 3 composites densified by spark plasma sintering," *Journal of the European Ceramic Society,* vol. 19, pp. 609-613, 1999.

[63] M. Tokita, "Trends in advanced SPS sparek plasma sintering systems and technology," *J. Soc. Powder Tech. Jpn.,* vol. 30, pp. 790-804, 1993.

[64] M. Tokita, *Handbook of Advanced Ceramics: Chapter 11.2. 3. Spark Plasma Sintering (SPS) Method, Systems, and Applications*: Elsevier Inc. Chapters, 2013.

[65] A. Morales–Rodríguez, A. Gallardo–López, A. Fernández–Serrano, R. Poyato, A. Muñoz, and A. Domínguez–Rodríguez, "Improvement of Vickers hardness measurement on SWNT/Al 2 O 3 composites consolidated by spark plasma sintering," *Journal of the European Ceramic Society,* vol. 34, pp. 3801-3809, 2014.

[66] G.-D. Zhan, J. Kuntz, J. Wan, J. Garay, and A. K. Mukherjee, "Alumina-based nanocomposites consolidated by spark plasma sintering," *Scripta Materialia,* vol. 47, pp. 737-741, 2002.

[67] G.-D. Zhan, J. Kuntz, J. Wan, J. Garay, and A. K. Mukherjee, "Spark-plasma-sintered $BaTiO_3/Al_2O_3$ nanocomposites," *Materials Science and Engineering: A,* vol. 356, pp. 443-446, 2003.

[68] H. Porwal, P. Tatarko, S. Grasso, J. Khaliq, I. Dlouhý, and M. J. Reece, "Graphene reinforced alumina nano-composites," *Carbon,* vol. 64, pp. 359-369, 2013.

[69] D. D. Jayaseelan, S. Ueno, T. Ohji, and S. Kanzaki, "Differential sintering by improper selection of sintering parameters during pulse electric current sintering," *Journal of the American Ceramic Society,* vol. 87, pp. 159-161, 2004.

[70] A. Kasperski, A. Weibel, C. Estournes, C. Laurent, and A. Peigney, "Preparation-microstructure-property relationships in double-walled carbon nanotubes/alumina composites," *Carbon,* vol. 53, pp. 62-72, 2013.

[71] K. Hirota, Y. Takaura, M. Kato, and Y. Miyamoto, "Fabrication of carbon nanofiber (CNF)-dispersed Al2O3 composites by pulsed electric-current pressure sintering and their mechanical and electrical properties," *Journal of materials science,* vol. 42, pp. 4792-4800, 2007.

[72] J. Liu, Y. Wang, F. Yang, K. Chen, and L. An, "Grain refining in spark plasma sintering Al 2 O 3 ceramics," *Journal of Alloys and Compounds,* vol. 622, pp. 596-600, 2015.

[73] R. Barea, M. Belmonte, I. Osendi, and P. Miranzo, "Thermal conductivity of Al 2 O 3/SiC platelet composites," *Journal of the European Ceramic Society,* vol. 23, pp. 1773-1778, 2003.

[74] K. Ahmad, P. Wei, and C. Wan, "Thermal conductivities of alumina-based multiwall carbon nanotube ceramic composites," *Journal of Materials Science,* vol. 49, pp. 6048-6055, 2014.

[75] G. Yamamoto, K. Shirasu, T. Hashida, T. Takagi, J. W. Suk, J. An, *et al.*, "Nanotube fracture during the failure of carbon nanotube/alumina composites," *Carbon,* vol. 49, pp. 3709-3716, 2011.

[76] A. C. Zaman, C. B. Üstündağ, A. Celik, A. Kara, F. Kaya, and C. Kaya, "Carbon nanotube/boehmite-derived alumina ceramics obtained by hydrothermal synthesis and spark plasma sintering (SPS)," *Journal of the European Ceramic Society,* vol. 30, pp. 3351-3356, 2010.

[77] K. Ahmad, W. Pan, and S.-L. Shi, "Electrical conductivity and dielectric properties of multiwalled carbon nanotube and alumina composites," *Applied physics letters,* vol. 89, p. 3122, 2006.

[78] M. Poorteman, M. Traianidis, G. Bister, and F. Cambier, "Colloidal processing, hot pressing and characterisation of electroconductive MWCNT-alumina composites with compositions near the percolation threshold," *Journal of the European Ceramic Society,* vol. 29, pp. 669-675, 2009.

[79] M. Estili, A. Kawasaki, and Y. Sakka, "Highly concentrated 3D macrostructure of individual carbon nanotubes in a ceramic environment," *Advanced Materials,* vol. 24, pp. 4322-4326, 2012.

[80] K. Niihara, A. Nakahira, G. Sasaki, and M. Hirabayashi, "Development of strong Al 2 O 3/SiC composites," in *MRS International Meeting on Advanced Materials, 1 st, Tokyo, Japan*, 1989, pp. 129-134.

[81] G. Pezzotti and W. H. Müller, "Strengthening mechanisms in Al 2 O 3/SiC nanocomposites," *Computational materials science,* vol. 22, pp. 155-168, 2001.

[82] Z.-Y. Deng, J.-L. Shi, Y.-F. Zhang, D.-Y. Jiang, and J.-K. Guo, "Pinning effect of SiC particles on mechanical properties of Al 2 O 3–SiC ceramic matrix composites," *Journal of the European Ceramic Society,* vol. 18, pp. 501-508, 1998.

[83] T. Ohji, T. Hirano, A. Nakahira, and K. Niihara, "Particle/matrix interface and its role in creep inhibition in alumina/silicon carbide nanocomposites," *Journal of the American Ceramic Society,* vol. 79, pp. 33-45, 1996.

[84] O. T. Johnson, P. Rokebrand, and I. Sigalas, "Microstructure and Properties of Al2O3–SiC Nanomaterials," in *Proceedings of the World Congress on Engineering,* 2014.

[85] L. Fabbri, E. Scafè, and G. Dinelli, "Thermal and elastic properties of alumina-silicon carbide whisker composites," *Journal of the European Ceramic Society,* vol. 14, pp. 441-446, 1994.

[86] D. Hasselman and L. F. Johnson, "Effective thermal conductivity of composites with interfacial thermal barrier resistance," *Journal of Composite Materials,* vol. 21, pp. 508-515, 1987.

[87] M. I. Collin and D. J. Rowcliffe, "Influence of Thermal Conductivity and Fracture Toughness on the Thermal Shock Resistance of Alumina—Silicon–Carbide–Whisker Composites," *Journal of the American Ceramic Society,* vol. 84, pp. 1334-1340, 2001.

[88] P. H. McCluskey, R. K. Williams, R. S. Graves, and T. N. Tiegs, "Thermal Diffusivity/Conductivity of Alumina—Silicon Carbide Composites," *Journal of the American Ceramic Society,* vol. 73, pp. 461-464, 1990.

[89] F. Lux, "Models proposed to explain the electrical conductivity of mixtures made of conductive and insulating materials," *Journal of Materials Science,* vol. 28, pp. 285-301, 1993.

[90] A. Borrell, I. Alvarez, R. Torrecillas, V. G. Rocha, and A. Fernández, "Microstructural design for mechanical and electrical properties of spark plasma sintered Al 2 O 3–SiC nanocomposites," *Materials Science and Engineering: A,* vol. 534, pp. 693-698, 2012.

[91] D. S. McLachlan and G. Sauti, "The AC and DC conductivity of nanocomposites," *Journal of Nanomaterials,* vol. 2007, p. 15, 2007.

[92] A. L. Vasiliev and N. P. Padture, "Single-wall carbon nanotubes at ceramic grain boundaries," *Scripta materialia,* vol. 56, pp. 461-463, 2007.

[93] C. B. Mo, S. I. Cha, K. T. Kim, K. H. Lee, and S. H. Hong, "Fabrication of carbon nanotube reinforced alumina matrix nanocomposite by sol–gel process," *Materials Science and Engineering: A,* vol. 395, pp. 124-128, 2005.

[94] S. S. Samal and S. Bal, "Carbon nanotube reinforced ceramic matrix composites-a review," *Journal of Minerals and Materials Characterization and Engineering*, vol. 7, p. 355, 2008.

[95] K. Ahmad and W. Pan, "Dramatic effect of multiwalled carbon nanotubes on the electrical properties of alumina based ceramic nanocomposites," *Composites Science and Technology*, vol. 69, pp. 1016-1021, 2009.

[96] K. Lee, C. B. Mo, S. B. Park, and S. H. Hong, "Mechanical and Electrical Properties of Multiwalled CNT-Alumina Nanocomposites Prepared by a Sequential Two-Step Processing of Ultrasonic Spray Pyrolysis and Spark Plasma Sintering," *Journal of the American Ceramic Society*, vol. 94, pp. 3774-3779, 2011.

[97] Y. Fei, C. Huang, H. Liu, and B. Zou, "Mechanical properties of Al 2 O 3–TiC–TiN ceramic tool materials," *Ceramics International*, vol. 40, pp. 10205-10209, 2014.

[98] K. Ahmad, W. Pan, and Z. Qu, "Multifunctional properties of alumina composites reinforced by a hybrid filler," *International Journal of Applied Ceramic Technology*, vol. 6, pp. 80-88, 2009.

[99] D.-Y. Lee and D.-H. Yoon, "Properties of alumina matrix composites reinforced with SiC whisker and carbon nanotubes," *Ceramics International*, vol. 40, pp. 14375-14383, 2014.

[100] J. Liu, Z. Li, H. Yan, and K. Jiang, "Spark plasma sintering of alumina composites with graphene platelets and silicon carbide nanoparticles," *Advanced Engineering Materials*, vol. 16, pp. 1111-1118, 2014.

[101] C. Suryanarayana and M. G. Norton, *X-ray diffraction: a practical approach*: Springer Science & Business Media, 2013.

[102] M. B. Heaney, "Electrical conductivity and resistivity," *The measurement, instrumentation and sensors handbook*, pp. 1332-1345, 2000.

[103] D. S. Smith, S. Fayette, S. Grandjean, C. Martin, R. Telle, and T. Tonnessen, "Thermal resistance of grain boundaries in alumina ceramics and refractories," *Journal of the American Ceramic Society*, vol. 86, pp. 105-111, 2003.

[104] F. Charvat and W. Kingery, "Thermal Conductivity: XIII, Effect of Microstructure on Conductivity of Single-Phase Ceramics," *Journal of the american ceramic society*, vol. 40, pp. 306-315, 1957.

[105] P. Auerkari, *Mechanical and physical properties of engineering alumina ceramics*: Technical Research Centre of Finland Finland, 1996.

[106] R. Chaim and M. Margulis, "Densification maps for spark plasma sintering of nanocrystalline MgO ceramics," *Materials Science and Engineering: A*, vol. 407, pp. 180-187, 2005.

[107] R. Chaim, "Densification mechanisms in spark plasma sintering of nanocrystalline ceramics," *Materials Science and Engineering: A,* vol. 443, pp. 25-32, 2007.
[108] S.-M. Choi and H. Awaji, "Nanocomposites—a new material design concept," *Science and Technology of Advanced Materials,* vol. 6, pp. 2-10, 2005.
[109] P. Rutkowski, P. Klimczyk, L. Jaworska, L. Stobierski, and A. Dubiel, "Thermal properties of pressure sintered alumina–graphene composites," *Journal of Thermal Analysis and Calorimetry,* vol. 122, pp. 105-114, 2015.
[110] D. Hasselman, K. Y. Donaldson, and A. L. Geiger, "Effect of reinforcement particle size on the thermal conductivity of a particulate-silicon carbide-reinforced aluminum matrix composite," *Journal of the American Ceramic Society,* vol. 75, pp. 3137-3140, 1992.
[111] E. L. Corral, H. Wang, J. Garay, Z. Munir, and E. V. Barrera, "Effect of single-walled carbon nanotubes on thermal and electrical properties of silicon nitride processed using spark plasma sintering," *Journal of the European Ceramic Society,* vol. 31, pp. 391-400, 2011.
[112] Q. Huang, L. Gao, Y. Liu, and J. Sun, "Sintering and thermal properties of multiwalled carbon nanotube–BaTiO 3 composites," *Journal of Materials Chemistry,* vol. 15, pp. 1995-2001, 2005.
[113] H. Zhang, J.-F. Li, K. Yao, and L. Chen, "Spark plasma sintering and thermal conductivity of carbon nanotube bulk materials," *Journal of applied physics,* vol. 97, p. 114310, 2005.
[114] J. Luo, R. Stevens, and R. Taylor, "Thermal diffusivity/conductivity of magnesium oxide/silicon carbide composites," *Journal of the American Ceramic Society,* vol. 80, pp. 699-704, 1997.
[115] H. Nakano, K. Watari, Y. Kinemuchi, K. Ishizaki, and K. Urabe, "Microstructural characterization of high-thermal-conductivity SiC ceramics," *Journal of the European Ceramic Society,* vol. 24, pp. 3685-3690, 2004.
[116] G. A. Slack, "Thermal conductivity of pure and impure silicon, silicon carbide, and diamond," *Journal of Applied Physics,* vol. 35, pp. 3460-3466, 1964.
[117] K. Yang, J. He, Z. Su, J. B. Reppert, M. J. Skove, T. M. Tritt, *et al.*, "Inter-tube bonding, graphene formation and anisotropic transport properties in spark plasma sintered multi-wall carbon nanotube arrays," *Carbon,* vol. 48, pp. 756-762, 2010.
[118] S. R. Bakshi, K. Balani, and A. Agarwal, "Thermal Conductivity of Plasma-Sprayed Aluminum Oxide—Multiwalled Carbon Nanotube Composites," *Journal of the American Ceramic Society,* vol. 91, pp. 942-947, 2008.

VITAE

Name	Umer Hayat
Nationality	Pakistani
Date of Birth	3/3/1992
Email	umerhayat99@gmail.com
Academic Background	MS Mechanical Engineering, January 2017 King Fahd University of Petroleum and Minerals (KFUPM), Dhahran, Saudi Arabia. BSc. Mechanical Engineering, November 2013 University of Engineering and Technology (UET) Peshawar, Pakistan

Research Publications

- “Temperature-dependent thermal properties of spark plasma sintered alumina”. Nouari Saheb, **Umer Hayat**. Accepted in Journal of Science of Sintering.

- “Electrical Conductivity and Thermal Properties of Spark Plasma Sintered Al_2O_3-SiC-CNTs Hybrid Nanocomposites”. Nouari Saheb, **Umer Hayat**. Submitted to Journal of Ceramics International.

- "Thermal conductivity of alumina hybrid nanocomposites: Experimental and numerical investigation". Muhammad Usama Siddiqui, **Umer Hayat**, Abul Fazal Arif, Nouari Saheb. Submitted to Journal of Materials Chemistry and Physics